

DETERMINATION OF THE DYNAMIC CONSTITUTIVE PROPERTIES
OF IN-SITU MATERIALS

AD 746194

PIFR-311

FINAL REPORT

by

Dr. Theodore F. Stubbs

April 1972

Details of illustrations in
this document may be better
studied on microfiche

Sponsored by

Advanced Research Projects Agency
ARPA Order No. 1579, Amend. 2
Program Code 1F10
Under Contract No. H0210015

The views and conclusions contained in this document
are those of the authors and should not be interpreted
as necessarily representing the official policies either
expressed or implied, of the Advanced Research Projects
Agency or the U.S. Government.

No Prior Report **DDO**

REFILED
AUG 4 1972
RECEIVED

DISTRIBUTION STATEMENT A

Approved for public release;
Distribution Unlimited

Reproduced by

**NATIONAL TECHNICAL
INFORMATION SERVICE**

U.S. Department of Commerce
Springfield VA 22151

PHYSICS INTERNATIONAL COMPANY

2700 MERCED STREET • SAN LEANDRO

ONE 357-4610 (415) • TWX 891-9689 (415)

This research was supported by the Advanced Research Projects Agency of the Department of Defense and was monitored by Bureau of Mines under Contract No. H0210015.

ADDITIONAL NO.	DATE	INITIALS
NO.	NO. 1000	Q
NO.	NO. 1000	Q
CHARACTER		
NO. 1000		
CONTINUED FROM PAGE 1000		
NO.	NO. 1000	
A		

DOCUMENT CONTROL DATA - R&D

(Security classification of title, body of abstract and indexing annotation must be entered when the overall report is classified)

1. ORIGINATING ACTIVITY (Corporate author) Physics International Company 2700 Merced Street San Leandro, California 94577		2a. REPORT SECURITY CLASSIFICATION Unclassified	
		2b. GROUP	
3. REPORT TITLE Determination of the Dynamic Constitutive Properties of In-Situ Materials			
4. DESCRIPTIVE NOTES (Type of report and inclusive dates) Final Report, January 1971 through February 1972			
5. AUTHOR(S) (Last name, first name, initial) Stubbs, Dr. Theodore F.			
6. REPORT DATE April 1972		7a. TOTAL NO. OF PAGES 109	7b. NO. OF REFS 12
8a. CONTRACT OR GRANT NO. H0210015		9a. ORIGINATOR'S REPORT NUMBER(S) PIFR-311	
b. PROJECT NO. ARPA Order No. 1579, Amend. 2		9b. OTHER REPORT NO(S) (Any other numbers that may be assigned this report)	
c. Program Code 1F10			
d.			
10. AVAILABILITY/LIMITATION NOTICES			
11. SUPPLEMENTARY NOTES		12. SPONSORING MILITARY ACTIVITY Advanced Research Projects Agency	
13. ABSTRACT See attached sheet.			

ABSTRACT

Calculations were performed leading to specifications for a gage system to determine the in-situ properties of natural material through application of the conservation equations to stress wave data. Based upon three different material models, the following conclusions were made for the case of a spherically symmetric stress wave:

- a. Specific volume (or density) is obtainable from particle motion data to a good accuracy during both the loading and unloading portions of the stress wave. Proper data processing techniques enable information to be used that has a large noise content or is inherently frequency limited. Under certain conditions the transition region between loading and unloading is not well represented if too much of the high-frequency information is removed by filtering.
- b. Optimum gage placement and the sensitivity of the gage system to errors in placement and asphericity of the measured disturbances were determined.
- c. Although theoretically possible, it is not feasible to calculate tangential stress from particle velocity and radial stress data. Therefore, a gage must be developed to measure tangential stress in order to define the complete stress field.

As a result of the above conclusion gages to measure tangential stress were designed, constructed, and tested using ytterbium as the active element. There were two major goals of the experimentation to test the efficiency of the gage design and to determine the most reliable materials with which to encase the piezoresistive elements. The tests resulted in the following conclusions:

- d. The gage, as designed, records tangential stress in a low-impedance, nearly hydrodynamic material. The required next step prior to field implementation is to test the device in a high-impedance, non-hydrodynamic material.
- e. Of the three substrate materials used (Lucalox, glass, and mica), only mica was found to distort the wavefront required. This was postulated to be due primarily to the anisotropy of sheet mica.
- f. More calibration work on ytterbium is required, particularly with respect to the unloading hysteresis.

14. KEY WORDS	LINK A		LINK B		LINK C	
	ROLE	WT	ROLE	WT	ROLE	WT
In-situ properties Tangential stress gage Equation of state						

INSTRUCTIONS

1. **ORIGINATING ACTIVITY:** Enter the name and address of the contractor, subcontractor, grantee, Department of Defense activity or other organization (*corporate author*) issuing the report.
- 2a. **REPORT SECURITY CLASSIFICATION:** Enter the overall security classification of the report. Indicate whether "Restricted Data" is included. Marking is to be in accordance with appropriate security regulations.
- 2b. **GROUP:** Automatic downgrading is specified in DoD Directive 5200.10 and Armed Forces Industrial Manual. Enter the group number. Also, when applicable, show that optional markings have been used for Group 3 and Group 4 as authorized.
3. **REPORT TITLE:** Enter the complete report title in all capital letters. Titles in all cases should be unclassified. If a meaningful title cannot be selected without classification, show title classification in all capitals in parentheses immediately following the title.
4. **DESCRIPTIVE NOTES:** If appropriate, enter the type of report, e.g., interim, progress, summary, annual, or final. Give the inclusive dates when a specific reporting period is covered.
5. **AUTHOR(S):** Enter the name(s) of author(s) as shown on or in the report. Enter last name, first name, middle initial. If military, show rank and branch of service. The name of the principal author is an absolute minimum requirement.
6. **REPORT DATE:** Enter the date of the report as day, month, year; or month, year. If more than one date appears on the report, use date of publication.
- 7a. **TOTAL NUMBER OF PAGES:** The total page count should follow normal pagination procedure, i.e., enter the number of pages containing information.
- 7b. **NUMBER OF REFERENCES:** Enter the total number of references cited in the report.
- 8a. **CONTRACT OR GRANT NUMBER:** If appropriate, enter the applicable number of the contract or grant under which the report was written.
- 8b, 8c, & 8d. **PROJECT NUMBER:** Enter the appropriate military department identification, such as project number, subproject number, system numbers, task number, etc.
- 9a. **ORIGINATOR'S REPORT NUMBER(S):** Enter the official report number by which the document will be identified and controlled by the originating activity. This number must be unique to this report.
- 9b. **OTHER REPORT NUMBER(S):** If the report has been assigned any other report numbers (*either by the originator or by the sponsor*), also enter this number(s).
10. **AVAILABILITY/LIMITATION NOTICES:** Enter any limitations on further dissemination of the report, other than those

imposed by security classification, using standard statements such as:

- (1) "Qualified requesters may obtain copies of this report from DDC."
- (2) "Foreign announcement and dissemination of this report by DDC is not authorized."
- (3) "U. S. Government agencies may obtain copies of this report directly from DDC. Other qualified DDC users shall request through _____."
- (4) "U. S. military agencies may obtain copies of this report directly from DDC. Other qualified users shall request through _____."
- (5) "All distribution of this report is controlled. Qualified DDC users shall request through _____."

If the report has been furnished to the Office of Technical Services, Department of Commerce, for sale to the public, indicate this fact and enter the price, if known.

11. **SUPPLEMENTARY NOTES:** Use for additional explanatory notes.
12. **SPONSORING MILITARY ACTIVITY:** Enter the name of the departmental project office or laboratory sponsoring (*paying for*) the research and development. Include address.
13. **ABSTRACT:** Enter an abstract giving a brief and factual summary of the document indicative of the report, even though it may also appear elsewhere in the body of the technical report. If additional space is required, a continuation sheet shall be attached.

It is highly desirable that the abstract of classified reports be unclassified. Each paragraph of the abstract shall end with an indication of the military security classification of the information in the paragraph, represented as (TS), (S), (C), or (U).

There is no limitation on the length of the abstract. However, the suggested length is from 150 to 225 words.
14. **KEY WORDS:** Key words are technically meaningful terms or short phrases that characterize a report and may be used as index entries for cataloging the report. Key words must be selected so that no security classification is required. Identifiers, such as equipment model designation, trade name, military project code name, geographic location, may be used as key words but will be followed by an indication of technical context. The assignment of links, roles, and weights is optional.

Contractor: Physics International Company
Effective Date of Contract: 15 January 1971
Contract Expiration Date: 15 February 1972
Amount of Contract: \$77,700
Contract Number: H0210015
Principal Investigator: T. Stubbs (Ph. 415-357-4610)
Project Scientist: Fred Sauer (Ph. 415-357-4610)

DETERMINATION OF THE DYNAMIC CONSTITUTIVE PROPERTIES OF IN-SITU MATERIALS

PIFR-311

FINAL REPORT

by

Dr. Theodore F. Stubbs

April 1972

Sponsored by

Advanced Research Projects Agency
ARPA Order No. 1579, Amend. 2
Program Code 1F10
Under Contract No. H0210015

Details of illustrations in
this document may be better
studied on microfiche

Preparing Agency

Physics International Company
2700 Merced Street
San Leandro, California 94577

ABSTRACT

Calculations were performed leading to specifications for a gage system to determine the in-situ properties of natural material through application of the conservation equations to stress wave data. Based upon three different material models, the following conclusions were made for the case of a spherically symmetric stress wave:

- a. Specific volume (or density) is obtainable from particle motion data to a good accuracy during both the loading and unloading portions of the stress wave. Proper data processing techniques enable information to be used that has a large noise content or is inherently frequency limited. Under certain conditions the transition region between loading and unloading is not well represented if too much of the high-frequency information is removed by filtering.
- b. Optimum gage placement and the sensitivity of the gage system to errors in placement and asphericity of the measured disturbances were determined.
- c. Although theoretically possible, it is not feasible to calculate tangential stress from particle velocity and radial stress data. Therefore, a gage must be developed to measure tangential stress in order to define the complete stress field.

As a result of the above conclusion gages to measure tangential stress were designed, constructed, and tested using ytterbium as the active element. There were two major goals of the experimentation: to test the efficacy of the gage design and to determine the most reliable materials with which to encase the piezoresistive elements. The tests resulted in the following conclusions:

- d. The gage, as designed, records tangential stress in a low-impedance, nearly hydrodynamic material. The required next step prior to field implementation is to test the device in a high-impedance, non-hydrodynamic material.

e. Of the three substrate materials used (Lucalox, glass, and mica), only mica was found to distort the wavefront required. This was postulated to be due primarily to the anisotropy of sheet mica.

f. More calibration work on ytterbium is required, particularly with respect to the unloading hysteresis.

CONTENTS

	<u>Page</u>
SECTION 1 INTRODUCTION	1
1.1 Objectives	1
1.2 Theoretical Background	2
1.3 Computational Procedures	5
1.4 Experimental Procedures	11
SECTION 2 RESULTS	17
2.1 Calculations	17
2.2 Experiments	57
SECTION 3 TECHNICAL REPORT SUMMARY	85
3.1 Technical Problems	85
3.2 General Methodology	85
3.3 Technical Results	88
3.4 DOD Implications	90
3.5 Implications for Further Research	90
REFERENCES	93
APPENDIX A: CONSERVATION EQUATIONS FOR SPHERICAL STRESS ANALYSIS	
APPENDIX B: SUPERIMPOSED GAUSSIAN NOISE	
APPENDIX C: DIGITAL LOW-PASS FILTERING	

ILLUSTRATIONS

<u>Figure</u>		<u>Page</u>
1.1	Ideal Input Velocity History	7
1.2	Typical Radial Stress-Time History of Compacting Material Model	9
1.3	Typical Tangential Stress-Time History Structural Concrete Model	10
1.4	Two Percent Noise on Ideal Velocity Record, Linear Elastic Model	12
1.5	Noisy Velocity Record Filtered at 1 kHz, Linear Elastic Model	13
2.1a	Comparison of True and Computed Tangential Stress Using Raw Data from Linear Elastic Model	19
2.1b	Comparison of True and Computed Tangential Stress Using High Digitation Rate and Low-Frequency Cut-Off Filter	20
2.2a	Volume Calculation for Gage Relative Separation of $\Delta h/h = 0.0206$	22
2.2b	Volume Calculation for Gage Relative Separation, $\Delta h/h = 0.080$	23
2.2c	Volume Calculation for Gage Relative Separation, $\Delta h/h = 0.182$	24
2.3a	Effect of Displacing Coordinate Origin by One-Fourth of the Gage Separation	25
2.3b	Effect of an Error in Gage Package Separation of 25 Percent	26

Preceding page blank

ILLUSTRATIONS (cont.)

<u>Figure</u>	<u>Page</u>
2.4 Pressure-Volume Curve Derived from a Plane-Wave Disturbance Analyzed as if it were Spherical	28
2.5a Pressure-Volume Data Derived from Information Having a Noise Level of 2 Percent on all Stress Data	29
2.5b Elimination of a 2 Percent Stress Noise Level by Low-Pass Filtering all Data at 4 kHz, Digitization Rate 50 kHz	30
2.6 The Effects of Low-Pass-Filtering Noisy Records	32
2.7 Effects Produced Either by a Phase Delay or Frequency Limit of Velocity Data	33
2.8a Effects of Low-Pass Filtering all Data at 4 kHz	34
2.8b Effects of Low-Pass Filtering all Data at 1 kHz	35
2.9 Compacting Model Volumetric Equation of State	37
2.10a Volume Calculation Using Compacting Model SED, $\Delta h/h \approx 0.11$	39
2.10b Volume Calculation Using Compacting Model SED, $\Delta h/h \approx 0.2$	40
2.11 Volume Calculation Using Concrete Model SED, $\Delta h/h \approx 0.9$	42
2.12a Volume Calculation Using Compacting Model SED, $\Delta h/h \approx 0.11$	43
2.12b Volume Calculation Using Compacting Model SED, $\Delta h/h \sim 0.11$	44
2.12c Volume Calculation Using Compacting Model, SED, $\Delta h/h \sim 0.11$	45
2.13a Pressure-Volume Calculation Using Concrete Model SED, $\Delta h/h \sim 0.9$	47
2.13b Pressure-Volume Calculation Using Concrete Model SED, $\Delta h/h \sim 0.9$	48

ILLUSTRATIONS (cont.)

<u>Figure</u>		<u>Page</u>
2.14	Effects of Noise on Concrete Model SED	49
2.15	Effects of Noise on Compacting Model SED	50
2.16a	Velocity History of Compacting Model SED; No Pre-Processing Applied	52
2.16b	Velocity History of Compacting Model SED With 2 Percent Gaussian White Noise Added	53
2.17	Velocity History of Compacting Model SED With 2 Percent Noise and Filtered with a Cut-off/ Digitization Rate Ratio of 0.06	54
2.18	Comparison of True and Calculated Tangential Stress Resulting from Compacting Model SED	55
2.19	Schematic Diagram of Experimental Arrangement	59
2.20	Tangential-Mode Gage Block in Process of Construction	61
2.21	Completed Gage Block Ready for Mounting	62
2.22	Mounting of Gage Blocks on Aluminum Sphere	63
2.23	Aluminum Sphere and Attendant Gage Blocks Installed in Concrete Form Awaiting Grout Covering	64
2.24	Radial Mode Stress Gage Data	68
2.25	Lucalox Substrate Tangential-Mode Gage Data	69
2.26	Glass Substrate Tangential-Mode Gage Data	70
2.27	Mica Substrate Tangential-Mode Gage Data	71
2.28	Numerical Simulation of Experiment--Radial Stress	73
2.29	Numerical Simulation of Experiment--Tangential Stress	74
2.30	Ytterbium Stress Transducer Calibration (M. J. Ginsberg, Reference 7)	78

ILLUSTRATIONS (cont.)

<u>Figure</u>		<u>Page</u>
2.31	Stress-Time Histories of Three Tangential-Mode Gages Including Effects of Assumed Hysteresis of Figure 2.31	80
2.32	Fractional Resistance Change Time Histories of Three Tangential-Mode Gages	82

GLOSSARY

- u Particle velocity along spatial variable
- r Spatial variable in inertial frame
- h Spatial variable in Lagrange frame
- $\left. \frac{\partial x}{\partial y} \right|_z$ The change in x due to a change in y while holding z constant
- V Specific volume
- t Time
- σ_r Radial stress (stress along spatial variable)
- σ_θ Tangential (or azimuthal) stress
- p Pressure
- K Bulk modulus
- $\tilde{\sigma}_\theta$ Tangential stress as derived from Equation (2)
- ϵ Noise/peak signal ratio input to data preprocessing codes
- SED Simulated experimental data

SECTION 1

INTRODUCTION

1.1 OBJECTIVES

The primary goal of this program was to address and solve those theoretical and experimental problems associated with the development of a gage system for determining the in-situ constitutive properties of geologic materials. In-situ properties may differ from those measured in the laboratory for several reasons. First, obtaining a test sample can alter its moisture content and its naturally existing state of stress. Second, it is very difficult to model accurately, in a laboratory specimen, any naturally occurring large scale fractures.

It has been pointed out that the equations of continuum mechanics can be cast in such a form as to yield the constitutive properties of materials from the time histories of stress and ground motion; (see Reference 1). For completeness we include a simplified theoretical discussion in this report. Although there have been some successes at obtaining the tangential stress from measured radial data (Reference 2) the full ramifications of in-situ measurements have not been reported previously. This investigation was one of the major tasks of this contract.

Computational work consisted of two parts: the first was the construction of a data processing code that would take experimental time-history data and convolve it in such a manner as to yield the constitutive properties of the material in which

gages were placed. The second part was the generation of such data to be analyzed by the code. To have precisely known material properties against which to calibrate the results of the analyses, these data were computed. Information sought consisted of the types of gages required, their frequency responses, gage placement, and sensitivity of the analysis techniques to gage noise. Other sources of error, such as waveform distortion were also considered.

The second major portion of the contract was the creation of a gage system to measure the in-situ properties of materials. As a result of the above calculations (reported, in part, in Reference 3) it was found that, from a practical standpoint, it was necessary to add a tangential stress gage to the gage package; (see Reference 3). It was necessary to design and test such a gage before the full package could be assembled. The second goal of the contract was thus directed to designing and testing candidates for a practical tangential stress gage.

1.2 THEORETICAL BACKGROUND

It is assumed that ground motion and stresses can be described completely in one space variable. For what follows, that variable will be radial position in spherical coordinates. Let $[r(h,t),t]$ be the space-time position referred to a fixed coordinate frame with the space-time position (h,t) that of a Lagrange coordinate system attached to the mass points of the material in question: $(h \equiv r(h,0))$.

Conservation of mass is expressed by

$$\left(\frac{\partial Q}{\partial u}\right)_h = -\frac{1}{C_u} \quad (1-1)$$

where

$$Q \equiv \left[\frac{v(h,t)}{v(h,0)}\right] \left[\frac{r(h,0)}{r(h,t)}\right]^m \quad (1-1a)$$

and

$$C_u \equiv \left(\frac{\partial h}{\partial t}\right)_u \quad (1-1b)$$

The coordinate symmetry is determined by the exponent m as follows:

$$m \equiv \begin{cases} 0 & \text{plane} \\ 1 & \text{cylindrical} \\ 2 & \text{spherical} \end{cases} \quad (1-1c)$$

C_u , the strain phase velocity, is defined as the rate at which the condition of a given particle velocity is transmitted through the medium. Clearly, if the relative volume, V , is to be obtained through Equation (1-1), the strain phase velocity must be determined experimentally, requiring a measurement of the particle-velocity history at a minimum of two values of h .

Conservation of momentum results in

$$\sigma_\theta = \sigma_r - \frac{r}{2} \left\{ \left(\frac{1}{QC_p}\right) \left(\frac{\partial \sigma_r}{\partial t}\right)_h + \frac{1}{v(h,t)} \left(\frac{\partial u}{\partial t}\right)_h \right\} \quad (1-2)$$

$$\sigma_\theta = \sigma_\theta(h,t)$$

$$\sigma_r = \sigma_r(h,t)$$

Here the stress phase-velocity is defined by

$$C_p \equiv \left(\frac{\partial h}{\partial t} \right)_{\sigma_r} \quad (1-2a)$$

and is the rate at which the condition of a given radial stress level is transmitted.

In order that the tangential stress, σ_θ , be calculated it is necessary to obtain C_p ; this is possible only through measurement of the radial stress history at a minimum of two values of h . The stresses are defined here to be positive in tension and the pressure is given as

$$p = -\frac{1}{3} \{ \sigma_r + 2 \sigma_\theta \} = p(h,t) \quad (1-3)$$

In principal, measurements of the time histories of radial velocity and stress at two values of initial radial position can be used to calculate tangential stress, pressure, and density at one of the positions.

Practical difficulties in applying the mass and momentum conservation equations may arise. Both the stress and strain phase velocities are computed from time differences taken between the records of two different gages, Equations (1-1b) and (1-2a). Although, in the case of Equation (1-1), random errors in these differences may be averaged out during integration to obtain the specific volume, systematic errors will not be. Secondly, Equation (1-2) contains the sum of two terms which include the time derivatives of experimental data; these two terms are generally of the same magnitude and of opposite sign. Significant trouble may be anticipated here.

Energy may also be calculated from the conservation of energy condition:

$$dE = - \left\{ \sigma_r dV + \frac{2V}{r} (\sigma_r - \sigma_\theta) dr \right\} \quad (1-4)$$

$$E = E(h,t)$$

The derivation of Equations (1-1), (1-2) and (1-4) is put forth in Reference 1, the essence of which is reproduced in Appendix A.

It is the purpose of the computational investigations to determine those measurements that are required in practice in addition to the constraints that must be imposed on the individual gage elements.

1.3 COMPUTATIONAL PROCEDURES

As explained above, the first task was to create a data reduction code designed to accept field velocity and stress history data. The time variation of the volume is obtained from Equation (1-1) using the measured velocity histories only, while the tangential stress history may be obtained from Equation (1-2) using time variations of both velocity and radial stress. Each of the two conservation equations may be tested separately as follows:

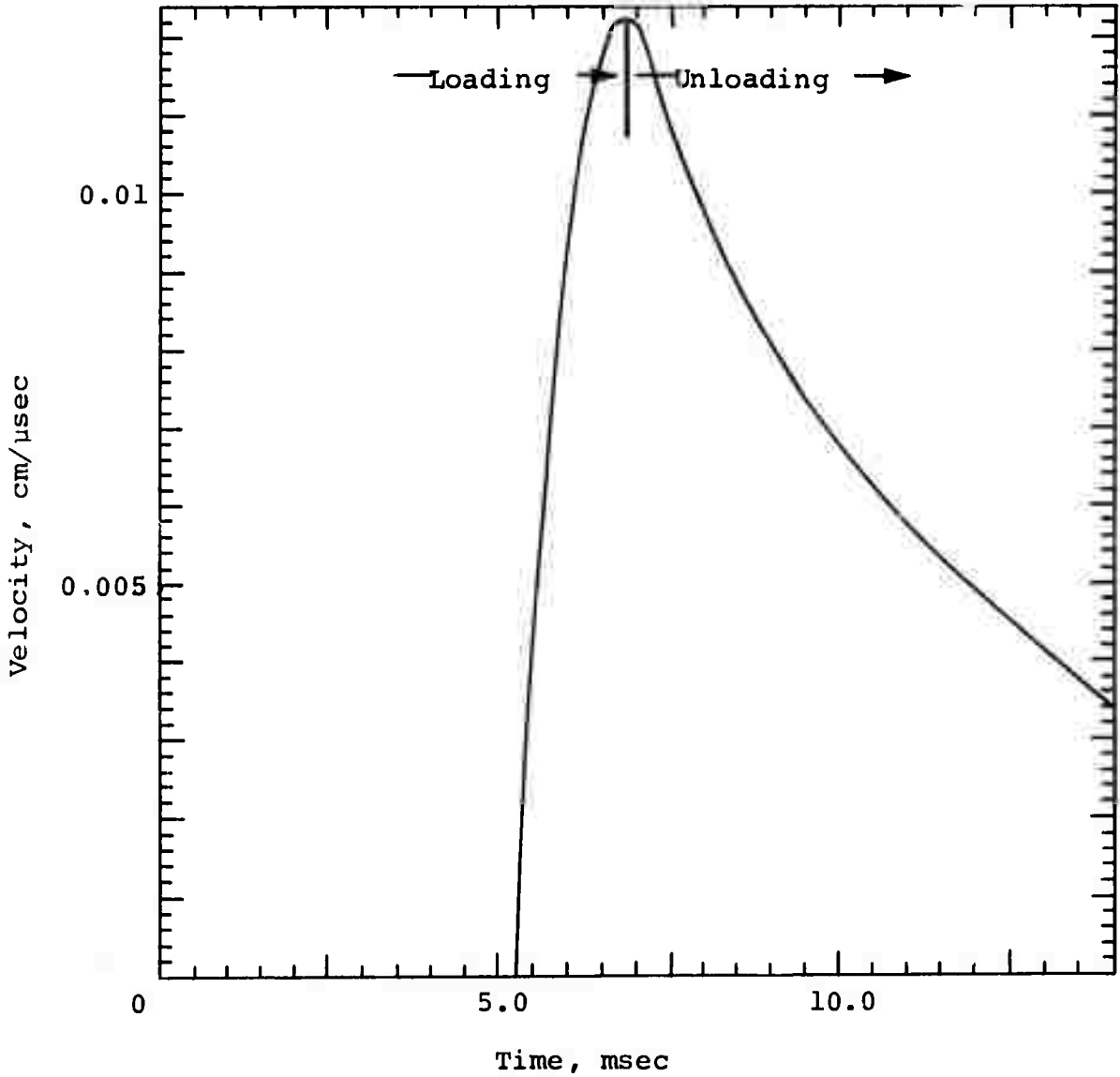
The conservation of mass Equation (1-1) is used to compute the relative volume as a function of time using the velocity data. The corresponding pressure history is taken directly from Equation (1-3) and is not a calculated quantity. The resulting pressure-volume data are then compared directly to the volumetric stress-strain data used to generate the simulated field data. The tangential stress is calculated from the conservation of momentum, Equation (1-2), and compared directly to the simulated experimental data of tangential stress.

The second task was to obtain data for the above analysis. Several rock mechanics computer codes exist at Physics International and two were selected to be used to generate simulated experimental data (SED) for the analytical investigations. Simulated data have a clear advantage over experimental data for this phase of the work; the constitutive properties to be obtained as the final product are known a priori. This information is part of the input to the rock mechanics codes. The efficiency of the analysis technique is thus measurable by comparing the derived equation of state to the precisely known one.

Three material models, each with a different complexity in the equation of state, were used to generate SED.

The first was a linearly elastic material, with a bulk modulus of $K = 0.5107$ Mbar and a Poisson's ratio of $1/4$. This is representative of the simplest possible non-trivial, material behavior. The mechanics code selected to use this equation of state in generating the required simulated data was one utilizing the method of characteristics (Reference 4). Representative of the data produced by this code and equation of state is the velocity history shown in Figure 1.1. All records produced by this code were smooth and free from round-off and difference-generated "noise" often exhibited by finite difference codes. Such records are ideal for investigating any shortcomings of the analysis techniques represented by Equations (1-1) through (1-3).

Details of the investigations using data generated by a linearly elastic material model were given in Reference 3 and will be recapitulated in Section 2 of this report.



Initial position = 130 meters
Digitization rate = 100 kHz

Figure 1.1 Ideal input velocity history.

A compacting material was used as the second model. The body is assumed to behave in a linearly elastic fashion during loading up to the pressure at which it begins to compact. Loading then proceeds linearly elastically, but with a lower bulk modulus than in the low-pressure portion of the loading. Unloading takes place with the maximum bulk modulus of the material. When the material reaches a predetermined, "fully compacted" condition, it then behaves as a linearly elastic material with the initial (high) bulk modulus.

A realistic model of good-quality, structural concrete was used for the third material. Here the equation of state was not only nonlinear, but also it had an energy contribution equivalent to a volume-dependent Grüneisen gamma. No compaction was considered.

As a characteristics computer code was unable to handle these relatively complicated equations of state, it was necessary to use a finite-difference rock-mechanics code to generate the required SED (Reference 5). Figure 1.2 is typical of the time histories produced using the compacting model, and Figure 1.3 shows a tangential stress-time history generated using the concrete equation of state. It must be noted that the compacting model had an essentially infinite tensile strength while the uniaxial tensile strength of the concrete was set at 40 bar. The computational noise (due to zoning) is clearly evident in Figure 1.2.

Two preprocessing options are available for making the SED either more realistic or more tractable. First, Gaussian white noise of any desired signal/noise ratio may be superimposed on any desired data record (Appendix B). This simulates the noise

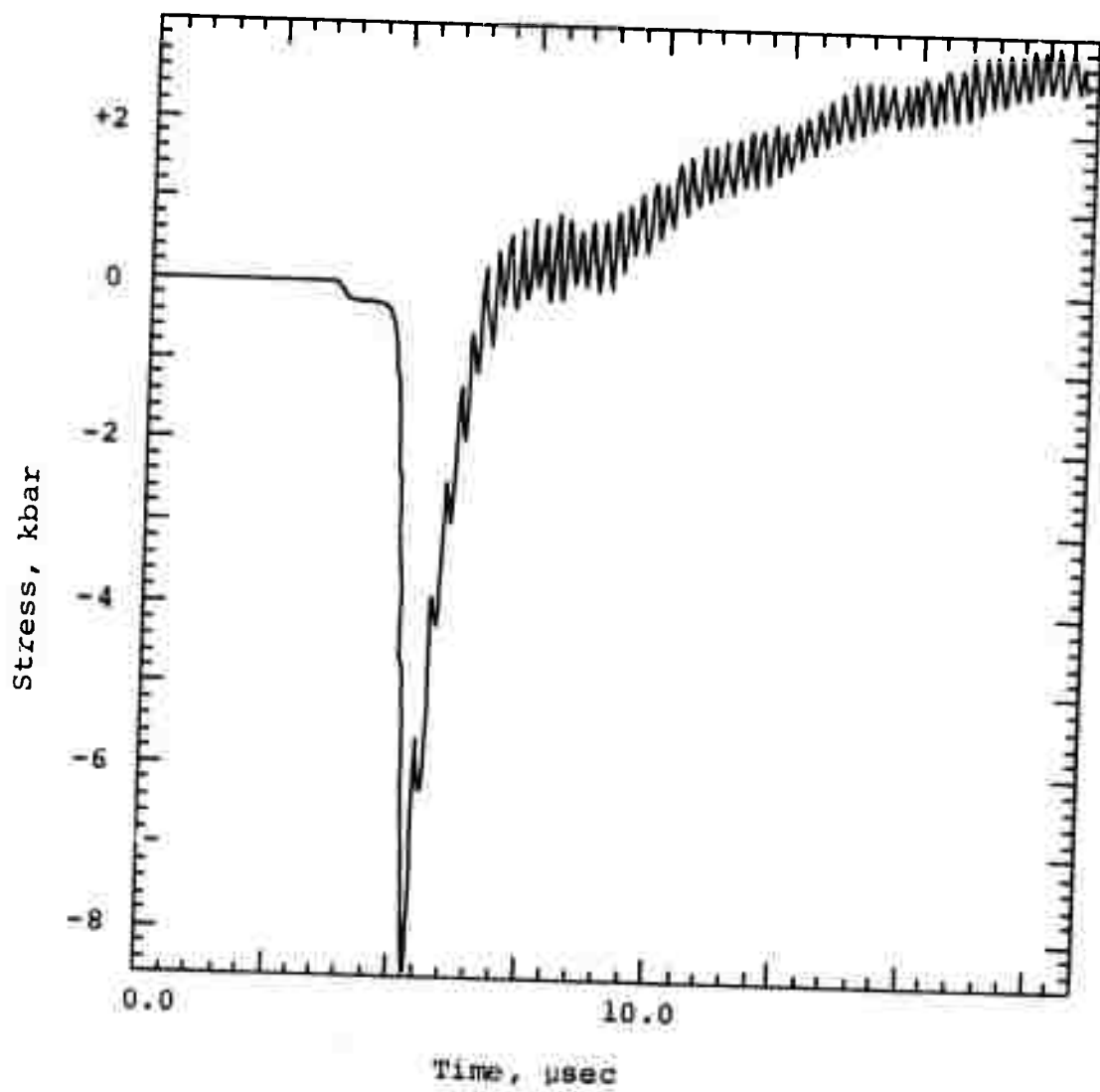


Figure 1.2 Typical radial stress-time history of compacting material model.

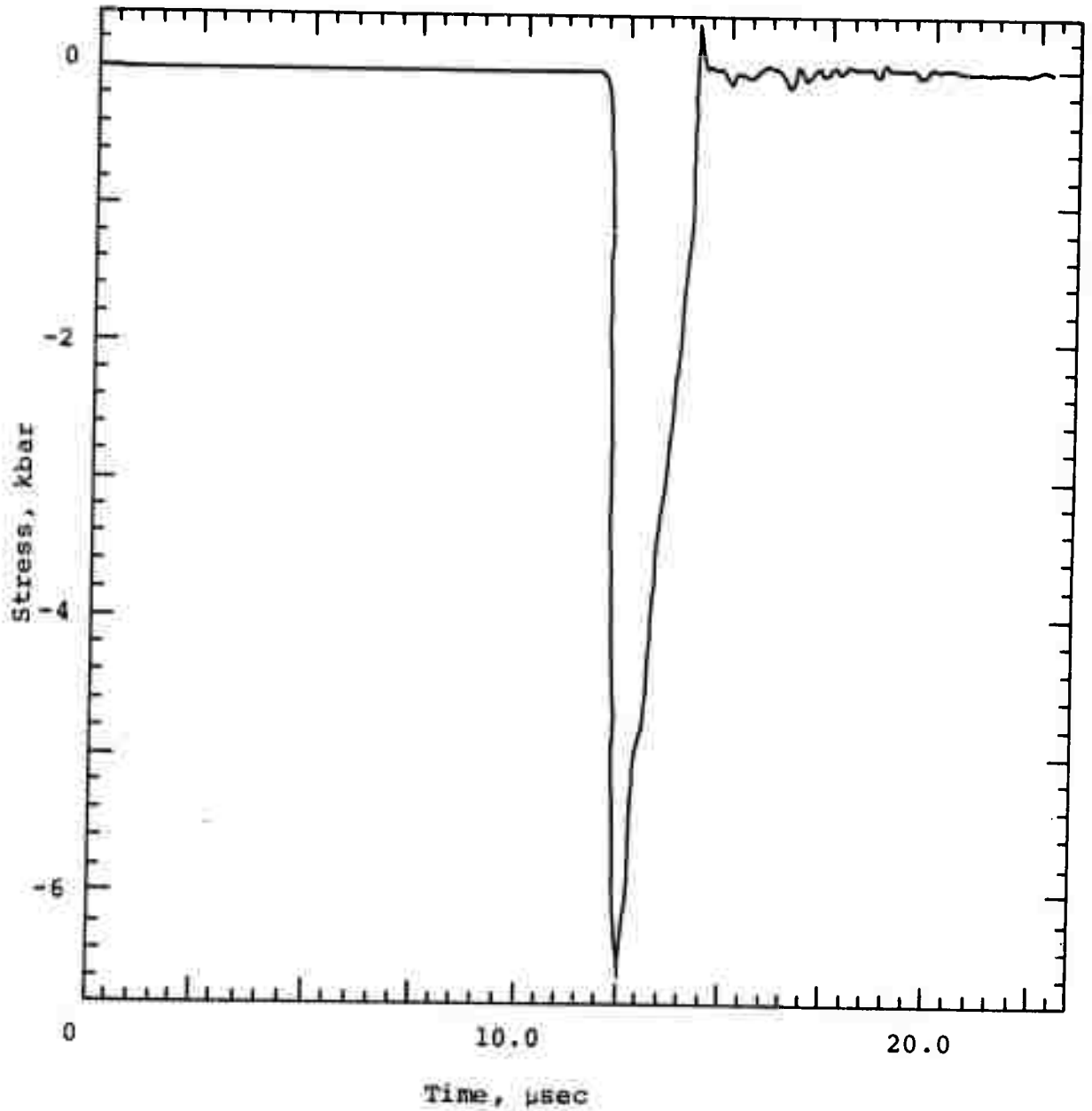


Figure 1.3 Typical tangential stress-time history structural concrete model.

that may be generated in an experimental data acquisition system. Second, high-frequency components of the data (raw or noisy) may be removed by processing the records through a digital low-pass filter (Appendix C). A typical record with noise added is shown in Figure 1.4, and the results of processing this noisy record through the low-pass filter are seen in Figure 1.5. Both of these preprocessing options will be available for the analysis of actual field data, although it is not expected to be desirable to add noise to these records.

Common to all data generation calculations was a pressure history obeying

$$p = p_{\max} \left(\frac{\alpha t}{2} \right)^2 t^2 e^{-\alpha t} \quad (1-5)$$

applied as a radial stress boundary condition of an inner radial position, R_0 , of the material being modeled. Time is measured in microseconds and the constants were set at $p_{\max} = 20$ kbar and $\alpha = 2.5 \mu\text{sec}^{-1}$. The resulting stress pulse was propagated outward through the material by the particular computer code used, and the stress and velocity histories calculated at various predetermined radial positions were recorded for use as the SED. Fourteen bit accuracy, commensurate with data attainable by normal analog-to-digital conversion, was maintained by reducing the SED on punched cards with five-significant-figure accuracy.

1.4 EXPERIMENTAL PROCEDURES

The active elements of all gages tested consisted of the piezoresistive material ytterbium. One of the goals of our investigation consisted of determining an appropriate material

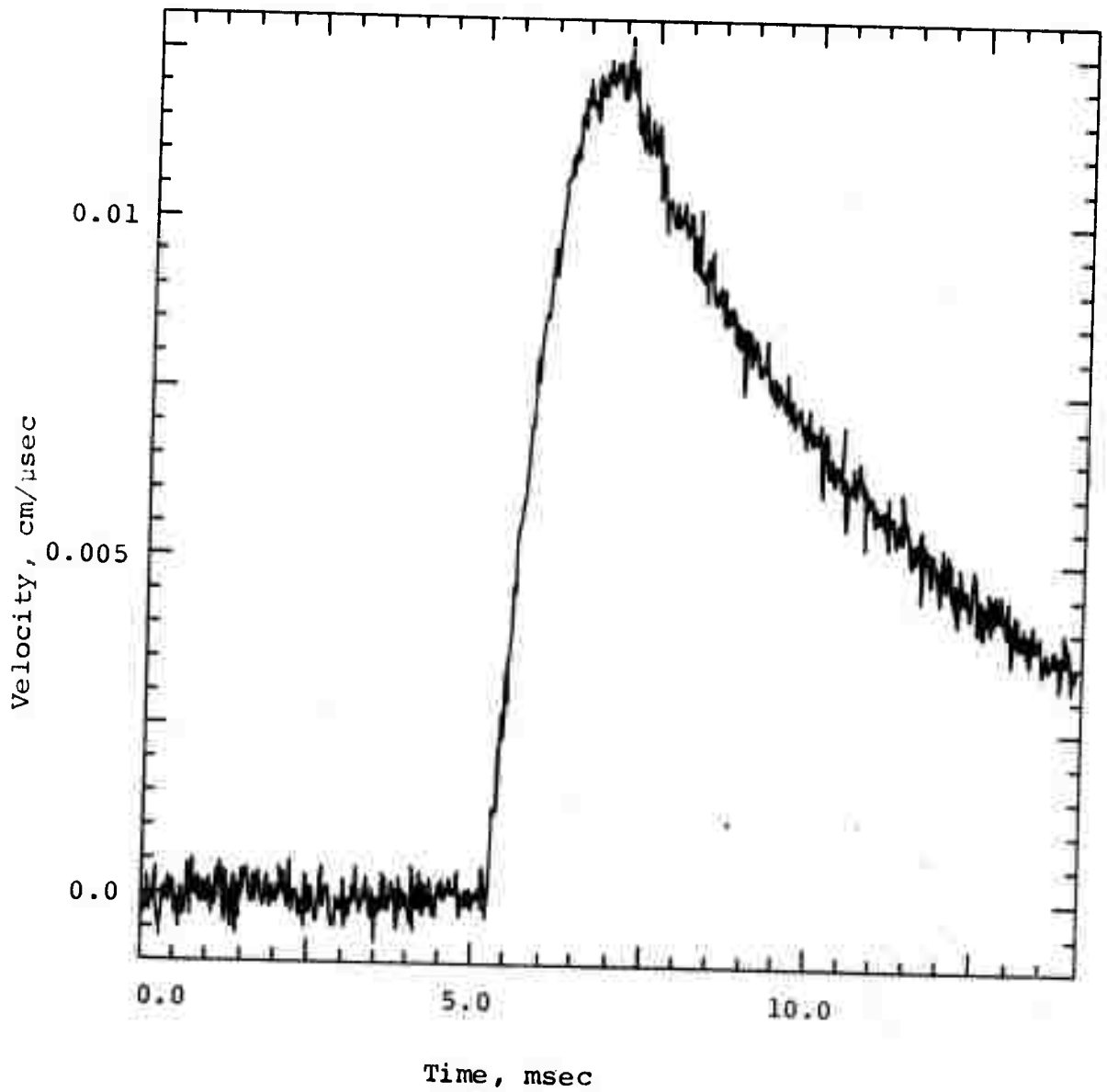


Figure 1.4 Two percent noise on ideal velocity record, linear elastic model.

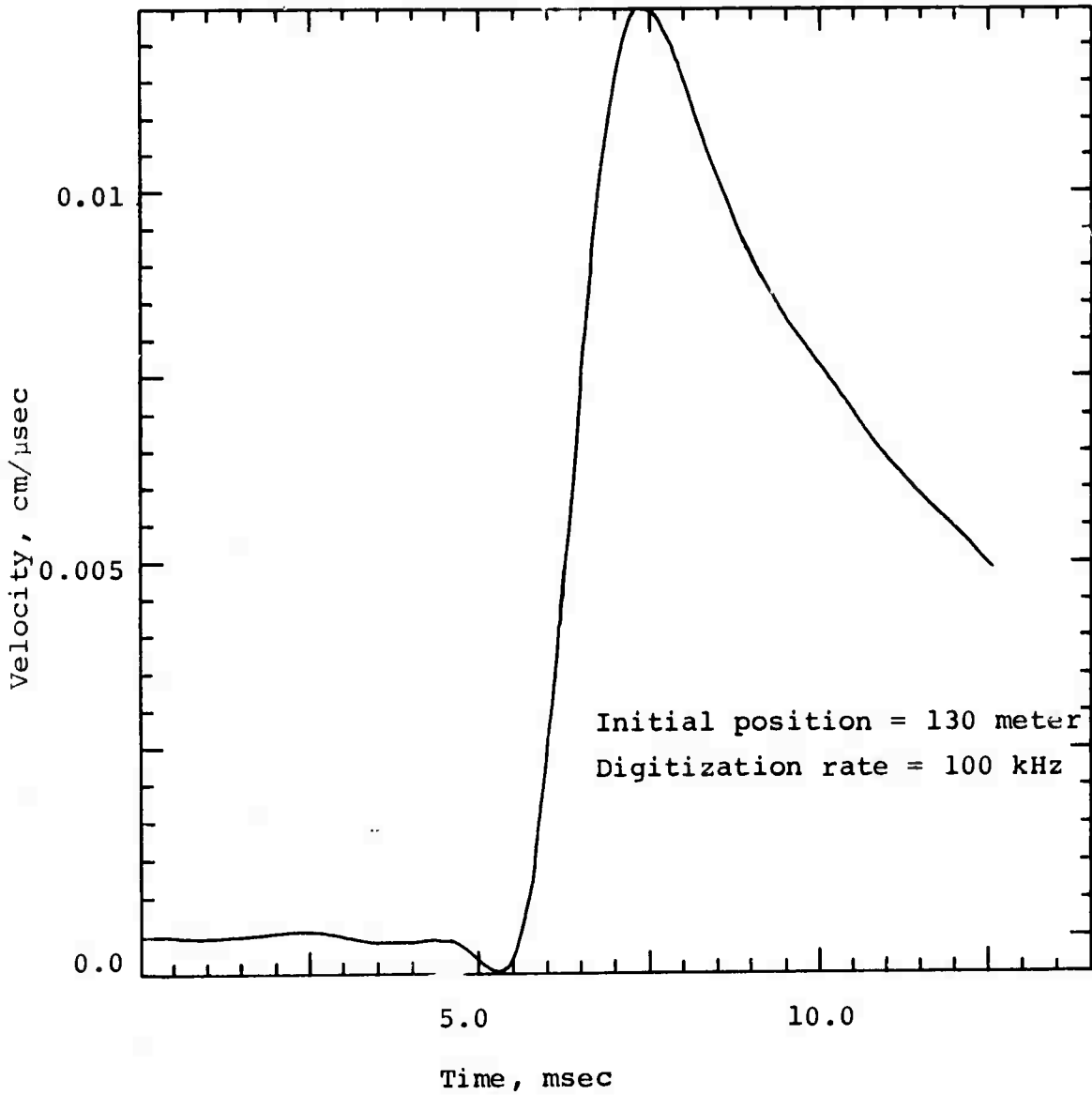


Figure 1.5 Noisy velocity record filtered at 1 kHz, linear elastic model.

on which to mount the gage elements. Such a material should match as closely as possible the rock in which the final gage is to be mounted. Thus, as two of our gage candidates, we chose mica and glass to be the backing materials. The third material, Lucalox, was chosen for its high impedance, allowing the gage to equilibrate to the in-situ stress very quickly. The thickness of the layers was kept to a minimum to prevent distortion of the wavefront by the gage. To minimize the risetime of the gage while maintaining a reasonable resistance for impedance matching to the field quality recording equipment, the geometry of the gages was long and thin, the width of the gage element being approximately one-fourth its total length. (This can be seen in Figure 2.20).*

The actual experiment was conducted in spherical geometry, the gages being cast in an essentially infinite sea of grout and placed at a fixed distance from a spherical high-explosive source. Gages placed in the radial mode had the normal to the wavefront normal to the gage surface whereas in the tangential mode, the normal to the wavefront was parallel to the gage surface. All gages were mounted so that their long axes were in the plane of the wavefront. The energy source was a sphere of LX-04 high explosive, surrounded by a spherical layer of water, the thickness of which was determined so that the peak shock stress at the water-grout interface would be about 10 kbar. The gages were then mounted at a fixed distance from this surface into the grout. Details on the gage construction and mounting are given in Section 2.2. The gage was made as the active element of a Wheatstone bridge so that a change in its resistance would result in a voltage which was then displayed on an oscilloscope screen. A

* Figure 2.20 appears in Section 2.2.

computational simulation of the experiment was performed using data taken statically on the same grout used in the experiment as part of the input. Results of the experiment and its simulation are compared in Section 2.

SECTION 2

RESULTS

2.1 CALCULATIONS

2.1.1 Linear Elastic Material. As noted in the preceding section, the SED resulting from the linear elastic model and method-of-characteristics code exhibited only the behavior of the material and had no computationally introduced aberrations. It is thus reasonable to expect that any difficulties found in using these data to compute time histories of volume and tangential stress via the use of Equations (1-1) and 1-2) would be magnified when the techniques are applied to actual field data.

The quality of the volume determination is seen by plotting the computed pressure-volume curve simultaneously with that used as input to the rock mechanics code. For this, the pressure is obtained from Equation (1-3) and the "measured" (SED) values of both σ_r and σ_θ .

2.1.1.1 Tangential Stress Determination. The quality of the calculating of σ_θ is measured by a direct numerical comparison of the computed and SED values. Define:

$$S = \frac{\sigma_\theta - \tilde{\sigma}_\theta}{\tilde{\sigma}_\theta} \quad (2-1)$$

where σ_θ is the tangential stress computed using Equation (1-2) and $\tilde{\sigma}_\theta$ is the SED value.

Preceding page blank

In Figure 2.1a we plot this function. It must be remembered that, although the SED are derived from an ideal source, they are presented to the analysis code as field quality; fourteen bit accuracy, comparable to analog-to-digital converters, is used with linear interpolation between the data points. The agreement is obviously poor enough to make using field-derived radial stress and velocity data in calculating the tangential stress unattractive.

Further manipulation of the raw data, redigitization at a higher sample rate, and low-pass filtering at a low-cut-off frequency to allow greater accuracy in computing the required derivatives result in the comparison plot of Figure 2.1b. Clearly, there is an improvement in the calculation of σ_{θ} . However, such manipulation is not always successful, as shall be seen later.

The conclusion to be made here is that tangential stress must be measured. It is not reasonable to expect that it can be calculated from field data of radial stress and velocities.

2.1.1.2 Optimum Gage Placement. Optimum spacing of the gage locations may also be made using the idealized SED of the linear elastic model. In Section 1 it was shown that to obtain the particle phase velocity, C_u , for use in Equation (1-1) it is necessary to obtain the velocity histories of two mass points at different values of the Lagrangian position, h . If the two are too closely spaced, C_u will be in error due to computational round-off in obtaining a small difference of two large numbers. If the gage locations are too widely separated, the nonlinear character of C_u precludes the calculation of a reasonable mean value for use in Equation (1-1). (Data from three gage locations could be used for a more accurate determination of C_u at one of them.)

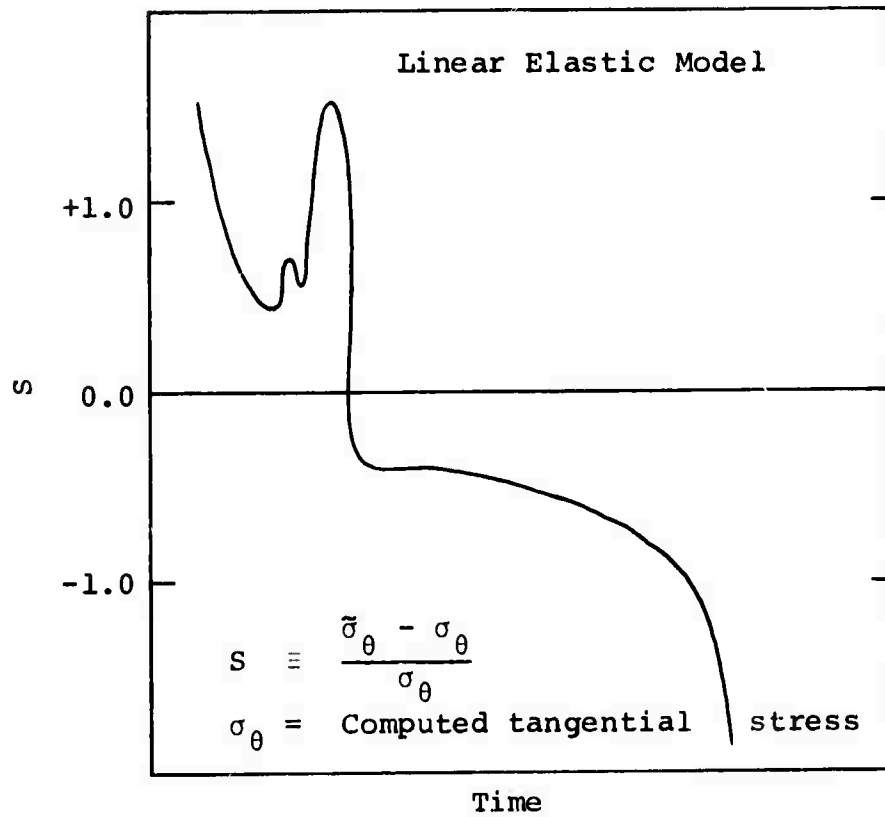


Figure 2.1a Comparison of true and computed tangential stress using raw data from linear elastic model.

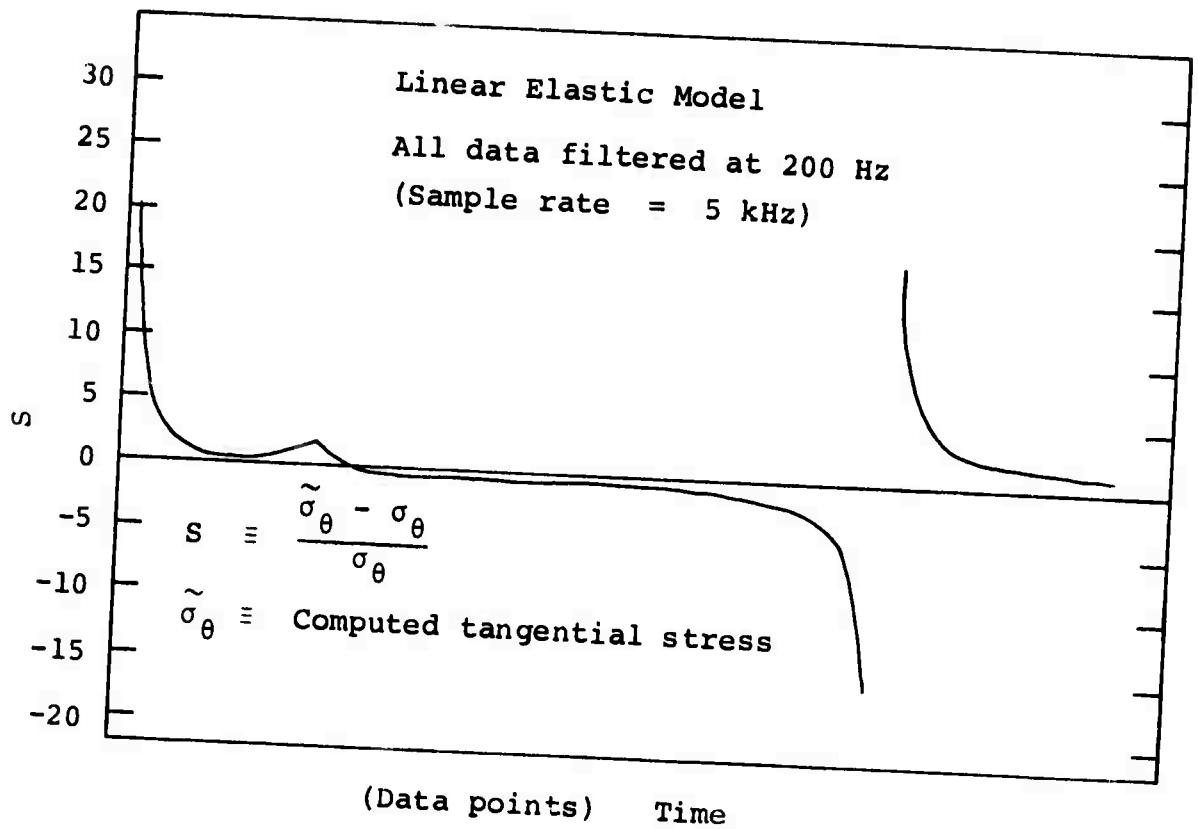


Figure 2.1b Comparison of true and computed tangential stress using high digitation rate and low-frequency cut-off filter.

Figures 2.2a, 2.2b, and 2.2c show the computed pressure-volume curves for relative gage separations of $\Delta h/h = 0.02, 0.08, \text{ and } 0.17$ respectively. It is seen that the quality of the calculations is not sensitive to the gage separation when $\Delta h/h = 0.08$ is near optimum. The results displayed in Figure 2.2b may be taken as indicative of the best agreement one should expect using field quality data.

2.1.1.3 Errors Due to Gage Misplacement. Errors in gage placement may also be determined. Figure 2.3a is the pressure-volume curve resulting from a 250-cm offset of both gage locations with respect to the working point. (Total distance of the gage pair to the working point is 12 meters.) It is seen that there is little difference between this and Figure 2.1c, the ideal case. However, when only one of the gages is offset by the same amount, the error introduced in the computed equation of state is substantial, as seen in Figure 2.3b.

It is necessary to know accurately the gage separation; (this quantity directly enters the calculation of C_u while the average radial position of the two with respect to the working point is a relatively insensitive parameter.

2.1.1.4 Errors Due to Asphericity of Wave. One further determination that may be made using linear-elastic ideal data is the effect of asymmetry of the strain wave on the analysis technique. Equation (1-1) is independent of the coordinate type and may be used directly to show the results of analyzing a plane or cylindrical wave as if it were spherical.

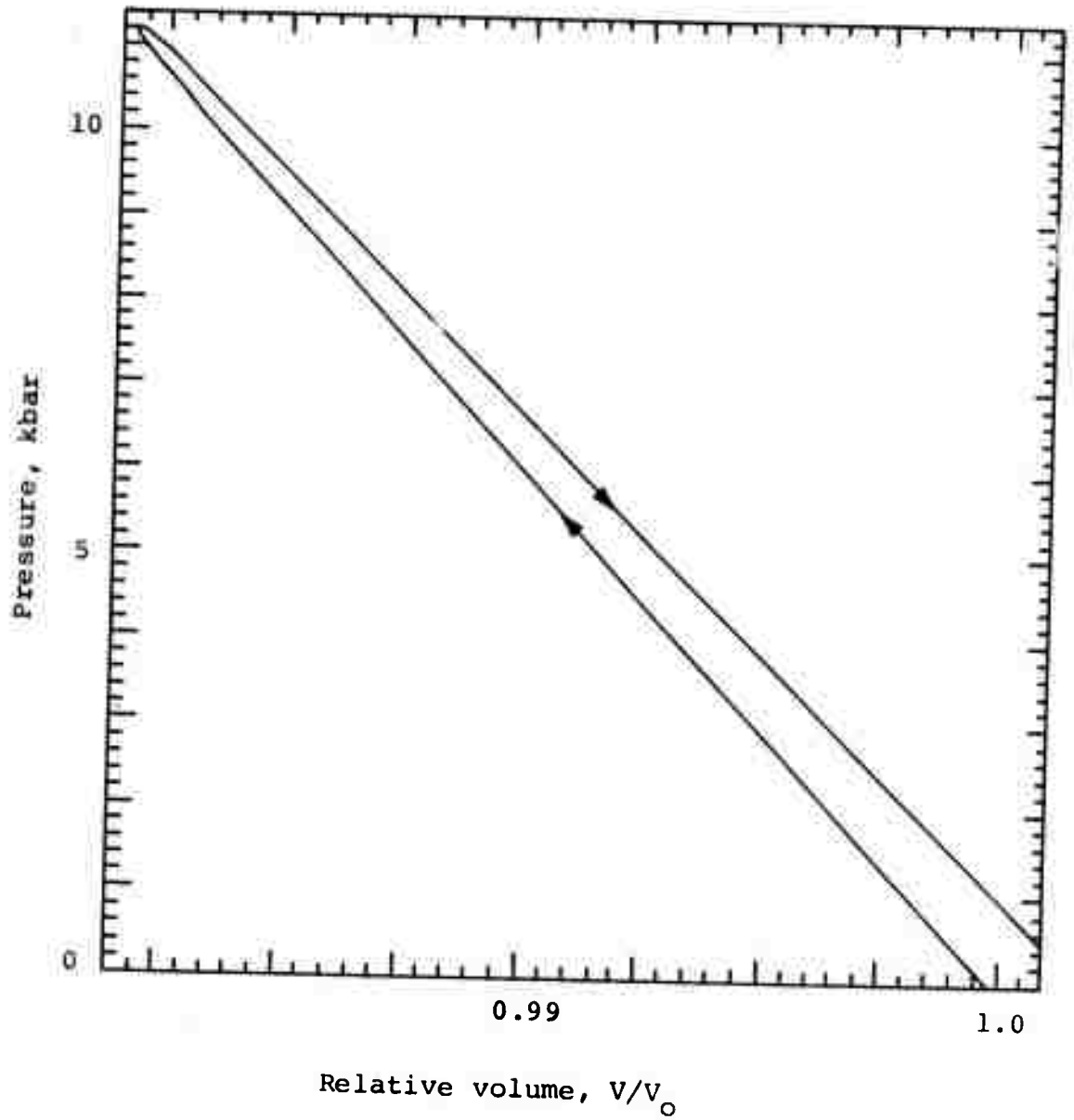


Figure 2.2a Volume calculation for gage relative separation of $\Delta h/h = 0.0206$.

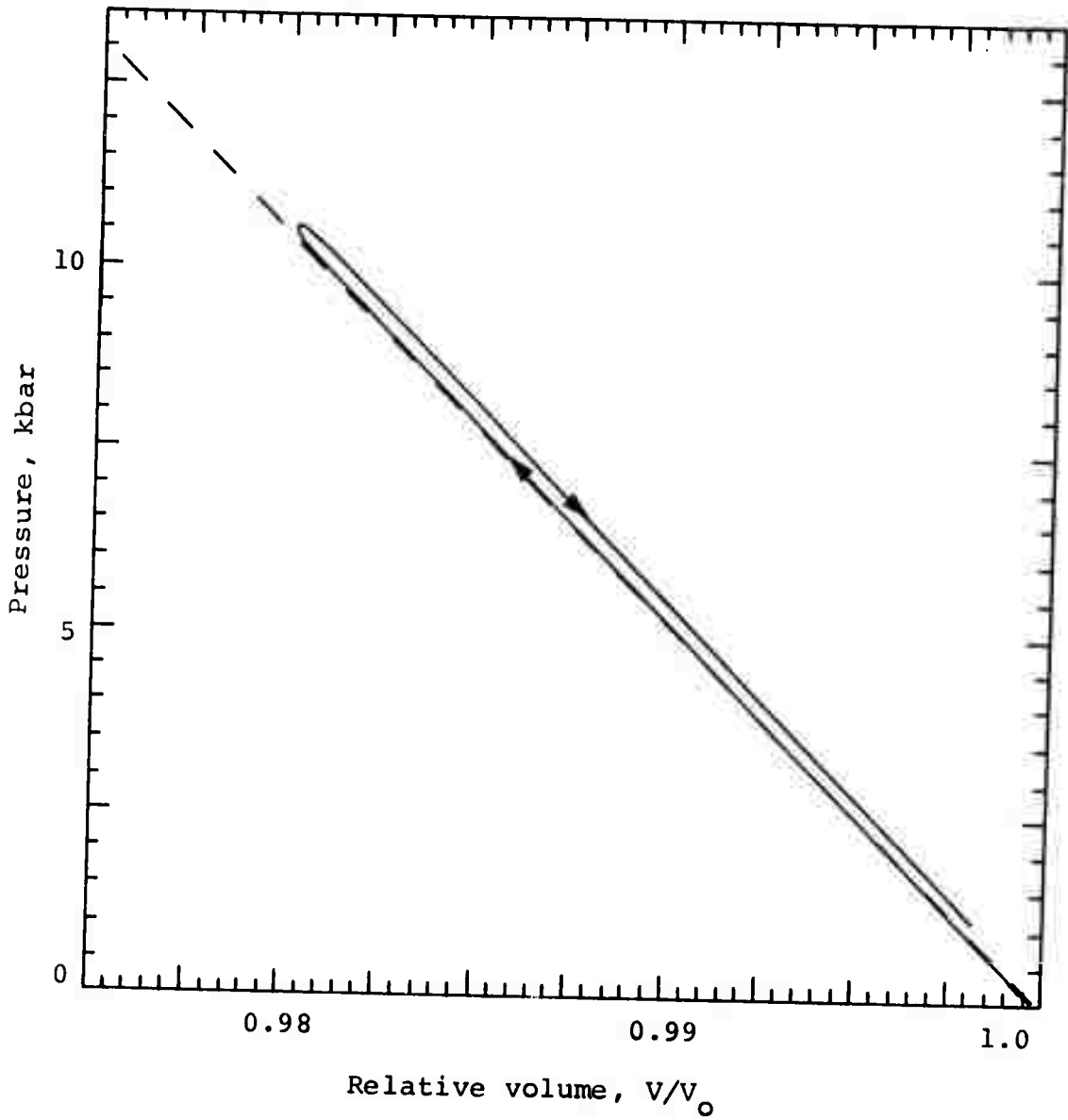


Figure 2.2b Volume calculation for gage relative separation, $\Delta h/h = 0.080$.

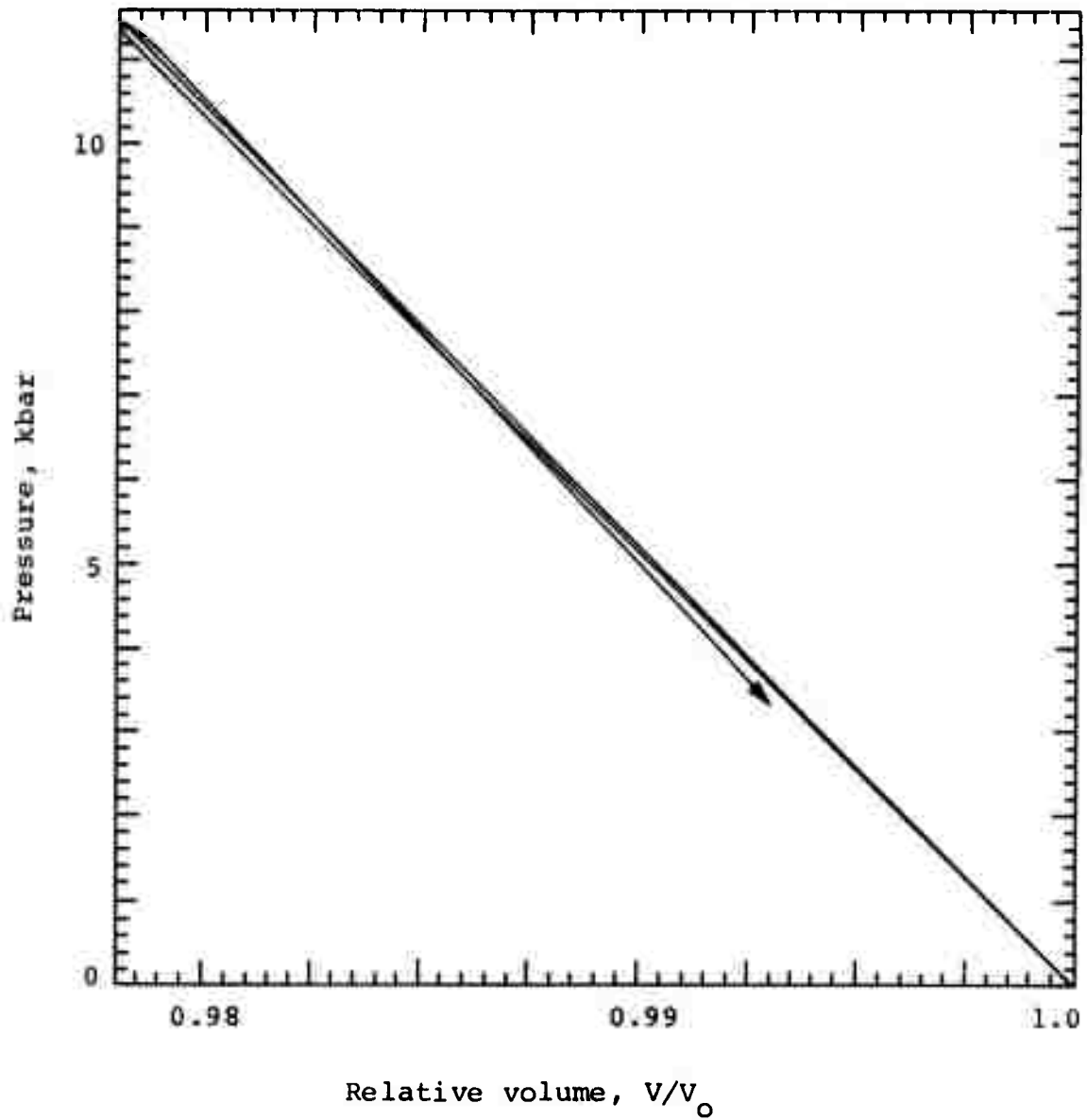


Figure 2.2c Volume calculation for gage relative separation, $\Delta h/h = 0.182$.

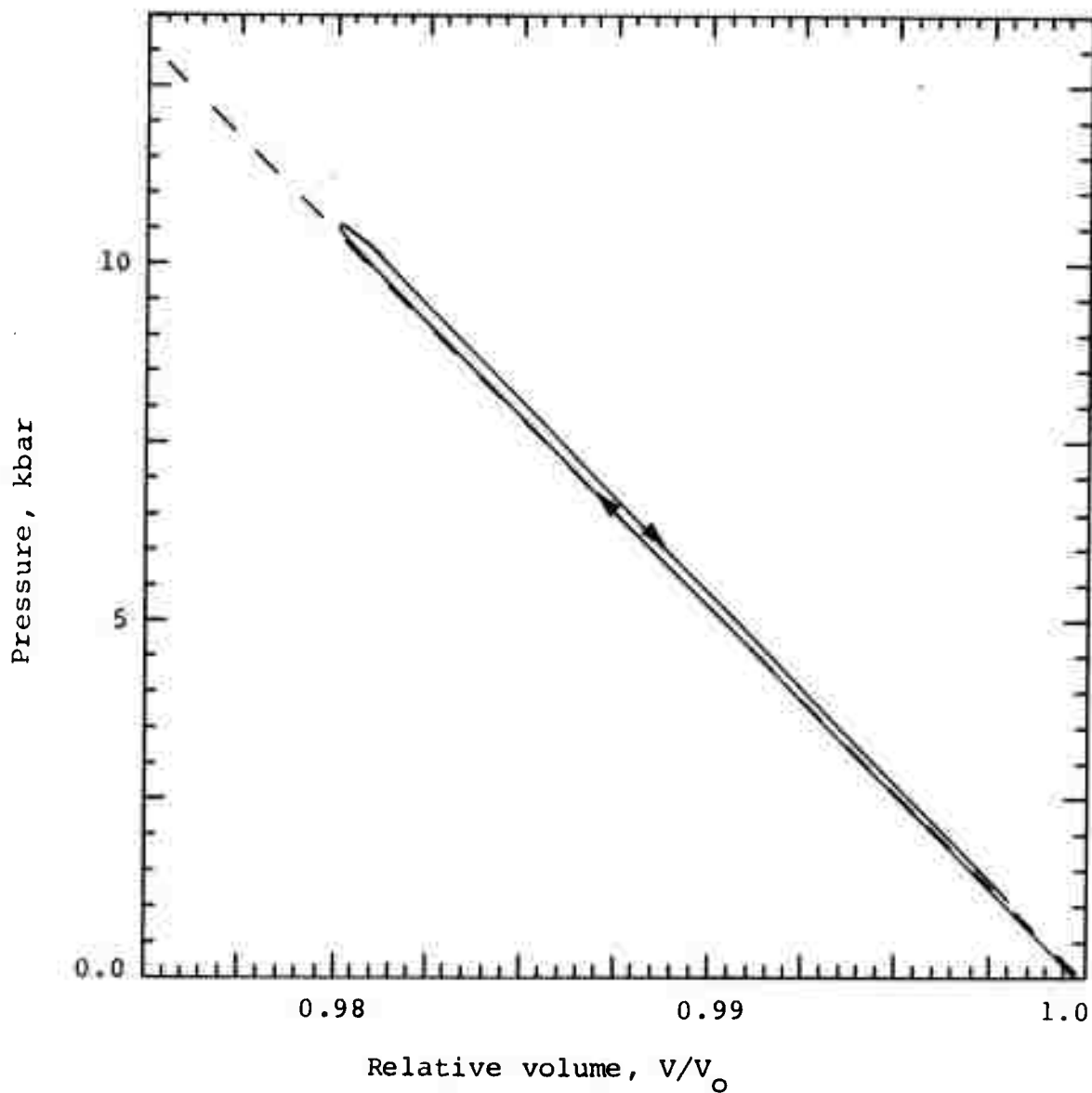


Figure 2.3a Effect of displacing coordinate origin by one-fourth of the gage separation.

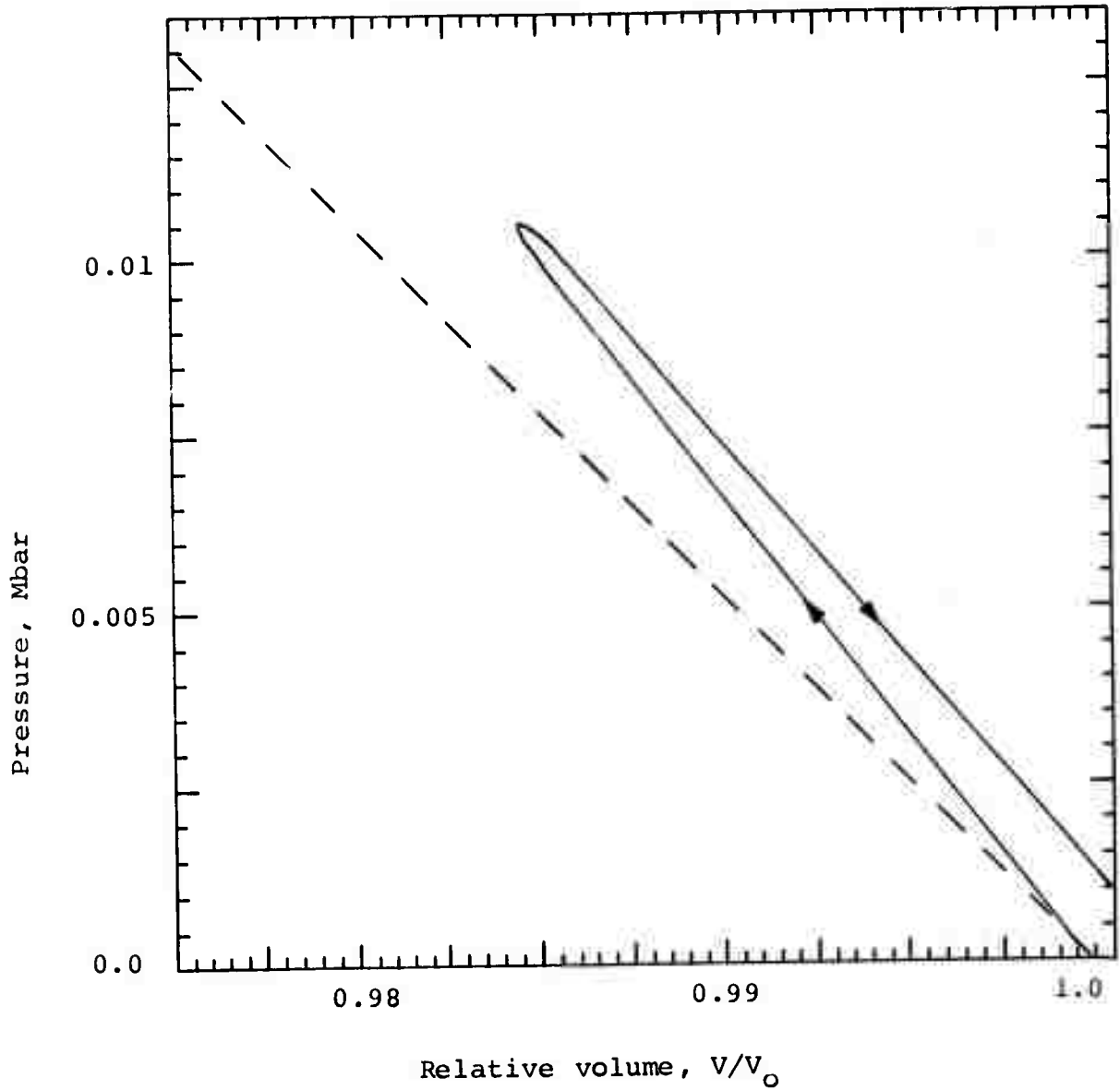


Figure 2.3b Effect of an error in gage package separation of 25 percent.

Consider a plane-wave disturbance. In this case $m = 0$ and C_u is constant. Integration of Equation (1-1) then leads to

$$Q = \left(\frac{v}{v_o} \right)_{\text{plane}} = \left(1 - u/C_u \right) \quad (2-2)$$

for the true relative volume. However, if the analysis were to proceed as if the wave were spherical, we would get

$$\left(v/v_o \right)_{\text{sphere}} = \left(\frac{r}{r_o} \right)^2 \left(\frac{v}{v_o} \right)_{\text{plane}} \quad (2-3)$$

A plot of this using the SED of Figure 2.2c is shown in Figure 2.4. (Similar behavior is displayed in Figure 2.38.) However, this is anomalous for materials in which shock heating plays no significant role.

The anomaly can be mitigated by altering the basic hypothesis of the analysis, either by assuming a different gage separation, a different wave symmetry ($m < 2$), or both.

2.1.1.5 Noise and Frequency-Response Requirements. In Figure 2.5a are shown the results of directly integrating Equation (1-1) using SED having a noise/peak signal ratio of 2 percent on the stress data. The known equation of state (dashed line) can be deduced from this with no further data processing. However, when the noisy SED are subjected to a digital low-pass filter and then analyzed, the results shown in Figure 2.5b are produced.

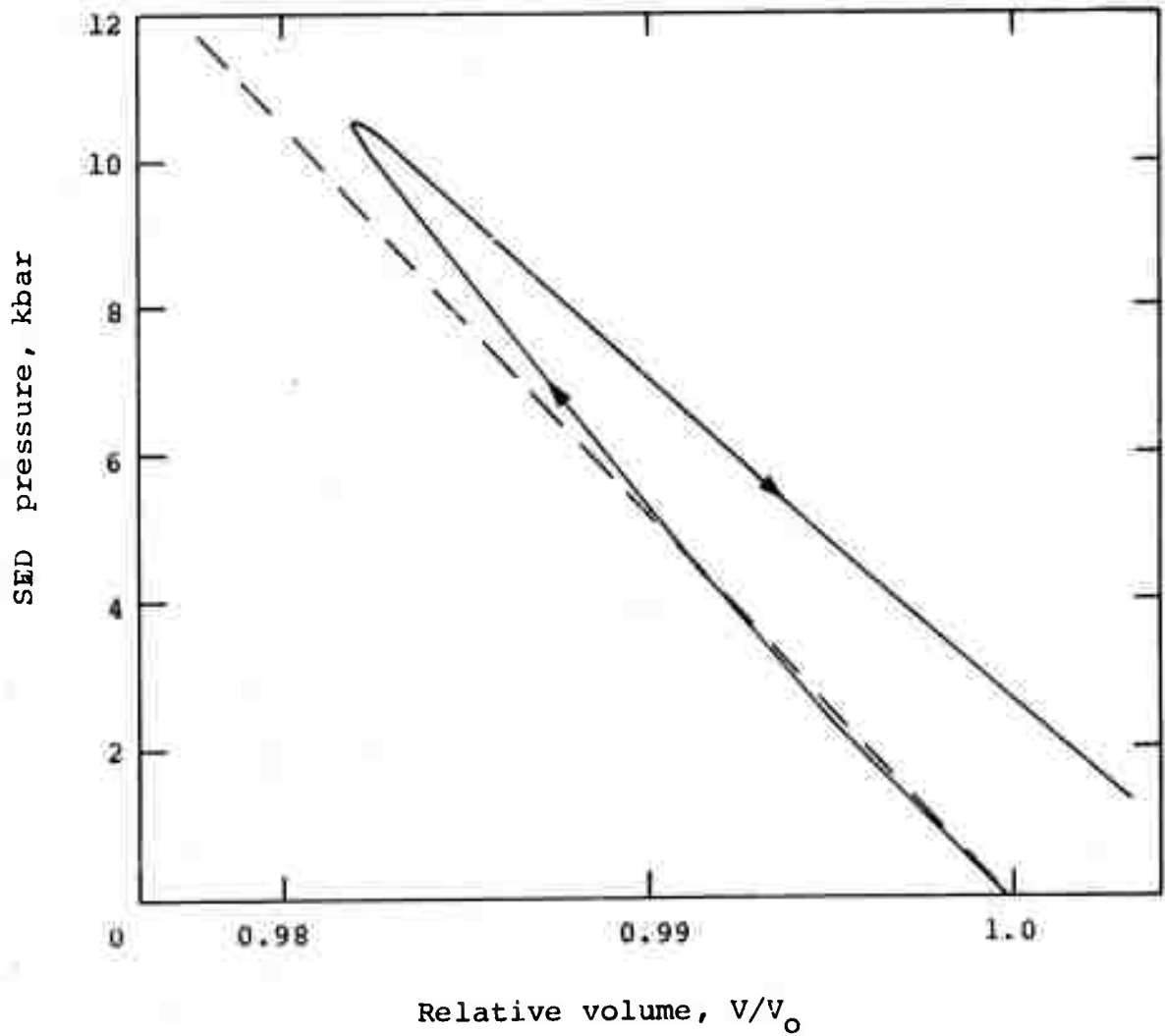


Figure 2.4 Pressure-volume curve derived from a plane-wave disturbance analyzed as if it were spherical.

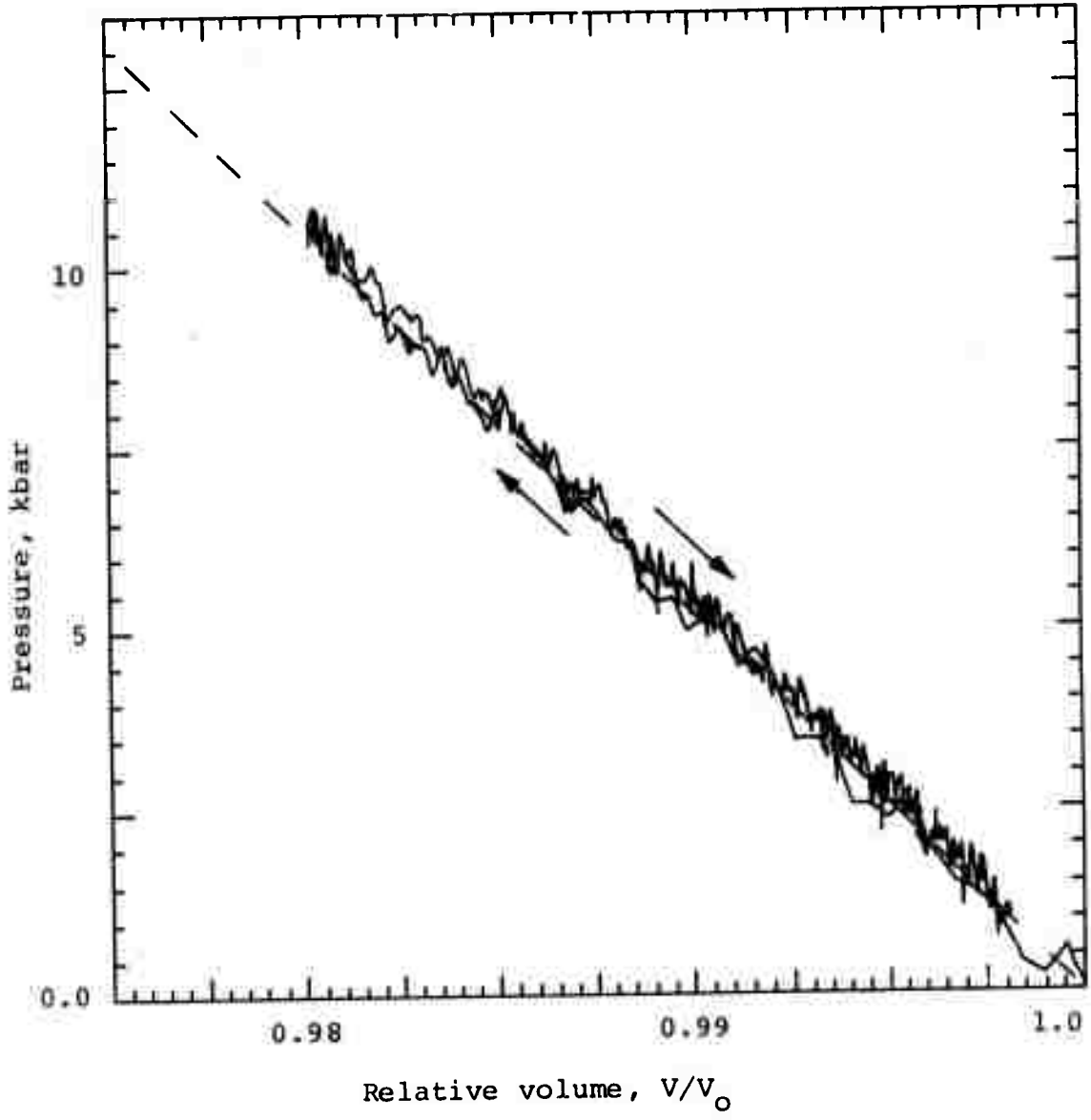


Figure 2.5a Pressure-volume data derived from information having a noise level of 2 percent on all stress data.

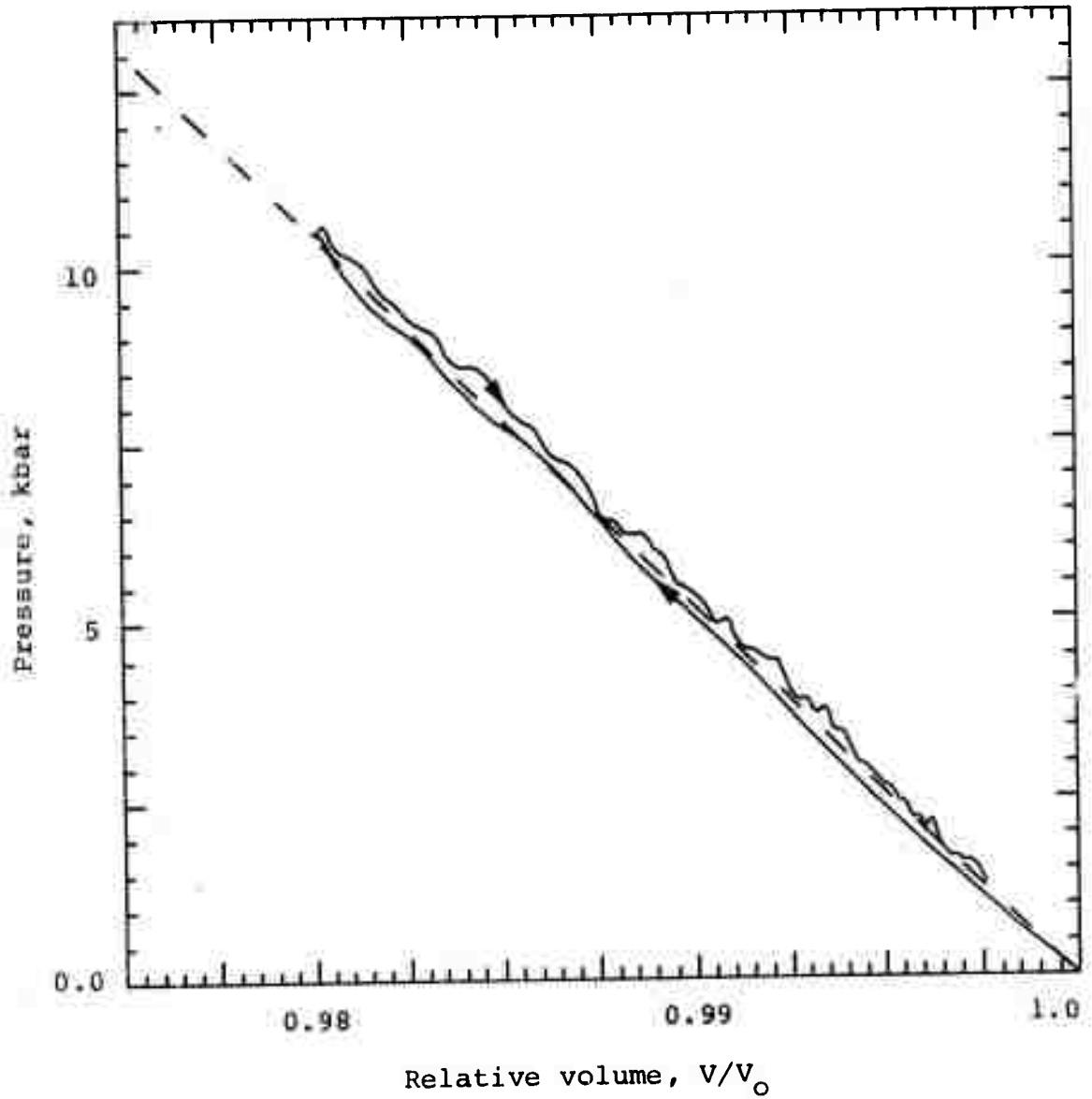


Figure 2.5b Elimination of a 2 percent stress noise level by low-pass filtering all data at 4 kHz, digitization rate 50 kHz.

In Figure 2.6 is indicated the quality of the pressure-volume calculation when each record of the SED has a different superimposed noise level and all records are subsequently processed through the same low-pass filter and analyzed.

It must be noted that all gage records comprising the SED were filtered at the same cut-off frequency for the above analysis. The effect of filtering only some of the records is shown in Figure 2.7 where only the velocity records were filtered (the SED had no noise superimposed for this test). The effect is that of delaying the velocity records with respect to the stress data. In principal the filter code computes its intrinsic delay and numerically corrects for its. However, due to an unresolved coding error, the phase shift is only about 80 to 90 percent removed. The apparent delay is due partly to altering the risetime of the filtered records and partly to the remaining time shift of the filter.

It is of interest to know the lower limits of the cut-off frequency/sample rate ratio. From Figures 2.8a and 2.8b it can be concluded that, in the case of a linearly elastic solid, the equation of state information is well represented in all frequency components of the transmitted signal. The loss of the higher frequencies, through filtering, does not mitigate the information content of the signal.

This is the behavior expected of an infinite, linearly-elastic solid; a sinusoidal signal of any frequency should be transmitted as well as any other. In the case of nonlinear-elastic or inelastic materials, these conclusions may be invalid. They clearly are invalid for solids whose material properties depend on the strain or stress rate.

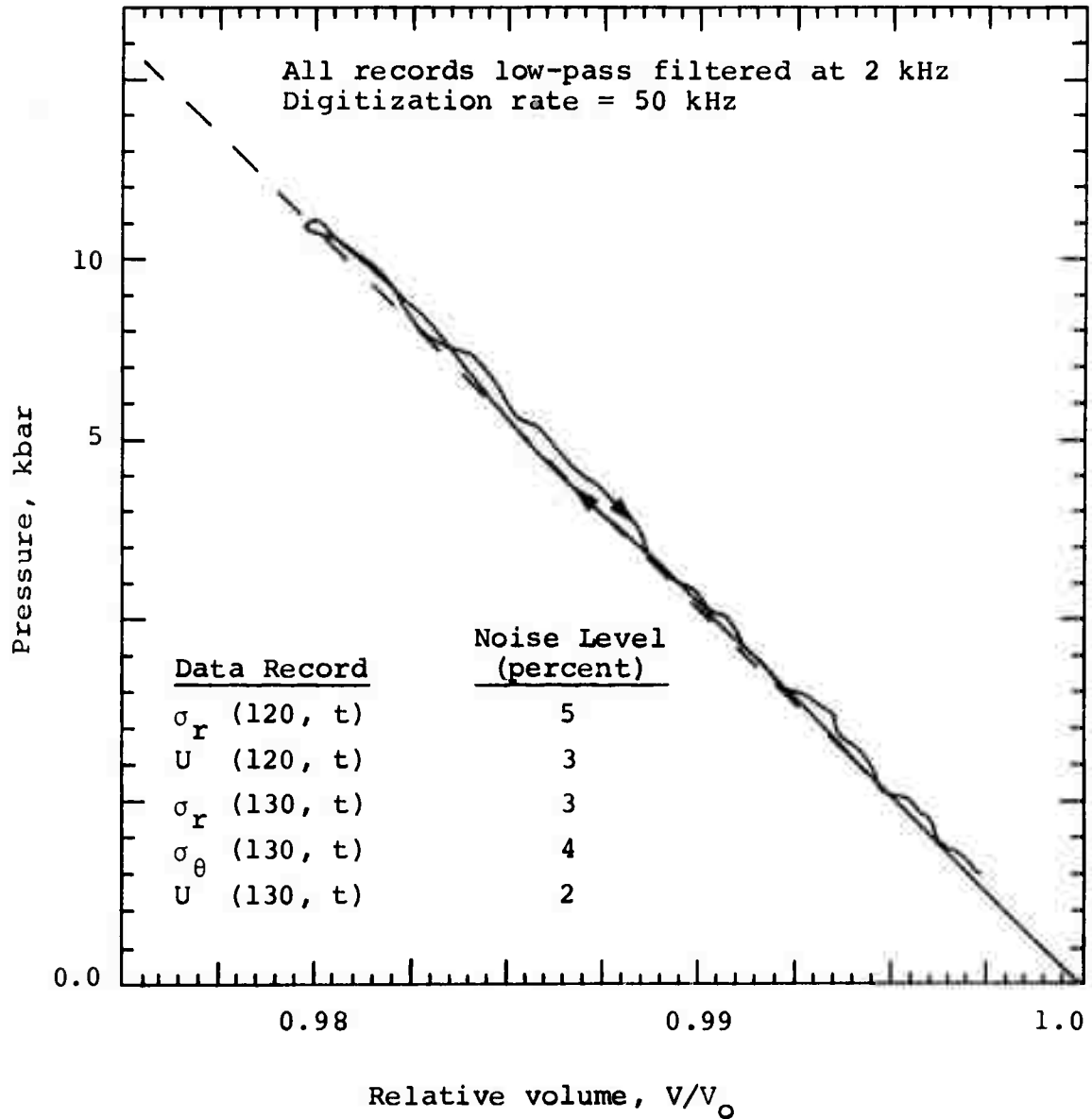


Figure 2.6 The effects of low-pass-filtering noisy records.

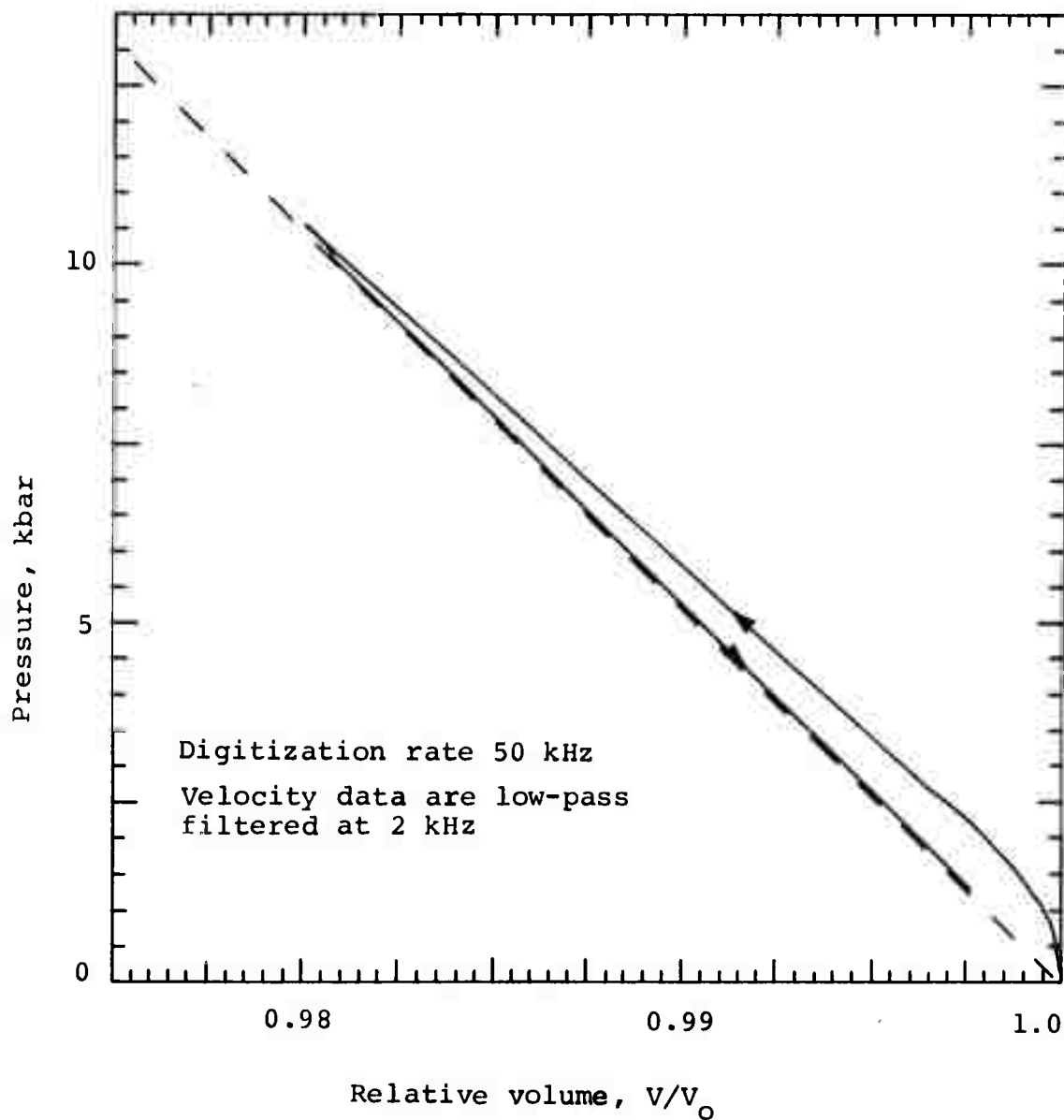


Figure 2.7 Effects produced either by a phase delay or frequency limit of velocity data.

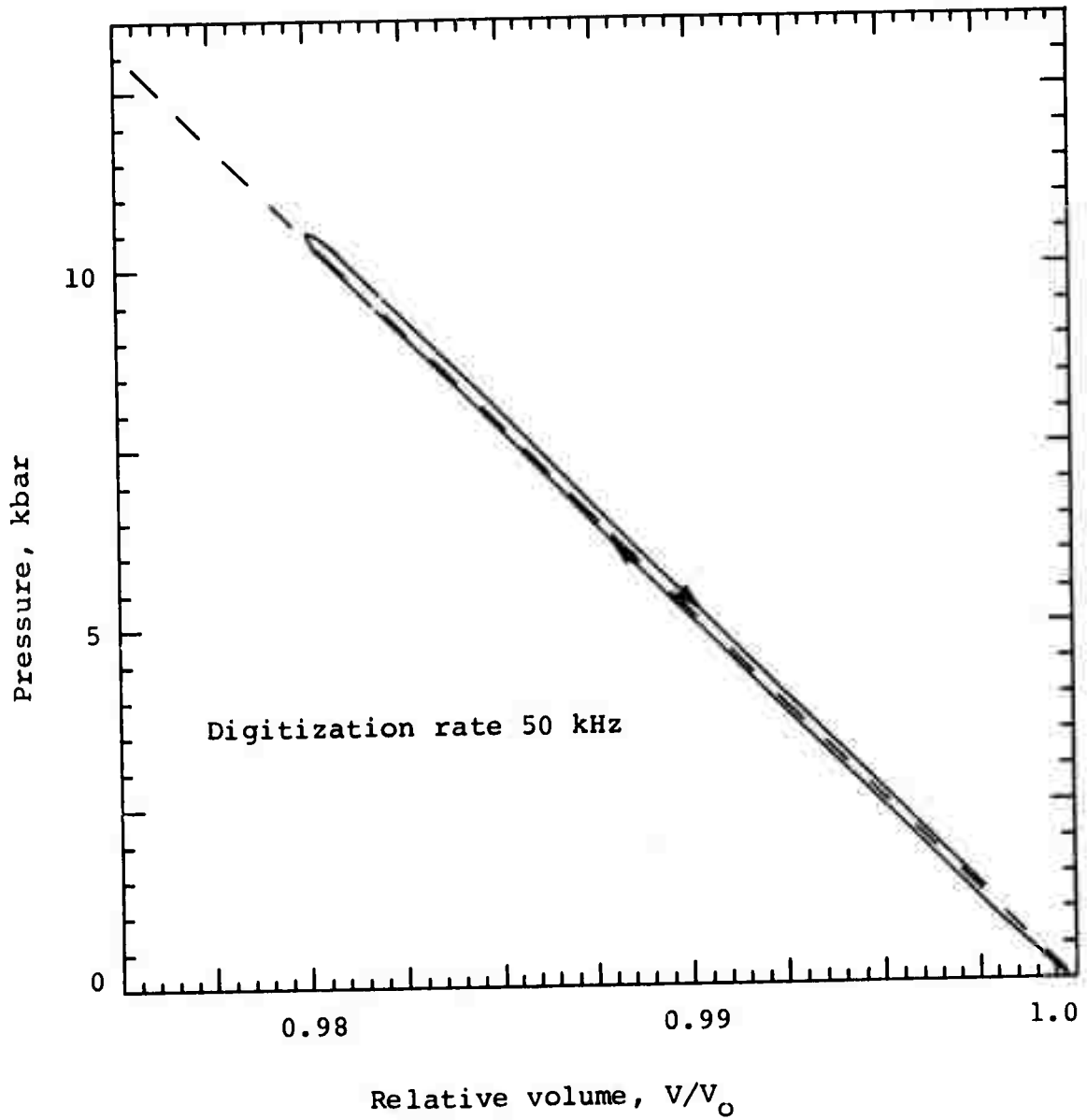


Figure 2.8a Effects of low-pass filtering all data at 4 kHz.

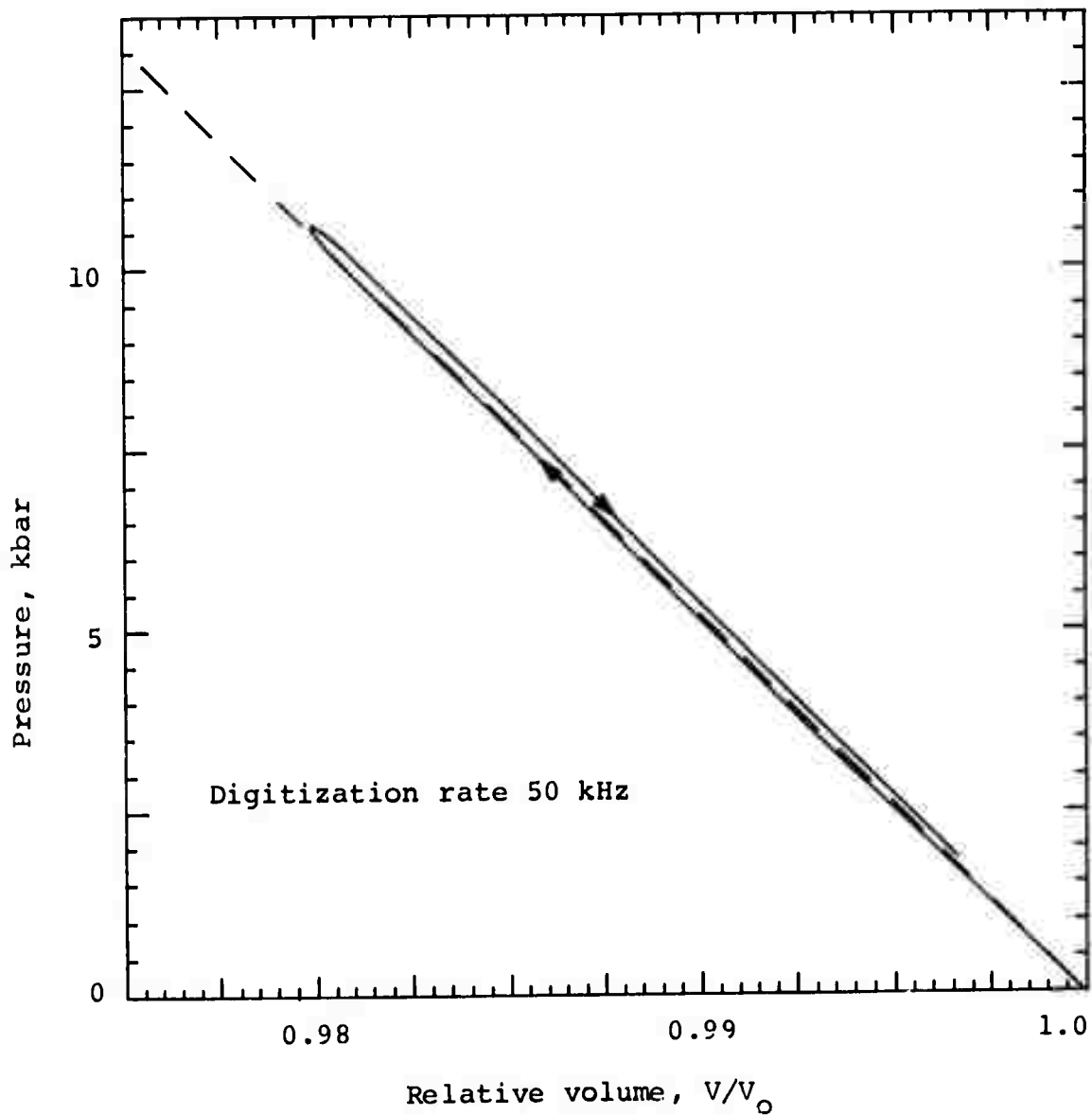


Figure 2.8b Effects of low-pass filtering all data at 1 kHz.

It is necessary to perform the same investigations on model materials having nonlinear elastic and inelastic behavior. A strain-rate-dependent model was not investigated, as such equations of state tend to have built-in computational instabilities and the effort to eliminate them was felt to be beyond the scope of this contract.

2.1.2 Nonlinear and Inelastic Materials. The two models used, as mentioned in Section 1, include both nonlinear elastic and inelastic behavior.

The compacting model loads along a given bulk modulus until it reaches a pressure-volume state at which compacting begins. Loading then continues along a lower bulk modulus. If the loading proceeds far enough, the material reaches a predetermined state of "full compaction" and both loading and unloading proceed from that time forward along a single curve in pressure-volume space determined by the initial (high) bulk modulus and the point in pressure-volume space at which full compaction occurred. Unloading from any state prior to reaching full compaction proceeds from that state along a curve determined by the initial (high) bulk modulus. Linear elasticity is observed during those phases of loading and unloading of the fully compacted material and loading and unloading for states below the compaction curve. Initial loading along the compaction curve is clearly inelastic and the overall behavior is nonlinear. See Figure 2.9.

The second nonlinear elastic model is that of a good quality structural concrete. A polynomial equation of state was assumed, of the form:

$$\rho(V,E) = a\mu + b\mu^2 + c\mu^3 + \frac{\Gamma'}{V} \left(\frac{1}{V^2} + 1 \right) E \quad (2-4)$$

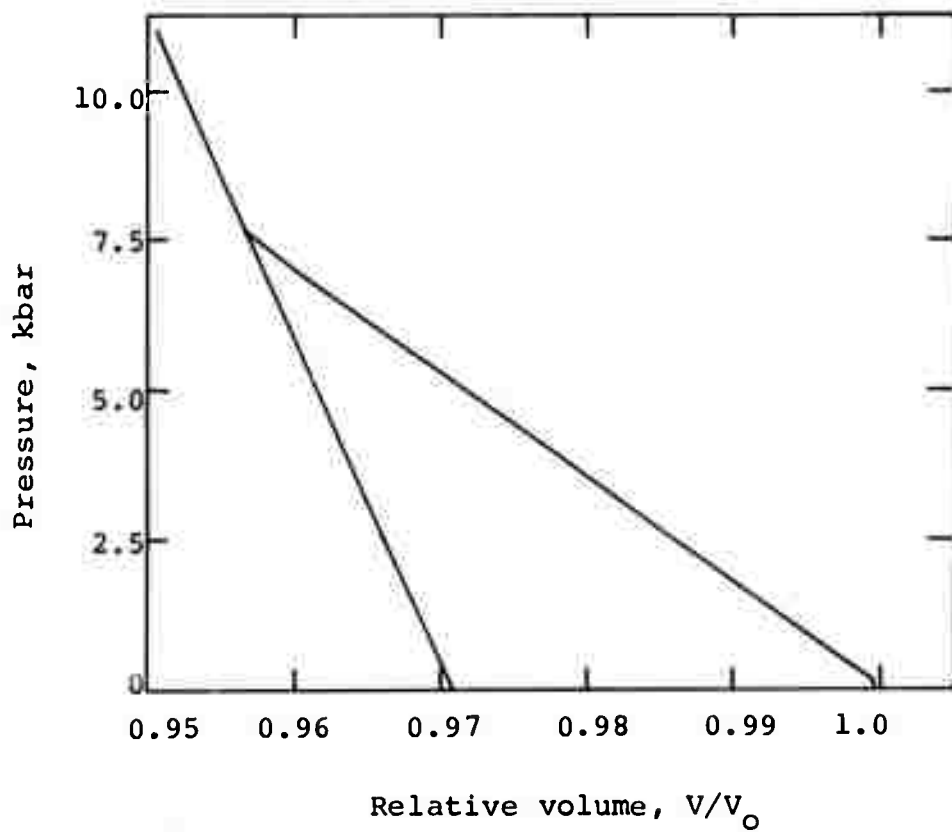


Figure 2.9 Compacting model volumetric equation of state.

where a is the low-pressure bulk modulus, $\mu = 1/V - 1$, and the term $\Gamma'(1/V^2 + 1)$ is identified as a volume-dependent Gruneisen Γ . Aside from the energy term, the material is reversible but nonlinear. Inelasticity is provided through the irreversible work represented by the energy term. Inelastic behavior is also exhibited through imposition of a yield surface bounded by a Mohr-Coulomb envelope having a von Mises limit of 15 kbar for compressive stress and a spall-fracture condition initiated by a uniaxial tensile strength of 40 bar. An initial bulk modulus of 256 kbar and constant shear modulus of 120 kbar were assumed.

It is felt that the questions of wave symmetry, and the gage types required were answered by the linear model. Work in this section concentrated on determining frequency-response limits and noise tolerances. Also, since the models are clearly nonlinear, it is conceivable that the rule-of-thumb for optimum gage separation of $h/h \approx 0.1$ may not be a valid one for these materials.

2.1.2.1 Optimum Gage Spacing. The (pressure, volume) point at which the compacting model becomes fully compacted is (7.7, 0.9566); that is, for any pressure greater than 7.7 kbar or relative volume less than 0.9566, the material must load and unload along the fully compacted curve. This pressure-volume curve is shown schematically in Figure 2.9. When the initial stress pulse peaks above this pressure, the material tends to develop a strong shock. We have chosen our gage locations so that the innermost of any pair is in this strong shock region while two others are in the region in which the material is never fully compacted. Figures 2.10a and 2.10b are the pressure-volume curves computed using the SED for this model derived with a finite-difference code. Figure 2.10a is the computed pressure-volume curve for a relative gage spacing of $\Delta h/h \approx 0.11$ while Figure 2.10b shows the effect of a relative gage spacing of $\Delta h/h \approx 0.2$.

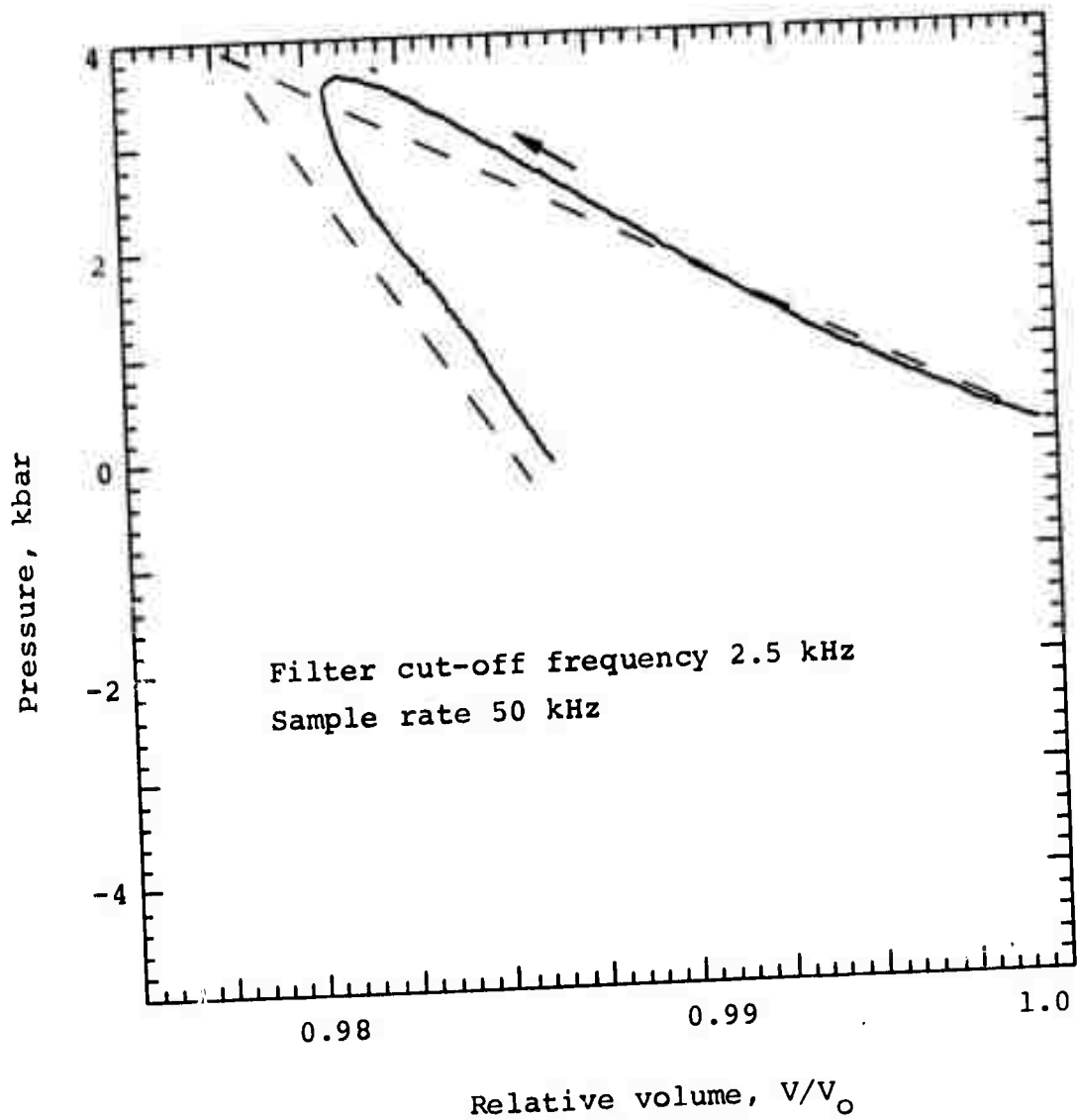


Figure 2.10a Volume calculation using compacting model SED,
 $\Delta h/h \approx 0.11$.

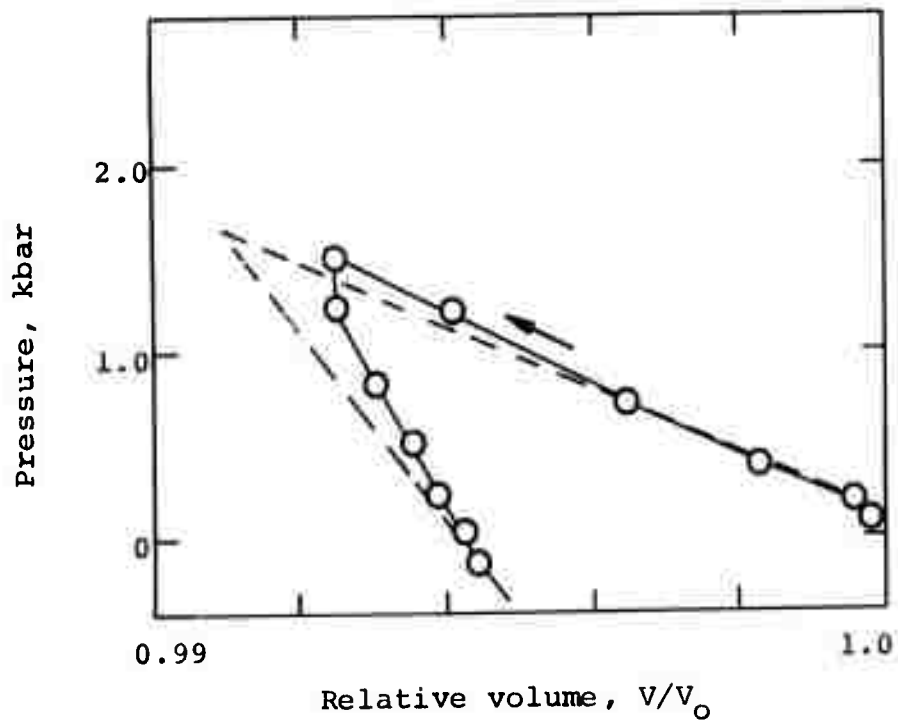


Figure 2.10b Volume calculation using compacting model SED,
 $\Delta h/h \approx 0.2$.

As will be seen (Figure 2.12a), the zoning noise mentioned earlier in connection with Figure 1.2 tends to mask the behavior of the analysis during the unloading portion of the stress pulse. For this reason, these two figures have been low-pass-filtered at 2.5 kHz (sample rate, 50 kHz) for clarity.

Figure 2.11 is the pressure-volume calculation using the SED of the concrete model derived, again, using a finite-difference code. A relative gage separation of $\Delta h/h = 0.09$ was used, again indicating the propriety of the $\Delta h/h \approx 0.1$ rule-of-thumb.

2.1.2.2 Frequency-Response Requirements. As before, the sensitivity of the computed equation of state to loss of high frequency-components is determined by processing the SED through a low-pass filter prior to analysis. With a sample rate of 50 kHz we have filtered the SED at cut-off frequencies of 3 kHz and 1 kHz. The effects of this are to round off the transition from loading on the compaction curve to unloading along the high bulk modulus curve (Figures 2.12a, 2.12b, and 2.12c). Clearly, the equation of state data, such as the compaction curve and unloading bulk modulus, are deducible from the analysis. However, the derived pressure-volume data never do reach the compaction experienced by the SED. Figure 2.10a conveniently fits into this section of the investigation between 2.12b and 2.12c.

It may thus be stated that the compacting equation of state parameters may be well approximated, although the ultimate (pressure, volume) state attained by the material at a given gage will not be faithfully reproduced in the analysis. Indeed, the ultimate computed state is a function of the cut-off frequency of the low-pass filter used in data processing. Therefore, no more filtering should be done than is required to reduce the data to a tractable state.

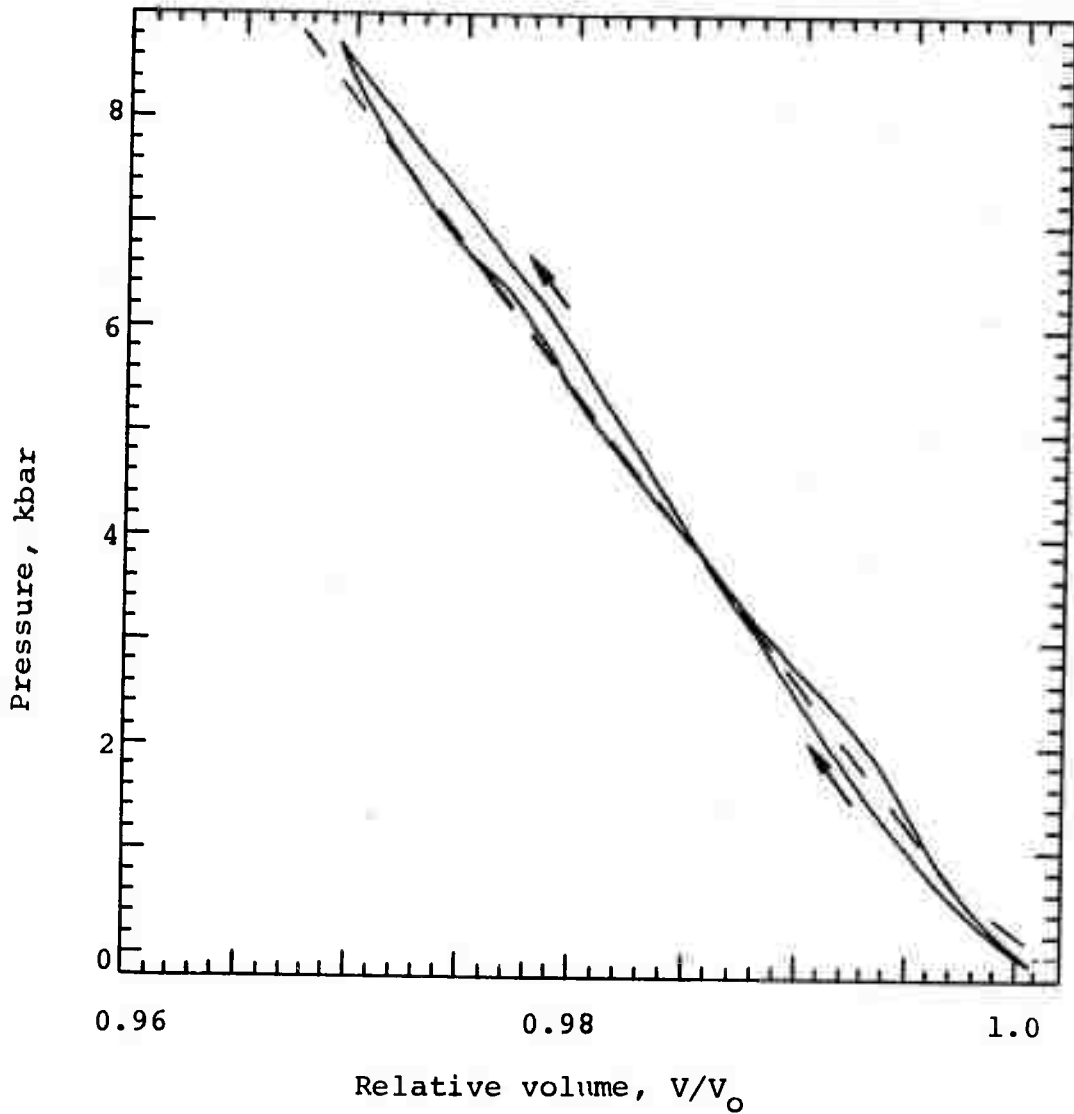


Figure 2.11 Volume calculation using concrete model SED, $\Delta h/h \approx 0.9$.

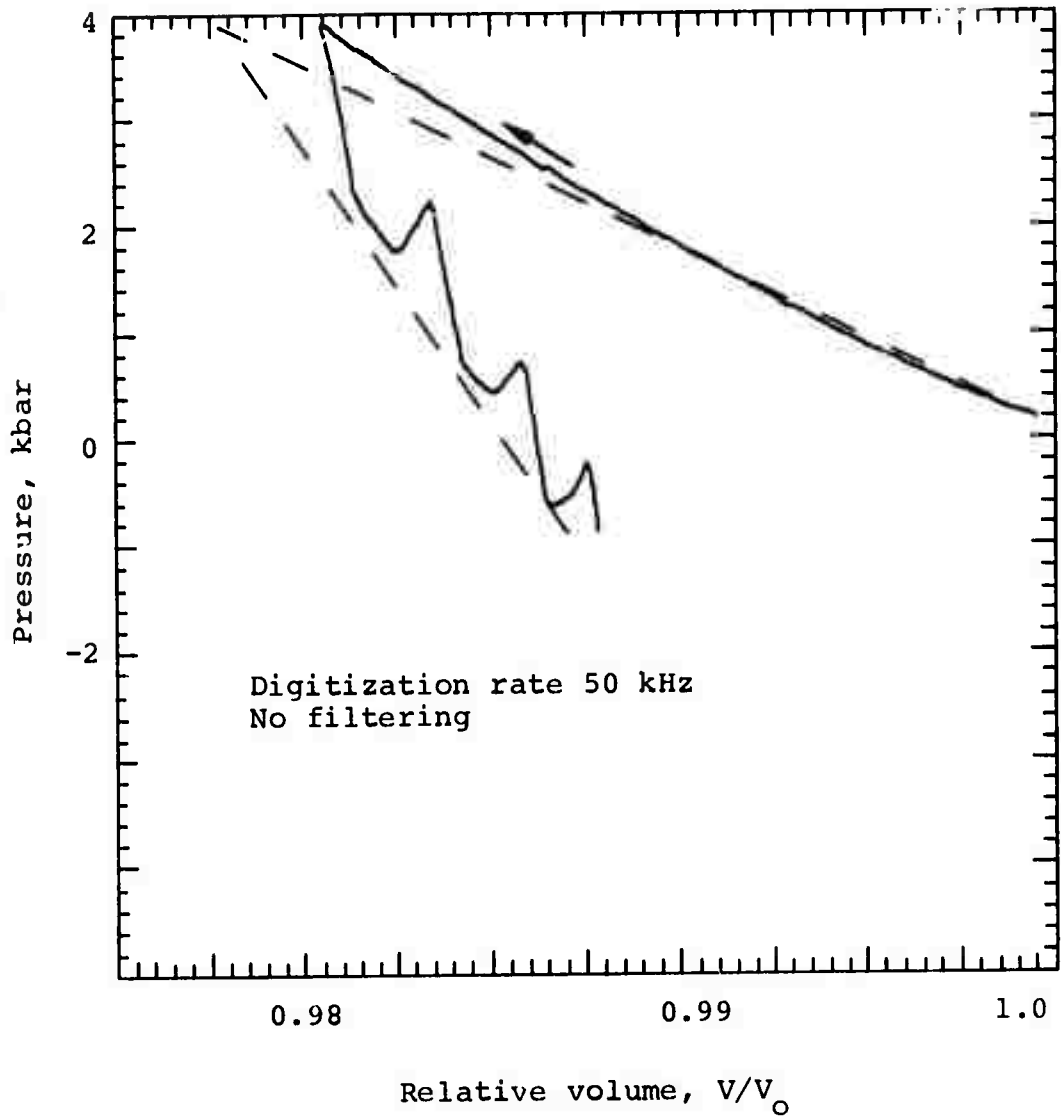


Figure 2.12a Volume calculation using compacting model SED,
 $\Delta h/h \approx 0.11$.

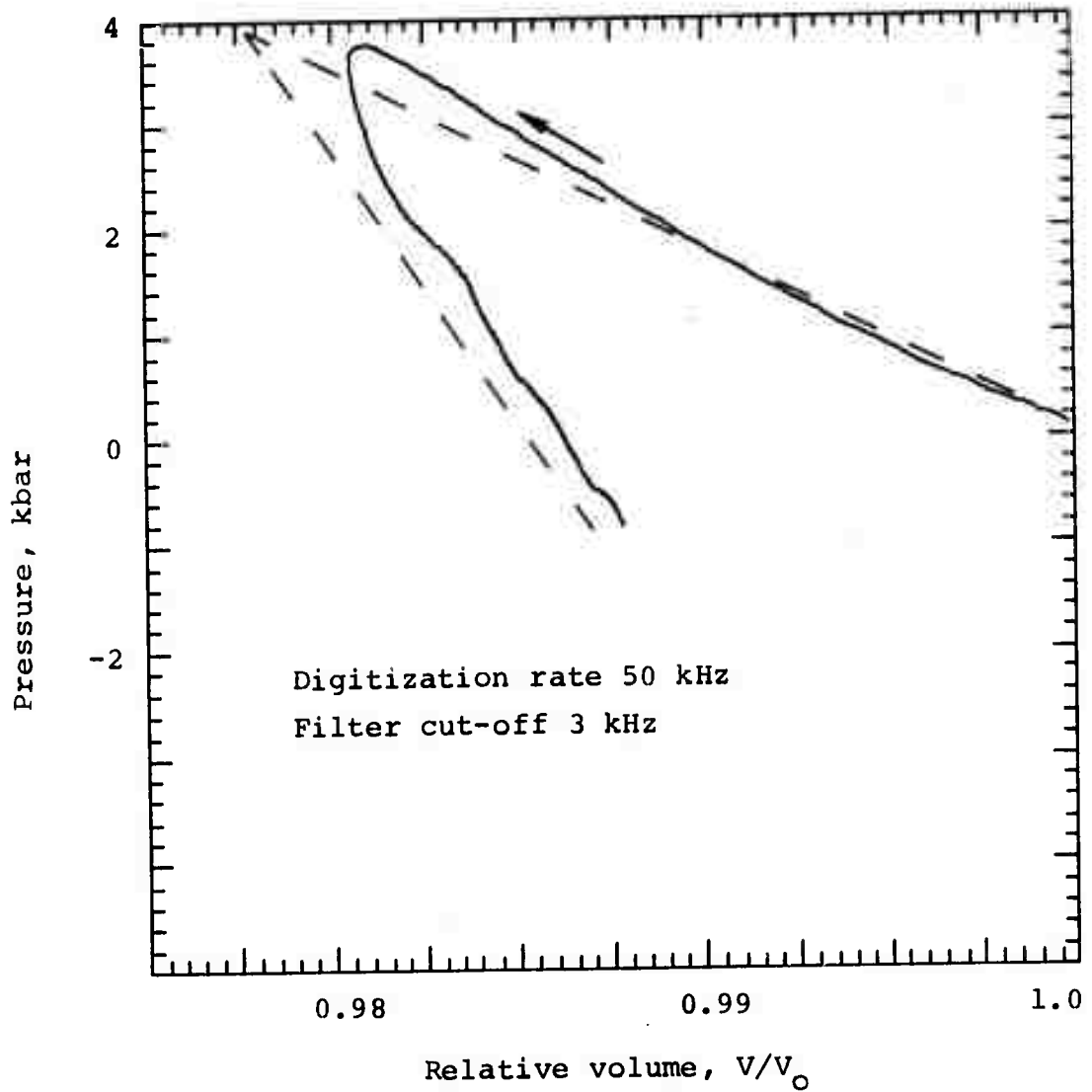


Figure 2.12b Volume calculation using compacting model SED,
 $\Delta h/h \sim 0.11$.

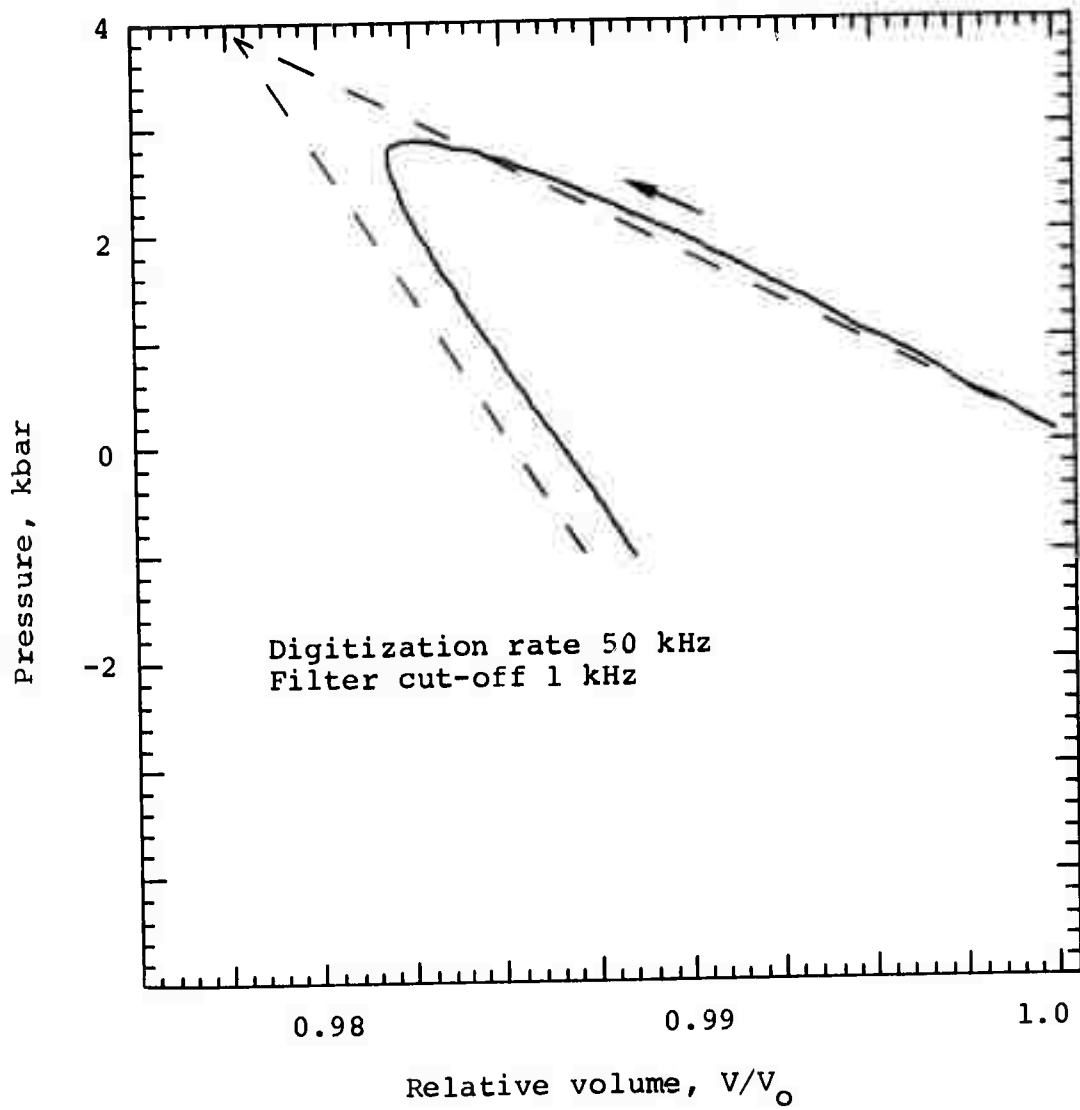


Figure 2.12c Volume calculation using compacting model, SED, $\Delta h/h \sim 0.11$.

Figures 2.13a and 2.13b represent the results of filter preprocessing applied to the SED of the concrete model. There is little difficulty in determining the pressure-volume equation of state corresponding to these data except at very low pressures. Referring to Figure 1.3, the material model is such that, when the tensile strength is exceeded, the material fractures and ensuing tensile stresses are forbidden. The analysis code is, at present, inadequate to handle second loading and unloading paths and should be terminated when such behavior occurs in the SED.

2.1.2.3 Noise Abatement. To determine the effects of system noise and subsequent low-pass filtering, various noise levels and cut-off filter frequencies were applied to the SED of both the compacting and concrete models. Representative of the results are Figures 2.14 and 2.15.

As the concrete model approximates a linear-elastic solid, most of the conclusions obtained from the work on linear material can be directly carried over. In particular, the conclusion that high-level noise may be removed by processing with a low enough cut-off frequency filter without substantial loss in pressure-volume equation of state information.

Analyzing noisy SED from the compacting model results in somewhat different conclusions. A comparison of Figures 2.12b and 2.15 indicates the effects of noise on the compacting model data. Unloading (where there are many data points) gives a good approximation of the true equation of state. However, addition of random noise to the few data points in the rapid loading portion of the SED leads to substantial error in the loading

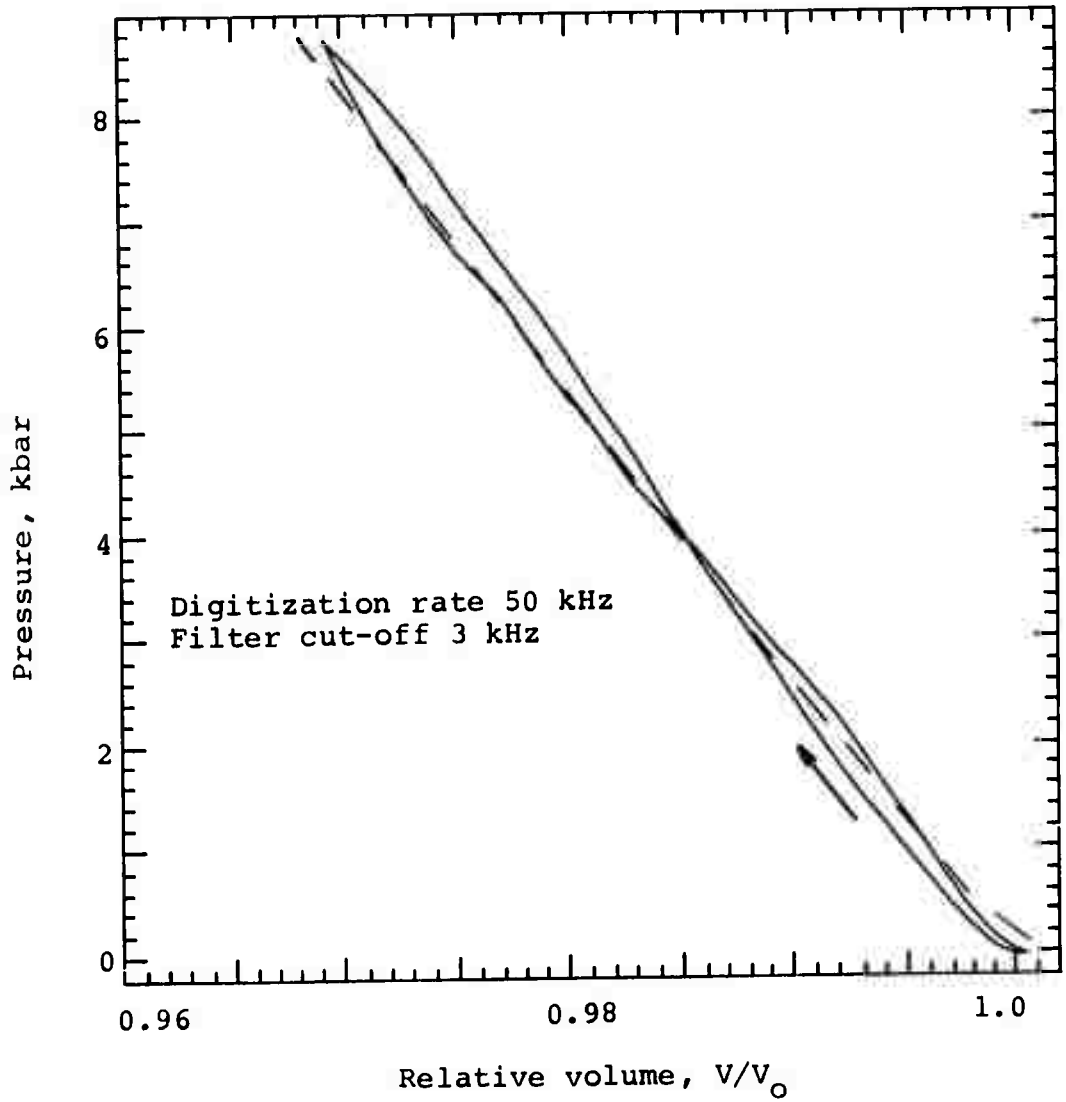


Figure 2.13a Pressure-volume calculation using concrete model SED, $\Delta h/h \sim 0.9$.

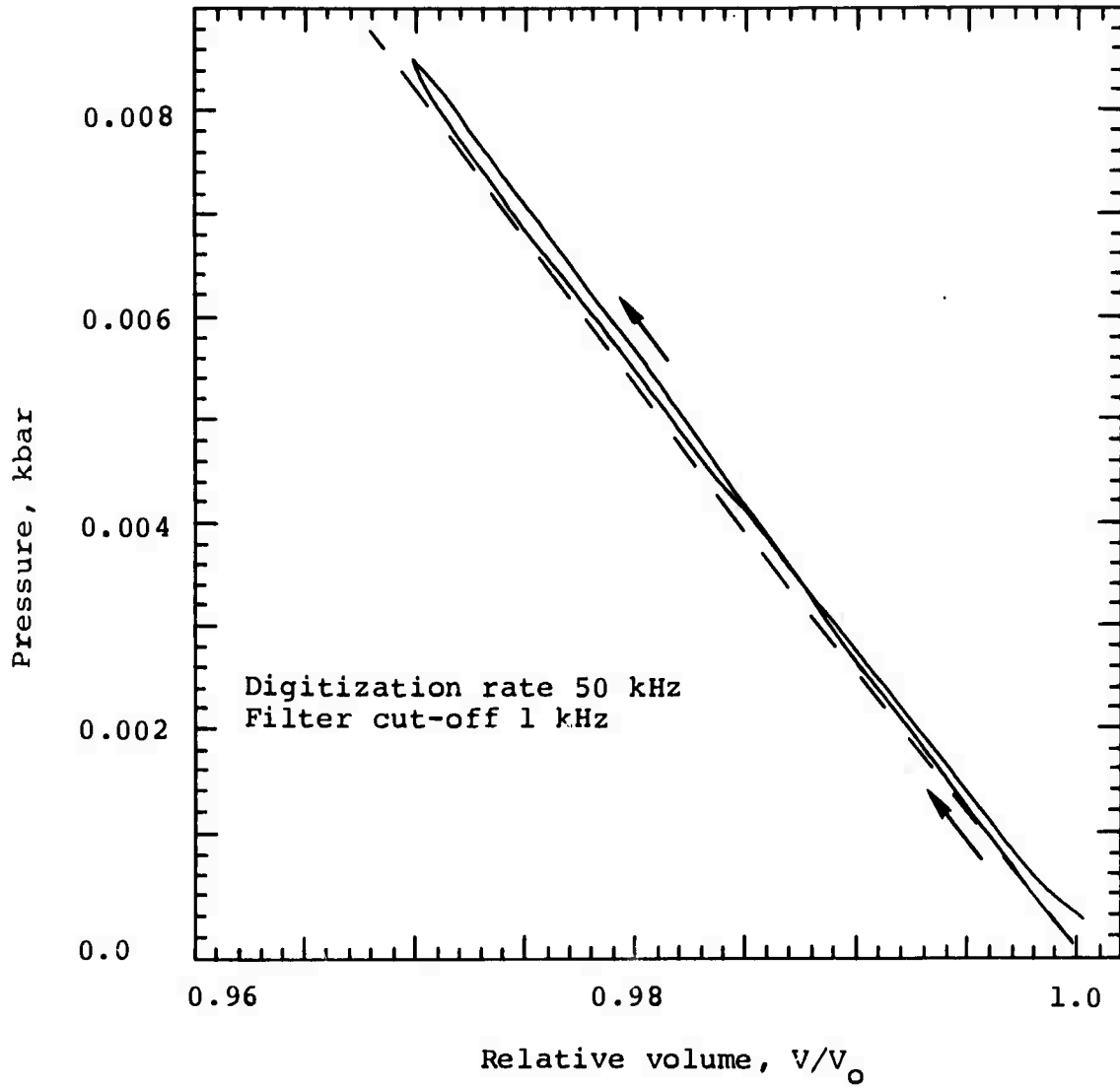


Figure 2.13b Pressure-volume calculation using concrete model SED, $\Delta h/h \sim 0.9$.

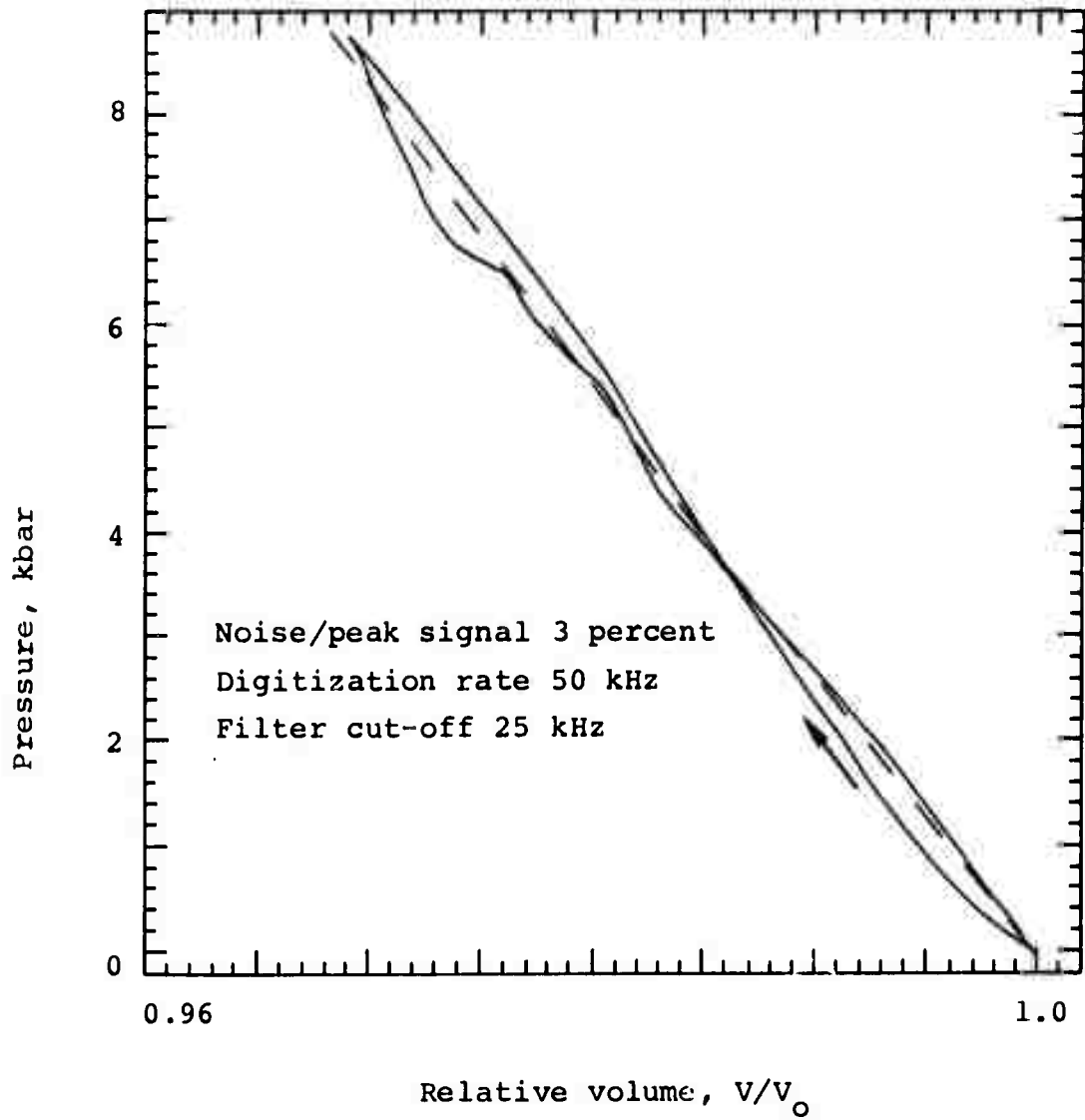


Figure 2.14 Effects of noise on concrete model SED.

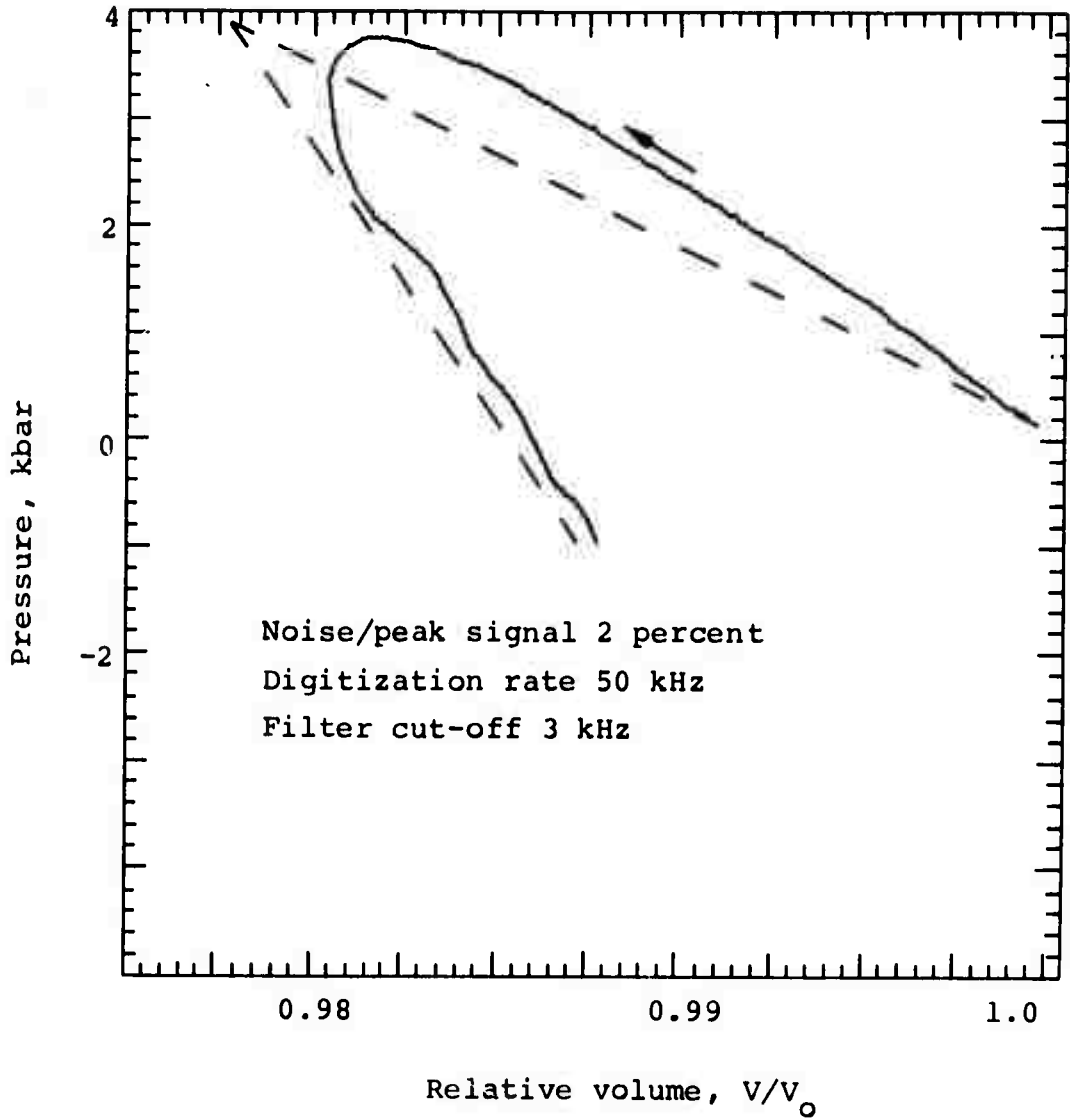


Figure 2.15 Effects of noise on compacting model SED.

equation of state. Additionally, as can be seen through the sequence of steps shown in Figures 2.16 and 2.17, the low-level precursor of the wave is very nearly lost in the noise.

2.1.2.4 Tangential Stress Calculations. In Figure 2.18 is plotted the comparison function of Equation (2-1) derived from data of the compacting material. Here the data were manipulated in the fashion of Figure 2.18, to yield the smoothest input data reasonably consistent with physical meaning. This was done to obtain the greatest possible accuracy of second order approximation of the derivatives required by Equation (1-2). It is seen that the calculation of σ_{θ} from radial data is not practical.

2.1.3 Discussion. The results of the foregoing analysis may be summarized in one sentence. Assuming the existence of an accurate tangential stress gage, there appear to be no theoretical or computational difficulties in determining the in-situ dynamic constitutive properties of a material during a single loading-unloading cycle. Specifically, this conclusion is based on the results of calculational investigations into the following categories:

a. Gages required. It was found that the tangential stress could not be calculated accurately through the conservation of momentum equation (1-2). This was due to the fact that the two terms in brackets are generally large, of opposite sign, and of very nearly the same magnitude. σ_{θ} then becomes dependent upon the small difference of two large quantities, both of which contain derivatives of measured quantities. It is thus imperative that the tangential stress, σ_{θ} , be measured to an accuracy comparable to that of σ_R so that the pressure (Equation 1-3) may be determined to the same accuracy.

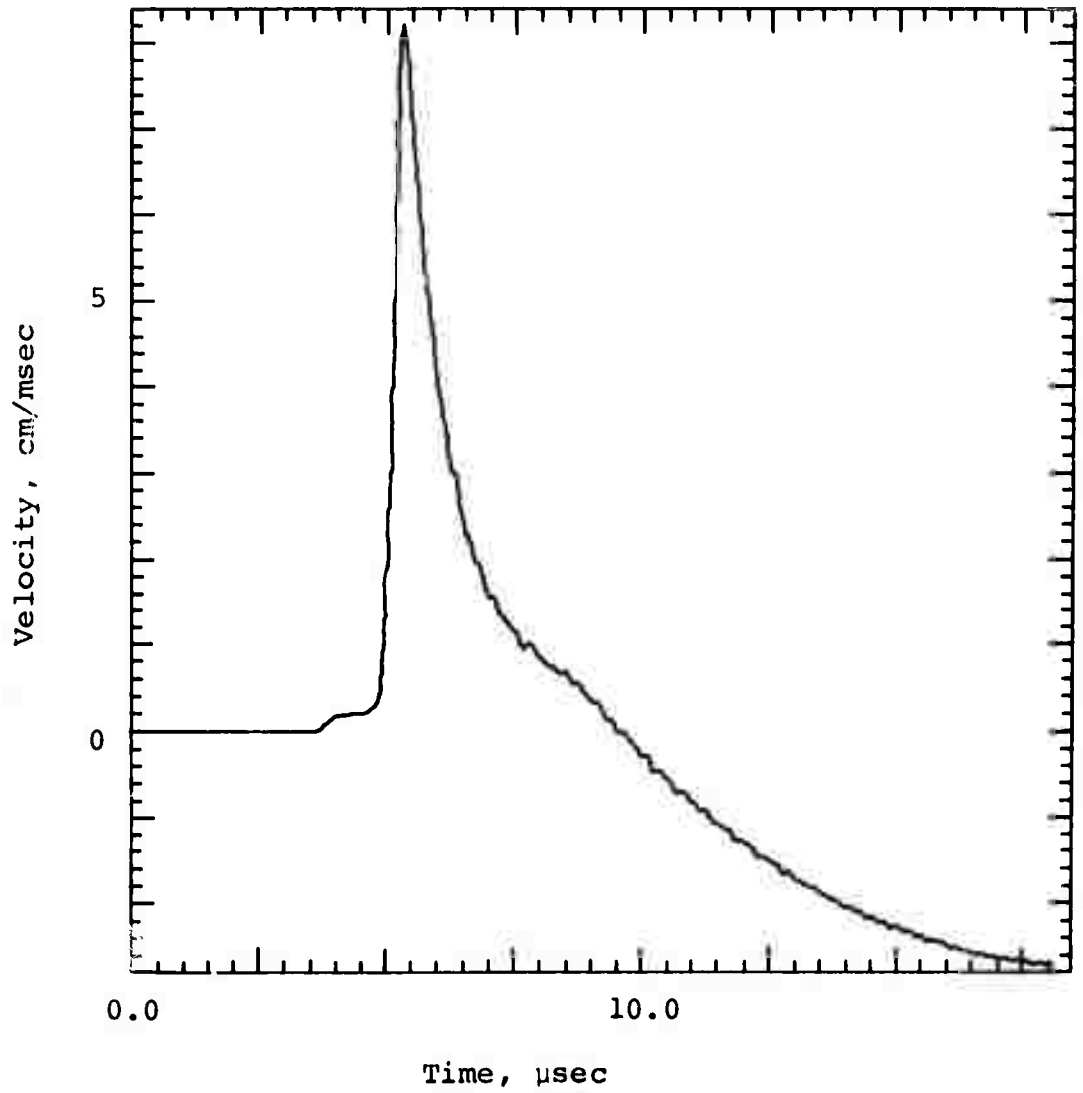


Figure 2.16a Velocity history of compacting model SED; no pre-processing applied.

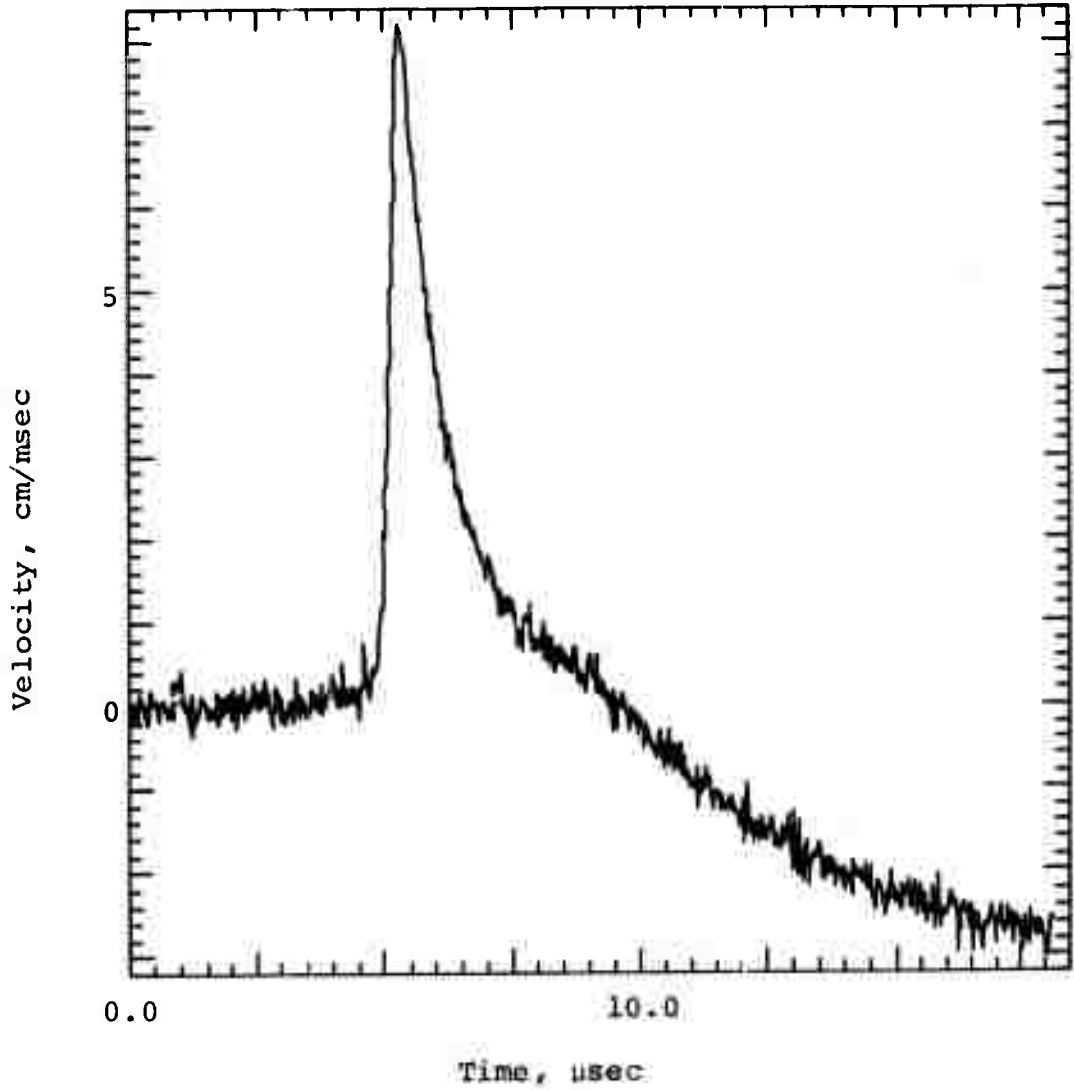


Figure 2.16b Velocity history of compacting model SED with 2 percent Gaussian white noise added.

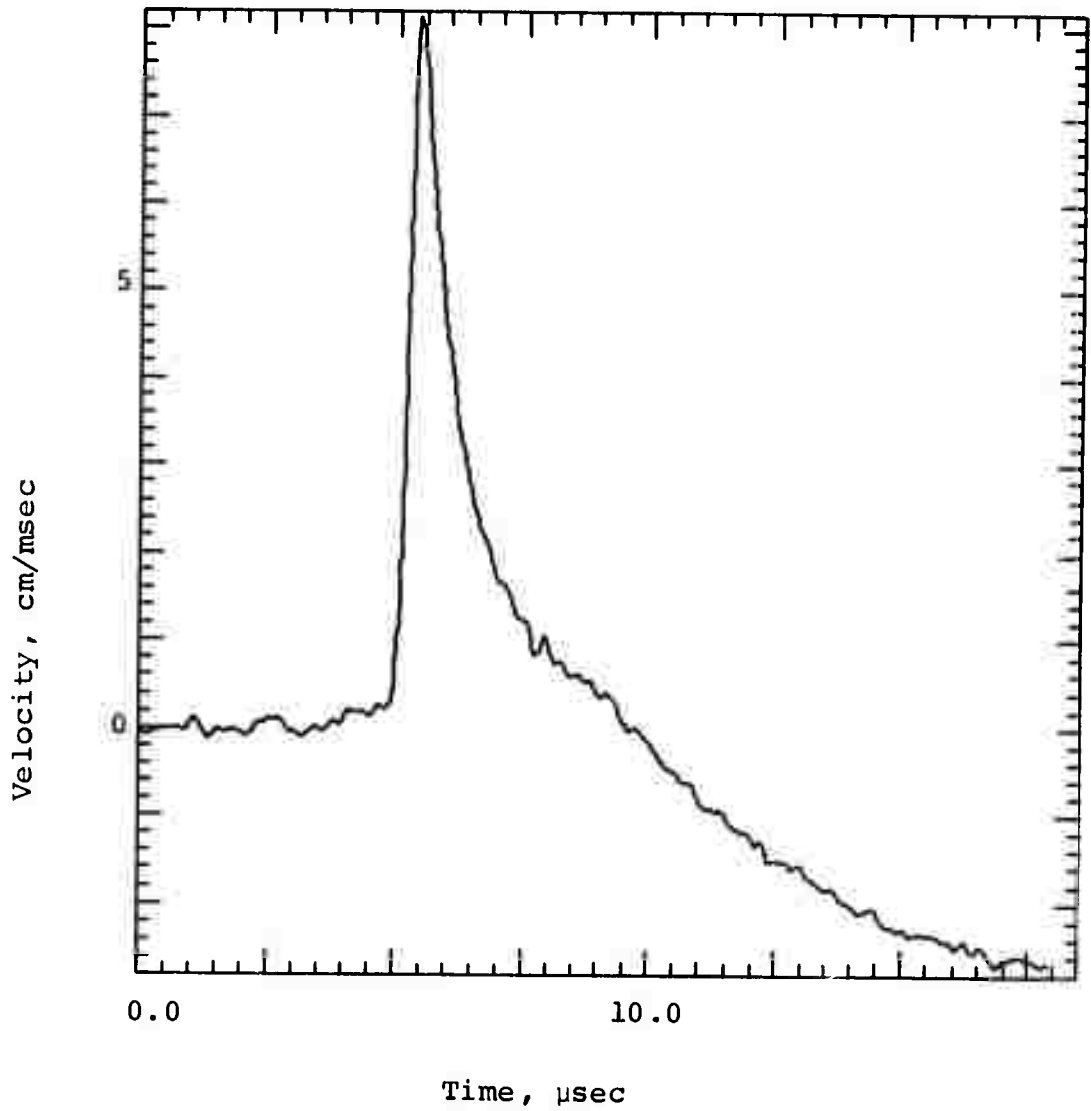


Figure 2.17 Velocity history of compacting model SED with 2 percent noise and filtered with a cut-off/digitization rate ratio of 0.06.

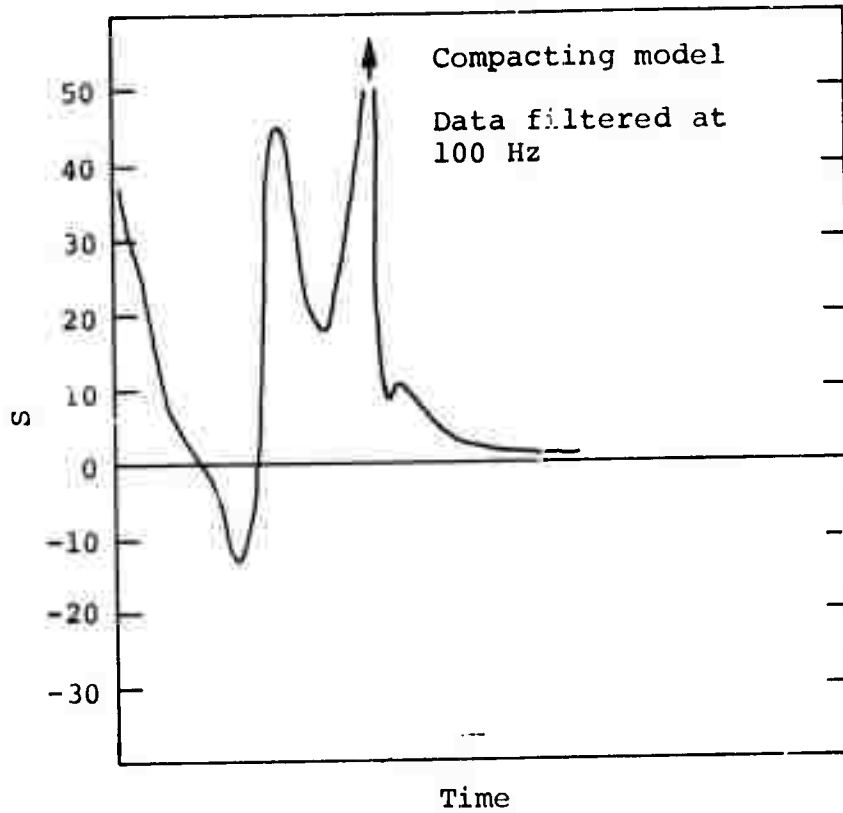


Figure 2.18 Comparison of true and calculated tangential stress resulting from compacting model SED.

b. Gage placement. There are required a minimum of two radial locations for ground-motion gages as seen from Equation (1-1b). Data derived from a linear-elastic solid model indicated that the optimum gage spacing, h , relative to the mean distance of the gage pair from the working point, h , was $\Delta h/h \approx 0.1$. Further investigations using more sophisticated material models did nothing to alter this conclusion.

Errors in gage placement fall into two categories: An error in h (e.g. improper locating of the working point) leads to a nearly undetectable change in the computed equation of state, and an error in Δh (e.g., a poor measurement of the position of one of the gages) leads, through Equation (1-1b), to a cumulative error in the calculation of relative volume Equation (1-1).

Insofar as the pressure-volume equation of state is concerned, alignment of the gage packages is not extremely critical. A 10-degree misalignment of all of the velocity (or accelerometer) gages introduces a constant 1.5 percent error in the volume history. If the stress-gage system is one in which all three normal axes are instrumented with identical gage elements, then the mean stress, or pressure, is independent of alignment. However, if the second stress invariant (including terms of the form $\sigma_R - \sigma_\theta$) is desired, then alignment is critical.

c. Frequency response and timing. By applying a digital low-pass filter to the simulated experimental data prior to analysis, it was determined that the loss of high-frequency data components had virtually no effect on the computed pressure-volume relationship of linear-elastic materials. The information of a constant bulk and shear modulus is carried equally at all frequencies for such a material.

There is a significant altering of the transition region between loading and unloading for materials that load and unload along different paths in pressure-volume space. However, outside of the transition region the equation of state is well approximated by analysis.

Filtering only some of the gage records tends to introduce what appears to be a time lag in those records due to an alteration of their risetimes. Any filter processing must be applied equally to all records. Low-pass filtering the entire set of records at a cut-off frequency at or below that of the lowest frequency response of the set should eliminate difficulties that may occur due to the inclusion of one gage element having a frequency response different than the others.

Information will be lost, however, if the material in question is one for which strain rate or strain hardening effects are important and the risetime of the signal is shorter than that which can be followed by the "slowest" gage of the set.

d. Noise limitations. As explained in Appendix C, in normal terminology "signal/noise ratio" refers to the mean signal. The noise added to the records in this work is referred to as the peak value of the signal in question. The quality of gage records that can be expected has a normal (signal/noise) ratio of about 20. This would imply a noise/(peak signal) = 0.025. Figures 2.10 and 2.11 indicate that noise of this magnitude and higher can successfully be eliminated by the application of a digital low-pass filter with loss of resolution in the region of transition from loading to unloading.

Evidently, the only apparent technical difficulty in developing a gage system to measure (or determine) the in-situ properties of geological materials is the development of a tangential stress gage.

2.2 EXPERIMENTS

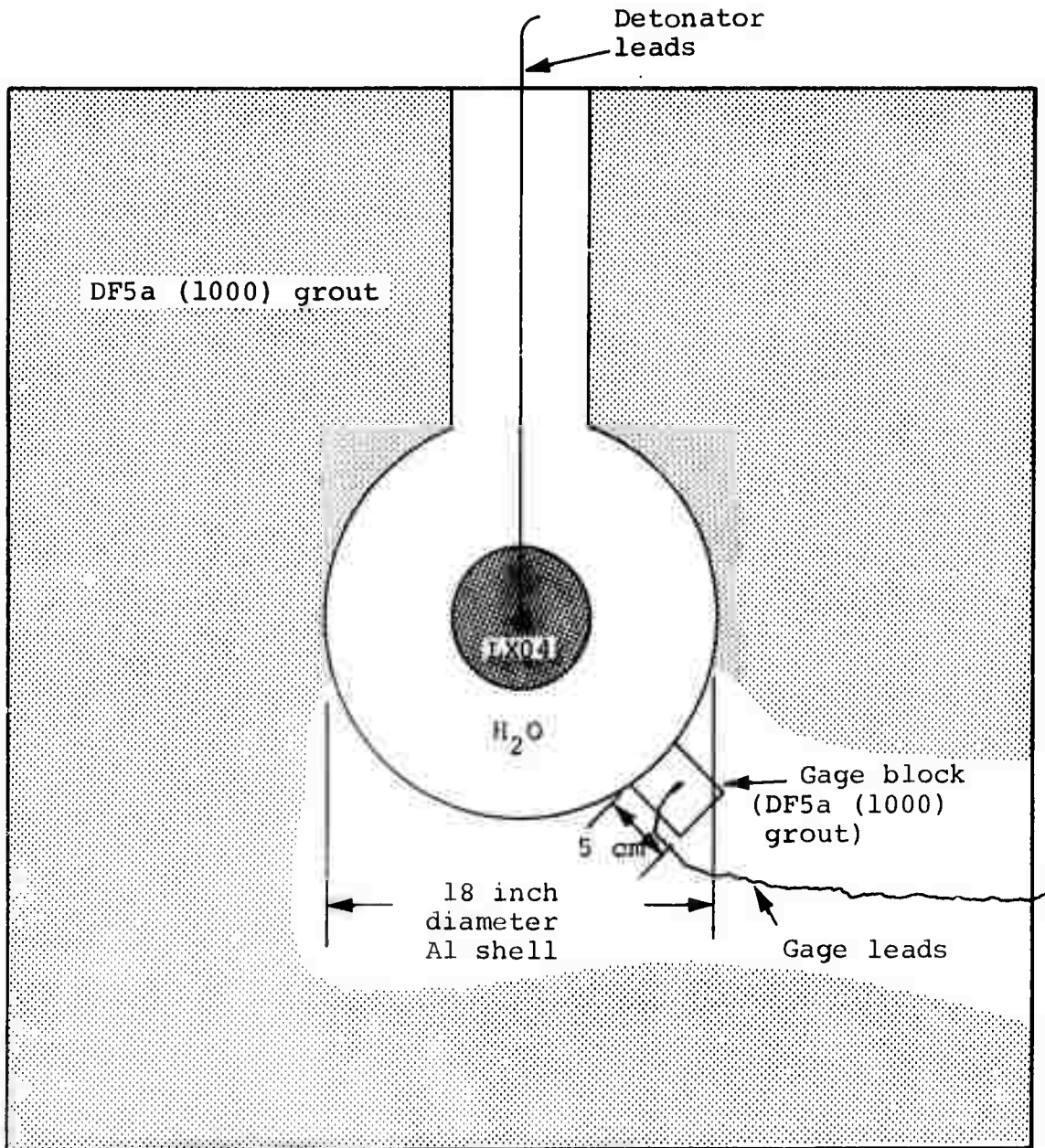
2.2.1 Engineering Description. All gages consisted of a one-mil foil of ytterbium deposited on a substrate and etched to give the desired grid pattern. The same substrate material was then overlaid on this grid, producing a three-layer gage of which the middle laminate was the ytterbium active element. Three different substrate materials: glass, mica, and Lucalox, were used to determine the effect of the substrate material on the quality of the data.

Glass and mica were chosen because they tend to match the properties of many geologic materials; Lucalox was used because of its high sound speed ($1 \text{ cm}/\mu\text{sec}$), allowing the gage to equilibrate in a very short time, considering the small substrate thickness used. Overall active grid dimensions were 1 inch x 1/4 inch x 1 mil. The glass substrate layers were 2 mils thick, the mica was 1 mil thick, and the Lucalox 3 mils thick.

The difference between the tangential and radial mode gages was their orientation. Both orientations had their long axes tangent to the surface of the shock front (assumed to be spherically diverging). Gages in the radial mode were mounted such that the normal to their surfaces was normal to the shock front, while the tangential gages were mounted so that the normal to the shock front was in the surface of the gage plane.

Three separate, identical, high-explosive experiments were conducted. Each shot was spherically symmetric and tested six gage elements. Two gages were mounted in the radial mode and four were mounted in the tangential mode for each shot. There was thus a total of 6 radial gages and 12 tangential gages tested in the 3 experiments. Figure 2.19 is a schematic diagram of the experimental arrangement for one such shot. A 6-inch-diameter sphere of high explosive (LX-04) was used as the energy source. To obtain a peak stress of about 10 kbar at the gage radius, the high explosive was surrounded by a spherical shell of water to a diameter of 18 inches. A thin-walled aluminum sphere of these dimensions contained the explosive and the water.

Gages were mounted as follows: Using the outside of this aluminum sphere as a base, a 4-inch-diameter Lucite ring, 5 cm high, formed a mold which was filled with DF5a(1000) grout.



Notes: LX04 radius = 3 inches
 Sphere radius = 9 inches
 Grout block = 48 inches x 48 inches

Figure 2.19 Schematic diagram of experimental arrangement.

While the grout in this first ring was still liquid, a gage was placed on the grout in the radial or the tangential mode; a second Lucite ring was placed on top and then filled with the grout. This block was then allowed to set up and the Lucite rings removed, thus forming a gage block which conformed to the outside of the aluminum sphere. Figure 2.20 shows the midpoint of this procedure with the gage being mounted in the tangential mode. A completed gage block is shown in Figure 2.21. In an attempt to preclude loss of signals due to shock-induced breakage of the leads as they exit the gage blocks, the leads were surrounded by a blob of silastic at that point. Rather than helping, this may have been detrimental, as will be seen later.

Each sphere was transported to the Physics International high-explosive test site with six such gage blocks epoxied to it as seen in Figure 2.22. The sphere was then mounted at the center of a 4-foot-cube concrete form and the form filled with the same grout as used for the gage blocks. This was allowed to set for two weeks prior to testing. Figure 2.23 shows one of the spheres with its attendant gage blocks just prior to filling the concrete form with the rock-matching grout.

Grout was used as the shot medium for reasons ultimately economic. It is easy to work with, allowing gages to be simply and accurately mounted in intimate contact with the medium they are to monitor. Precision machining is not required and the materials are inexpensive.

2.2.2 Data Acquisition System. A transient power supply impresses a voltage across a Wheatstone bridge, one arm of which includes the gage element. Stress-induced changes of resistance of this piezoresistive material are then seen as a voltage change



Figure 2.20 Tangential-mode gage block in process of construction.



Figure 2.21 Completed gage block ready for mounting.



Figure 2.22 Mounting of gage blocks on aluminum sphere.



Figure 2.23 Aluminum sphere and attendant gage blocks installed in concrete form awaiting grout covering.

which is recorded as oscilloscope trace. To double the probability of getting a record, each gage feeds both beams of a dual-beam oscilloscope. Each beam has a different sweep speed and a different voltage amplification. Further, each beam has a different delay time so that the arrival time of the shock should appear at about the same position on the scope screen for both traces. Hard-copy Polaroid pictures are taken of each screen and become a permanent record of experimental data. Calibrations of voltage amplification and sweep speed are made of every trace of all oscilloscopes at shot time. These calibration traces are also recorded as permanent Polaroid pictures.

2.2.3 Data. Table 2.1 is a summary of the peak stresses obtained by the gages and includes comments on the quality of the records. It will be noted that on the first shot, all of the gages survived for nearly the full length of the scope trace, four of the six giving clear records. One of the mica tangential gages was off-scale preshot for both of its traces while the other mica-backed tangential gage gave a poor quality record.

In the second shot, both radial gages broke up just after they reached the peak, as did one of the Lucalox-backed tangential gages. The character of the break indicates that the leads failed and not the gage itself. The other records lasted throughout the sweep time on the scope.

On the third shot, the glass-backed radial gage was shorted out preshot and one of the glass tangential gages was not properly recorded, because the Polaroid film did not make full contact with the developer. The other radial gage backed by mica broke up again after about 5 μ sec. This also had the characteristics of a loss of signal due to a break of the leads. Three of the

TABLE 2.1
SUMMARY OF EXPERIMENTAL PEAK STRESS MEASUREMENTS

<u>Gage</u> ^a	<u>Peak Stress</u> (kbar)	<u>Comments</u>
LIR	7.7	
LITI	7.4	
LIT2	7.0	
MIR	6.5	
MITI	4.4 ^b	
MIT2		Trace off-scale preshot
L2R	8.2	c
L2TI	8.9	d
L2T2	8.3	
G2R	7.1	c
G2TI	7.5	
G2T2	8.2	
G3R		Gage shorted out preshot
G3TI	5.9	
G3T2		Faulty developer in Polaroid film
M3R	6.9	c
M3TI	7.7	
M3T2	8.0	

a. Legend (backing), (shot number), (gage mode), (gage number)

1. Backing: Lucalox, mica, glass
2. Gage mode: radial, tangential

b. This record rejected from statistical averaging.

c. Gage record terminated about 5 μ sec after reaching peak stress.

d. This is the only tangential mode gage that failed at peak stress.

other four gages gave good records and lasted the full length of the sweep time of the scope.

Figure 2.24 shows scope traces of both of the radial gages that did not break up, and for completeness, one that did. Records of the nine surviving tangential-mode gages are seen in Figures 2.25, 2.26, and 2.27. Static tests performed on grout samples taken from the pour of the shot blocks and cured at 100 percent humidity resulted in the following data. The density was $2.12 \pm 0.07 \text{ gm/cm}^3$, the sound velocity $0.269 \pm 0.003 \text{ cm}/\mu\text{sec}$, and the unconfined compressive strength is 100 bars. Hugoniot data on very much the same type of grout (DOOR MIST) indicate that, at a pressure of 115 kbar, the relative volume is 0.58.

The gage blocks were allowed to cure under dry conditions prior to being surrounded by the final grout shot block. Observation of the experimental records yields a good measure of the shock speed in the gage block grout: The shock may be seen to cross the individual elements of the grid giving a shock velocity of about $0.15 \text{ cm}/\mu\text{sec}$, nearly a factor of 2 below the sound speed of the wet-cured surrounding grout. Additional measurements on the density of a large piece of similar material that was allowed to air-cure indicate a density as low as 1.8 gm/cm^3 .

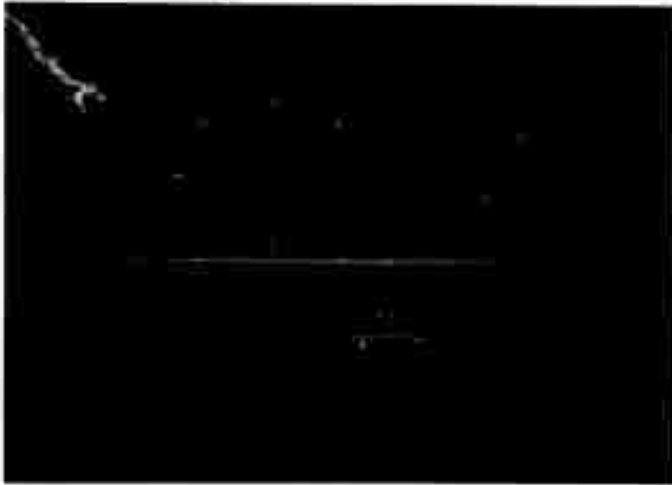
The above considerations lead to a simple approximation of the equation of state for the gage block given by

$$p(v) = 0.02 \mu + 0.14 \mu^2 \text{ Mbar} \quad (2-5)$$

where

$$\mu = \left(\frac{V_0}{V} - 1 \right)$$

Reproduced from
best available copy.

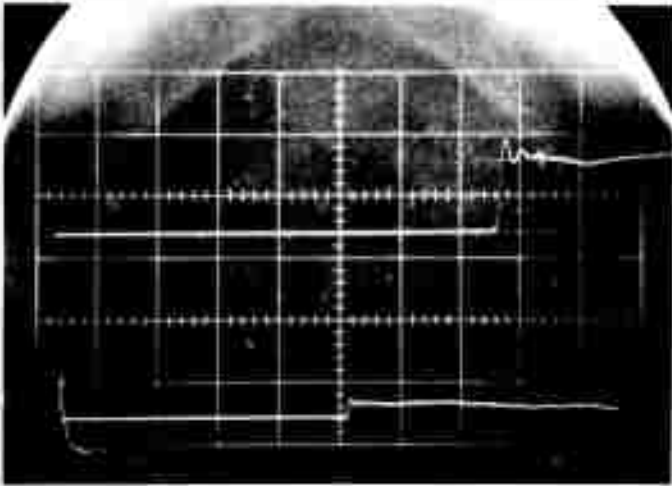


a. Lucalox substrate

Upper trace: 1 V/cm

Lower trace: 2 V/cm

L1R

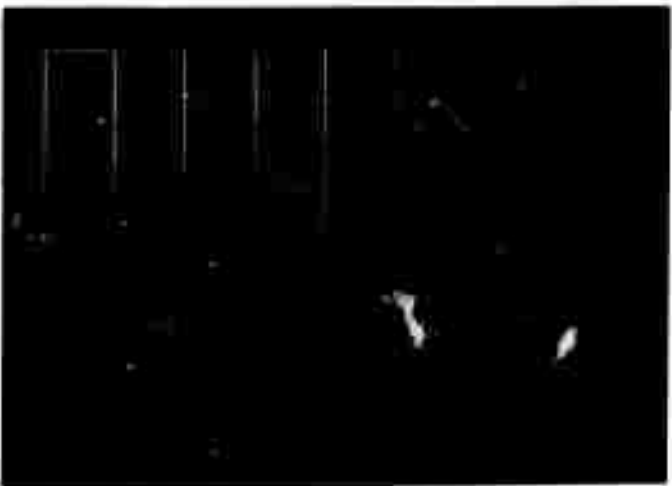


b. Mica substrate

Upper trace: 1 V/cm

Lower trace: 2 V/cm

M1R



c. Glass substrate

Upper trace: .5 V/cm

Lower trace: 1 V/cm

G2R

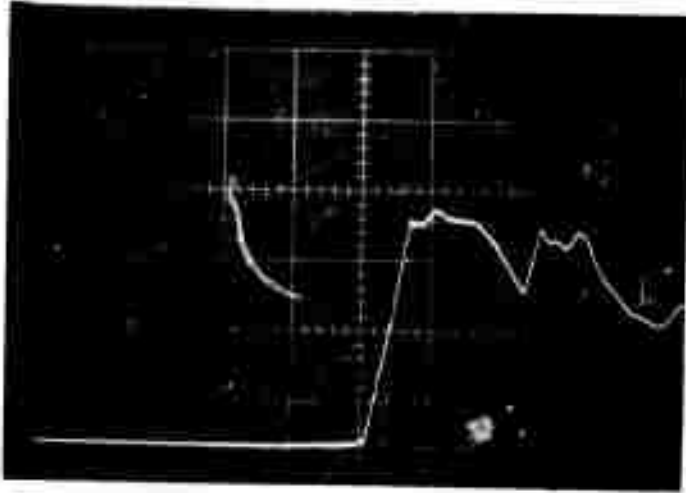
Sweep rate

Upper trace: 5 μ sec/cm

Lower trace: 10 μ sec/cm

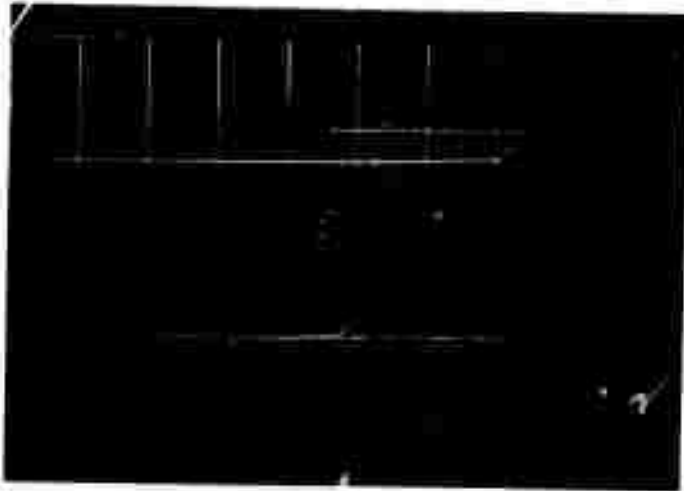
Figure 2.24 Radial mode stress gage data.

Reproduced from
best available copy.



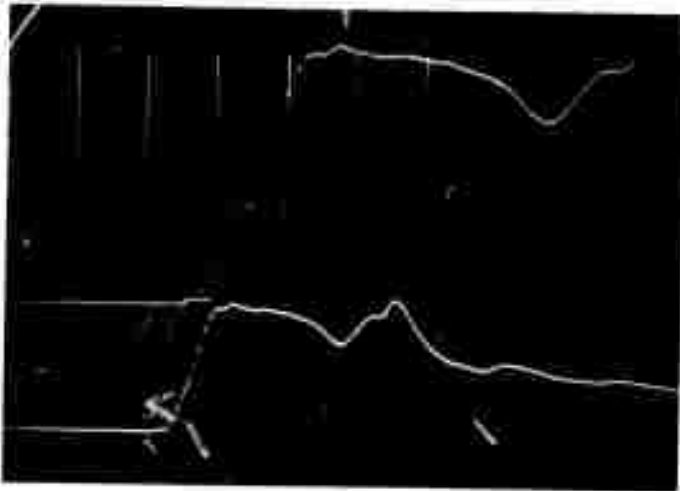
- a. Lower Trace: .5 V/cm
Sweep rate: 10 μ sec/cm

L1T1



- b. Lower trace: .5 V/cm
Sweep rate: 10 μ sec/cm

L1T2



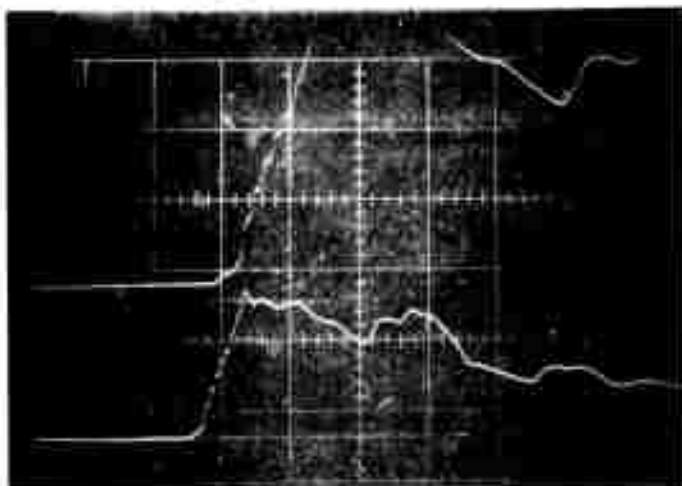
- c. Upper trace: .5 V/cm
Sweep rate: 5 μ sec/cm
Lower trace: 1 V/cm
Sweep rate: 10 μ sec/cm

L2T2

Figure 2.25 Lucalox substrate tangential-mode gage data.

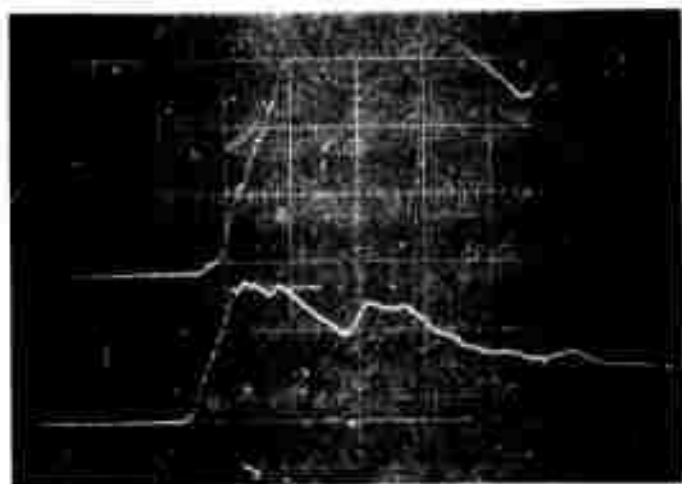
AL1010

Reproduced from
best available copy.



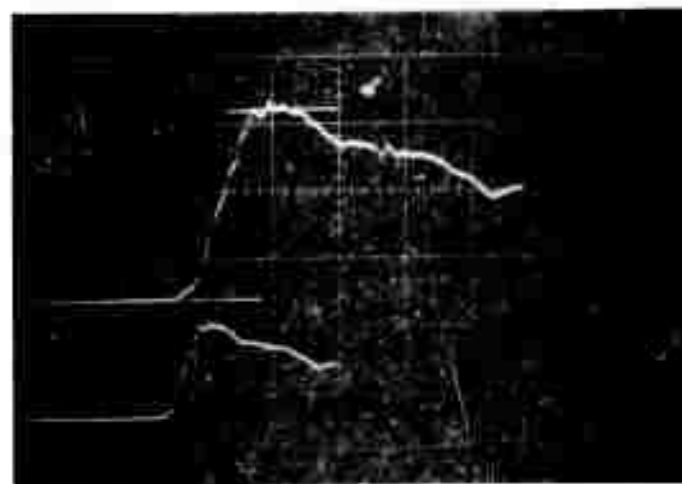
a. Upper trace: .5 V/cm
Lower trace: 1 V/cm

G2T1



b. Upper trace: .5 V/cm
Lower trace: 1 V/cm

G2T2



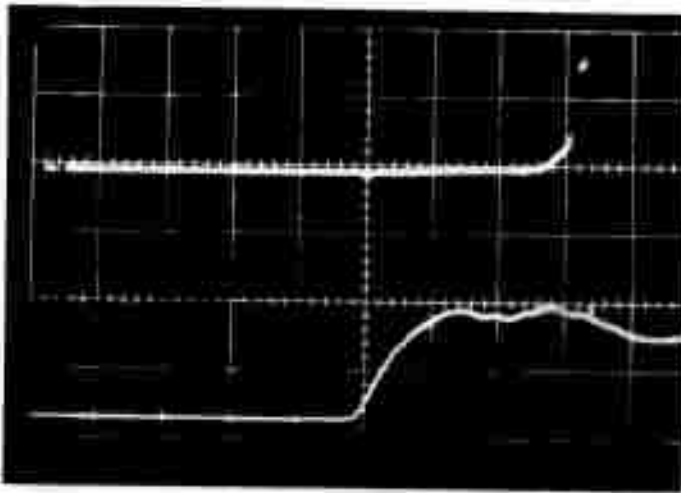
c. Upper trace: .5 V/cm
Lower trace: 1 V/cm

G3T1

Sweep rate

Upper traces: 5 μ sec/cm
Lower traces: 10 μ sec/cm

Figure 2.26 Glass substrate tangential-mode gage data.



a. Lower trace: .5 V/cm

M1T1



b. Upper trace: .5 V/cm
Lower trace: 1 V/cm

M3T1



c. Upper trace: .5 V/cm
Lower trace: 1 V/cm

Sweep rate M3T2
Upper traces: 5 μ sec/cm
Lower traces: 10 μ sec/cm

Figure 2.27 Mica substrate tangential-mode gage data.

We have assumed a simple von Mises limit of 100 bar, the unconfined compressive strength. The calculation comprised the explosion of the sphere of high explosive and transmission of the resulting shock through water and the gage block material. This latter was taken to be 7.6 cm thick, surrounded by an infinitely thick layer of material having the same equation of state with the exception that the bulk modulus at zero stress for this second layer was 0.096 Mbar and its density was taken as 2.2 gm/cm³ consistent with, but somewhat more dense than, the cylindrical samples of the wet-cured grout. The results of our numerical simulation of the experiment are presented in Figures 2.28 and 2.29.

2.2.4 Analysis and Discussion. The radial gage records show (Figure 2.24) a very sharp shock front and display a few cycles of megahertz ringing. This ringing may have its origin in several sources: it may be associated with a frequency limit of the electronics (acting as a low-pass filter with a band edge at about 1 MHz, it may be direct observation of the equilibration process in the gage, or it may be more subtle. The thickness of most of the gage packages was about 0.02 cm and the particle velocity of the grout matrix is computed to be about 0.02 cm/ μ sec. Sharpness of the shock front is also evidenced in the tangential mode gages, as the wave may be observed as it crosses each of the eight "wires" of the gage grid, reducing the risetime of these devices.

Also noted is a secondary stress pulse that occurs about 25 μ sec after shock arrival (Figures 2.24 through 2.27). An additional smaller pulse shows in several of the records at around 50 μ sec, possibly indicating a periodic phenomenon. The magnitude of the pulse is variable from moderate, as seen in gage

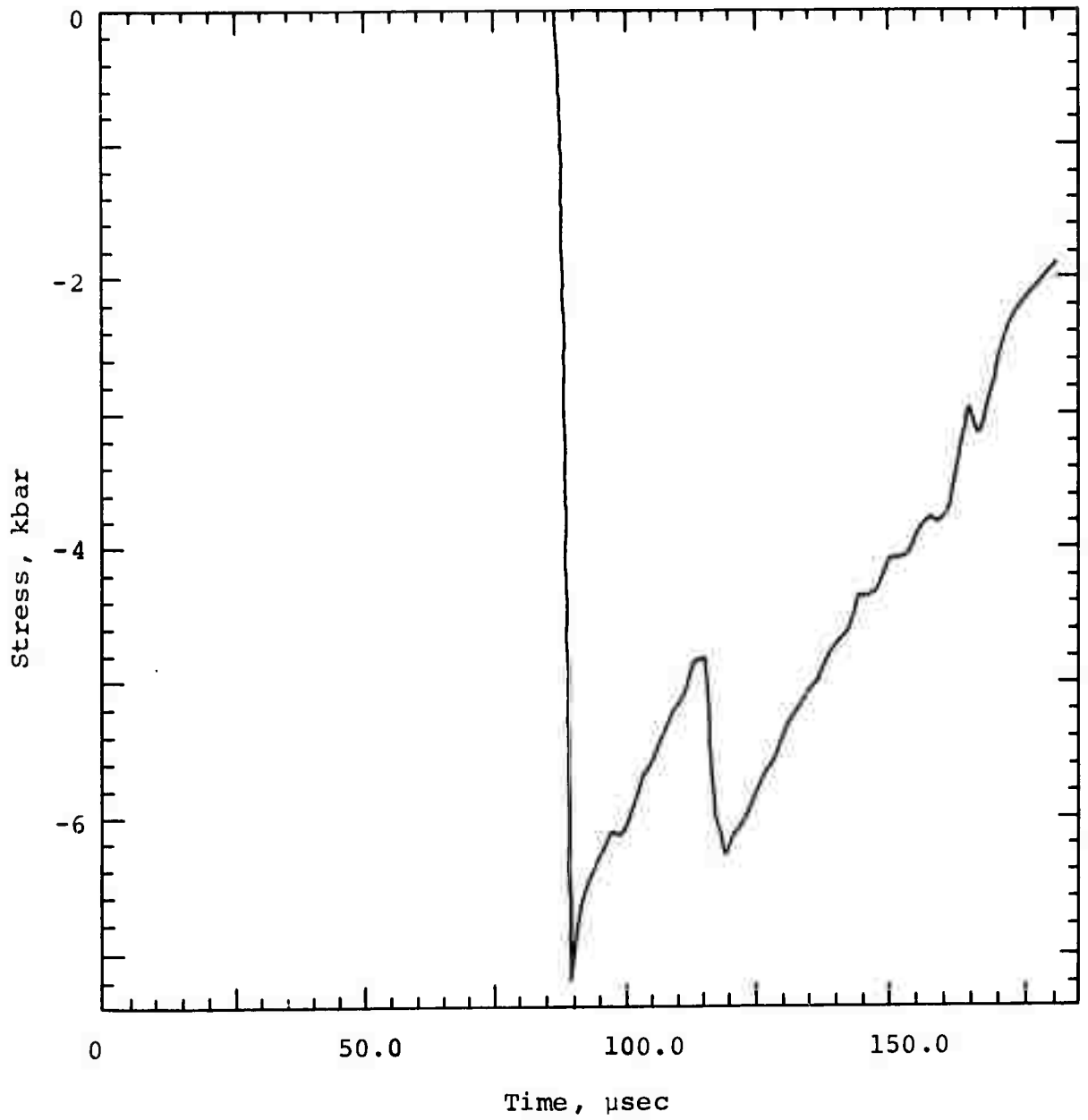


Figure 2.28 Numerical simulation of experiment--radial stress.

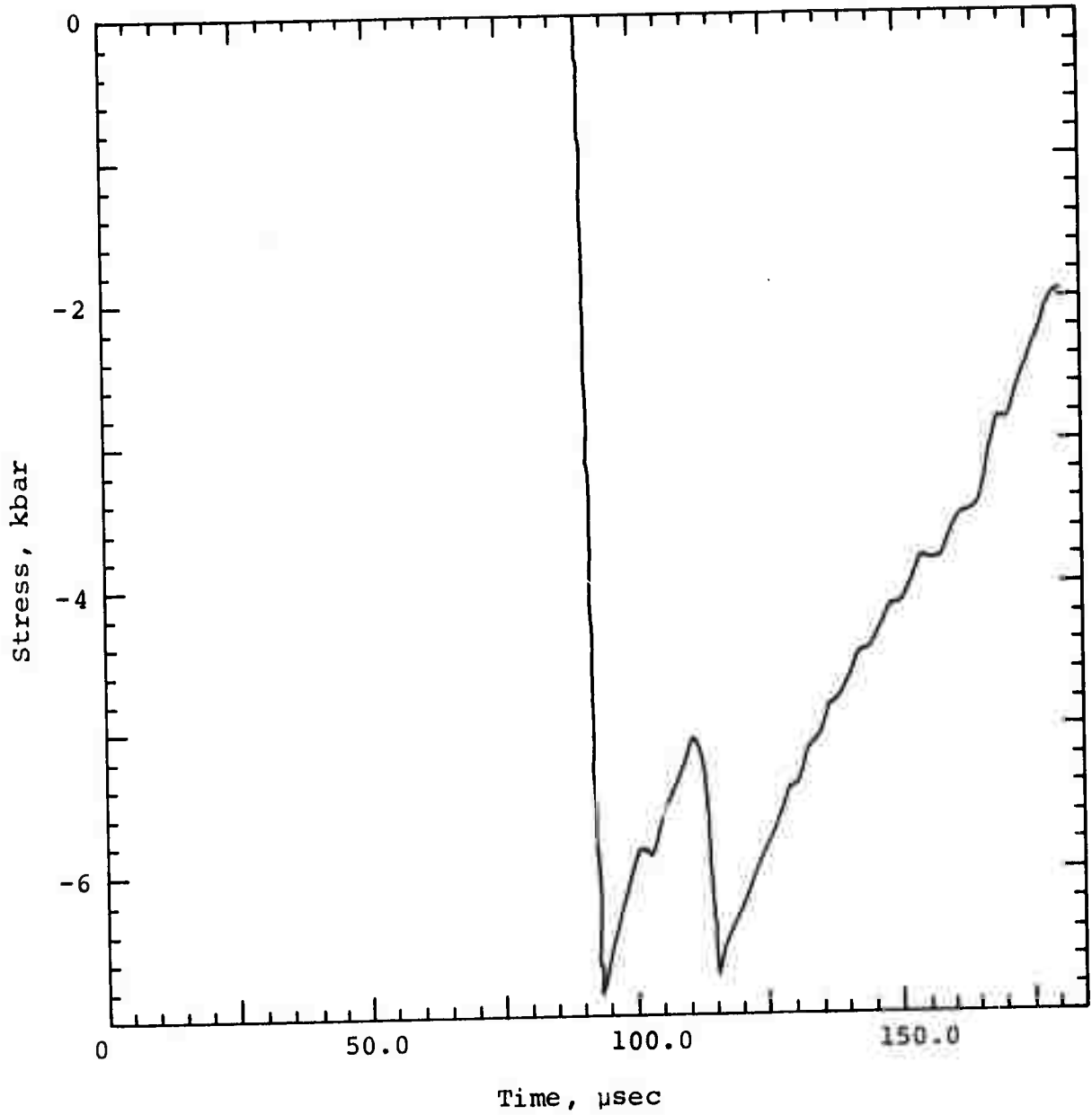


Figure 2.29 Numerical simulation of experiment--tangential stress.

G2T2, to overwhelming in MIT2, where the peak in question is at least 50 percent greater than the magnitude of the initial shock-induced peak. (This gage is not shown, as its baseline is off-screen preshot and the scope sweep delay was set so that the record is not displayed much beyond the "spurious" pulse.)

The origin of this pulse is a reflection from the downstream face of the gage block. The gage blocks were allowed to cure in air for a few days prior to the final pour. The downstream face is 1/2 to 3/4 inch from the edge of the tangential gages. Observation of the stress wave crossing the grid leads to a shock velocity in the gage block of about 0.15 cm/ μ sec, about one-half the measured sound velocity measured in sample of the final pour that was cured under 100 percent humidity conditions. Recent measurements on a very large block of grout that had dry curing conditions indicate substantially lower density and sound velocity than sample cylinders of the same material cured under wet conditions. Because of differences in curing, the gage blocks had a different (lower) impedance than the surrounding grout.

The numerical simulation of this experiment discussed in the previous section yields a peak stress of approximately the correct magnitude and a reflection pulse (from the interface of the two types of grout) having about the correct timing and magnitude. This is taken as strong evidence that the second peak in the experimental data is such a reflection pulse.

The mica-backed tangential gages did not appear to have the fidelity displayed by the other materials. There was no obvious difference due to backing materials when the gages were used in the radial mode. However, it is to be noted that in the tangential orientation a radial stress wave is propagated along

The natural layering of the mica while the radial stress is propagated normal to these layers. The anisotropy of mica could well lead to a distortion of the wavefront as seen by the gage elements. For this reason it is recommended that mica not be the substrate of gages used in this mode.

The loss of all radial gages, except those in the first experiment where the amplifier gains and oscilloscope delays were set to yield short, low-amplitude records, combine to preclude the deduction of much more than peak stress from the radial gages. However, such information is made useful in the following manner. Table 2.2 summarizes the peak stress data of all of the gages, the first part in the table assumes all gages are accurate and averages the output of the three experiments separately; the second assumes all shots were physically identical and averages the results of the gages with different substrate materials separately, and finally all gages and all shots are averaged. Gage MITI was excluded from the averaging process because its peak stress reading varied by more than two standard deviations from the mean.

The conclusions to be reached here are that the peak stress declared by the gage element is independent of backing material and that the radial and tangential peak stresses are identical within the limits of the experimental error. As the grout is almost certainly behaving hydrodynamically at these stress levels, the equality of radial and tangential peak stresses indicates that the tangential mode gages are operating properly. Also the difficulties experienced by other investigators (Reference 6), arising from Mach jetting of the epoxy matrix in which the gage elements were mounted in their work, are not encountered here.

TABLE 2.2
AVERAGE PEAK STRESS

<u>Item</u>	<u>Stress Radial Mode (kbar)</u>	<u>Stress Tangential Mode (kbar)</u>
Shot 1	7.1±0.6	7.2±0.2
Shot 2	7.7±0.6	8.2±0.5
Shot 3	6.9	7.2±0.9
Lucalox	7.9±0.3	7.9±0.8
Mica	6.7±0.2	7.8±0.2
Glass	7.1	7.2±0.9
All gages	7.3±0.6	7.7±0.8

Note: Gages MIR and G3TI depart by about two standard deviations from the mean of their classes and should have been rejected. They are included in the above compilation.

Stress histories were obtained by hand digitizing the voltage records and converting these points to gage resistance and finally to stress by reading points from Figure 2.30. Although tedious, this has the advantage that estimates to the effects of the ytterbium hysteresis may be folded into the results automatically. Loading data are taken from the loading path given by Ginsberg (Reference 7) and unloading data are read from the postulated unloading paths. Data are presented in Reference 7 giving the zero-stress residual resistance as a function of the peak stress. Specifically there is claimed to be a residual

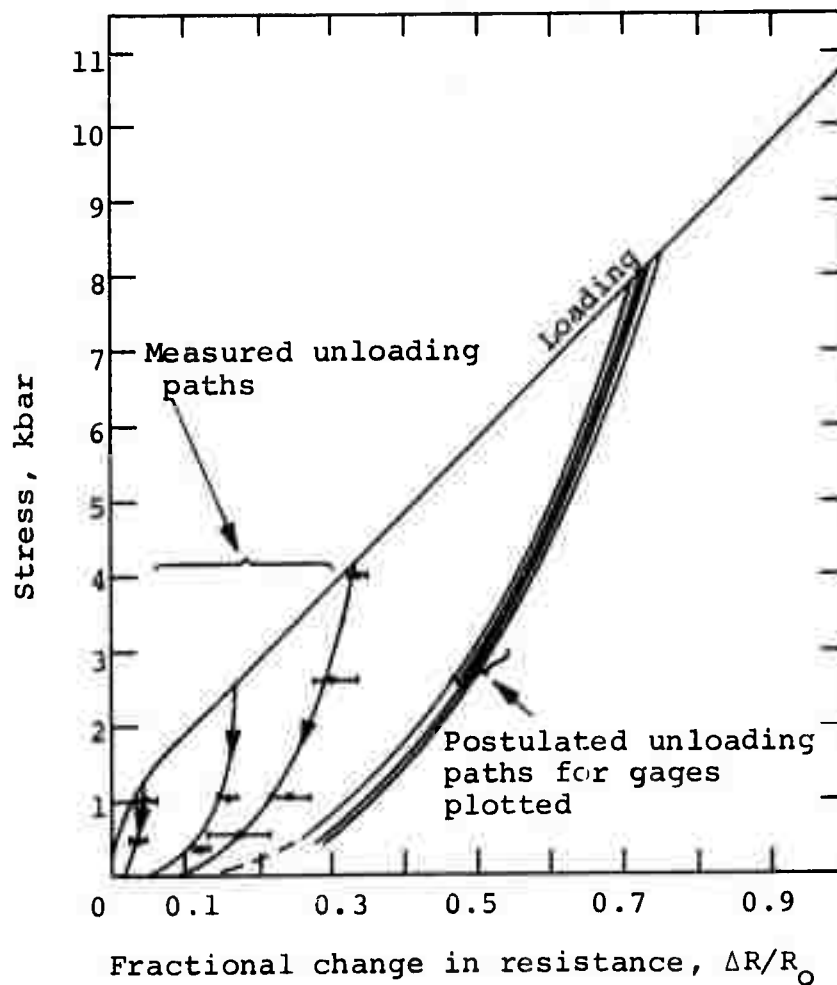


Figure 2.30 Ytterbium stress transducer calibration (M. J. Ginsberg, Reference 7).

$\Delta R/R_0 \approx 0.13$ for a peak stress of about 7.8 kbar. The postulated unloading path for a gage loaded to this stress is a smooth curve following the trend of lower peak stress unloading paths and connecting these two paths. The unloading data of Keough (Reference 8) appear to be somewhat inconsistent with those of Ginsberg and in the interest of consistency we have chosen to adhere to the latter.

In Figure 2.31 are plotted the three long-time tangential-mode stress records remaining after exclusion of the mica-backed gages for the reasons stated above. These consist of two glass and one Lucalox gages. Also included are points taken from Figure 2.29 (the computed tangential stress).

In the case of Gage L2TI, both the high and low gain traces are available to be analyzed for the peak stress. There was found to be a discrepancy of 12 percent between the peak stress values obtained from the two traces, making the reported value and the plotted stress history somewhat suspect as to its magnitude. Discrepancies of 3 percent and 10 percent were found by similar analyses on two other oscilloscopes. As a result, the voltage magnitude records must be considered as accurate to not better than 5 percent.

The general behavior of the stress wave as calculated is that of the measured behavior: the second pulse observed in all of the records is clearly due to an impedance mismatch between the gage block and the surrounding grout. However, the assumption that the ytterbium unloads along the postulated path of Figure 2.30 leads to stresses that are nearly an order of magnitude below the computed values. That there should be a difference between the computed and measured stress histories is not surprising. The equation of state used in the calculations is only

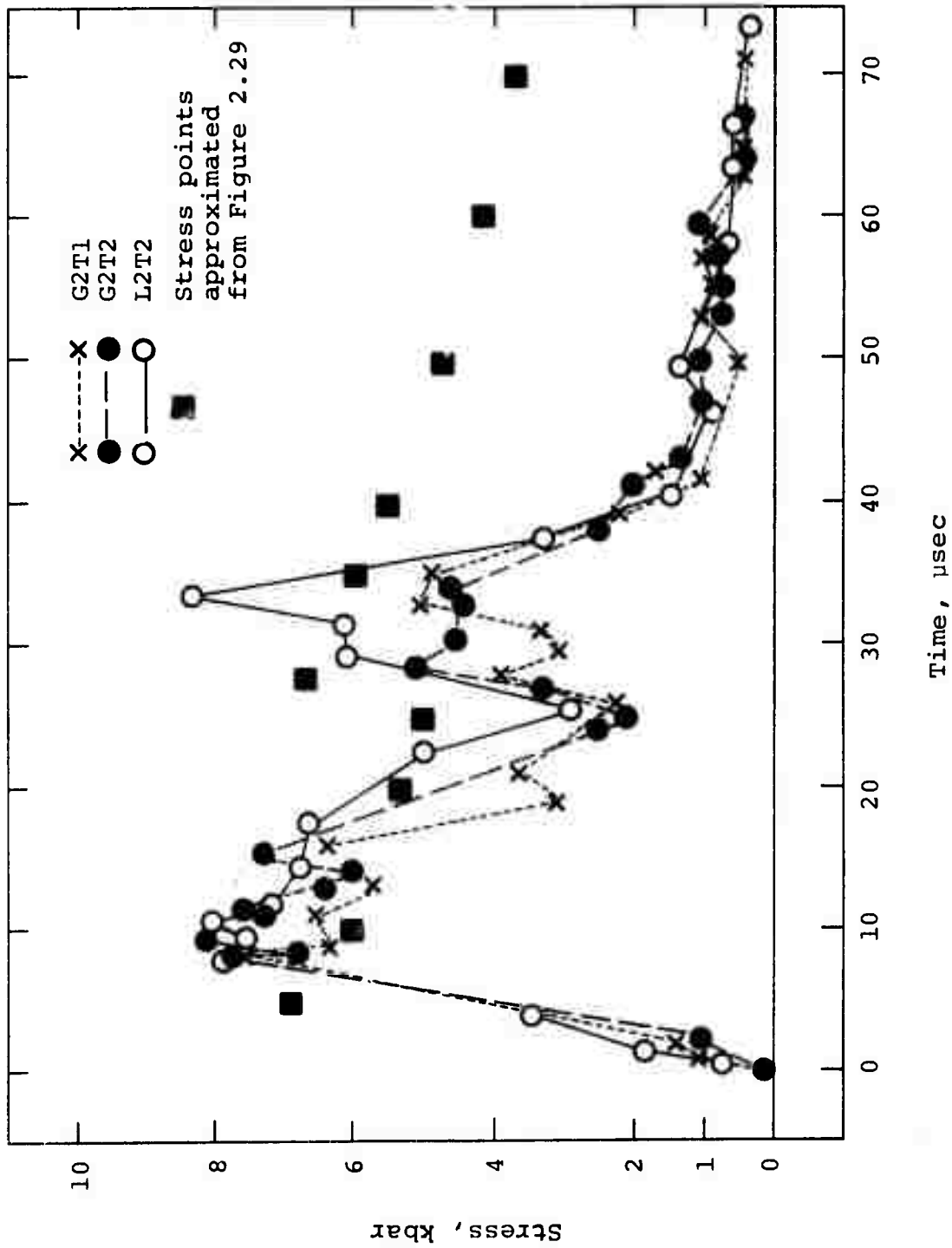


Figure 2.31 Stress-time histories of three tangential-mode gages including effects of assumed hysteresis of Figure 2.31.

approximate, including no effects of compaction, and the two-dimensional character of the actual shock wave traveling past a small gage block imbedded in a semi-infinite region of different material will feed energy into the block from the tangential dimensions, thus distorting the wave, to second order.

It is difficult to explain the large discrepancy at late times by other than an improper assumption as to the unloading path of the ytterbium. For completeness we have also plotted (Figure 2.32) the fractional change in resistance of the three gages as a function of time and have scaled the computed stress by a factor given by the slope of the loading curve of Figure 2.30. In effect, we are comparing, in Figure 2.32, the computed stress and the measured behavior assuming no hysteresis. These results plainly call for further investigation in the behavior of ytterbium.

Similar results were noted by Smith (Reference 9) in field tests of similar gages emplaced in Nevada Test Site tuff. A second stress pulse was noted and the suggestion was that it may have originated from air pockets within the grout packing. In the work of this report, we have shown that mismatching impedances resulting from different grout curing procedures can lead to similar phenomena. Further, Smith also finds a measured stress that decays faster than the theoretical and, likewise, for one of his gages, shows a better agreement between theory and experiment when ytterbium hysteresis is neglected.

We may conclude that the device design used in these experiments is long-lived at these stress levels and that the strongly divergent flow is not detrimental to gage integrity. Loss of information is thought to have been due to the intentional insertion of a discontinuity around the electrical leads as they emerge from the gage mounting block.

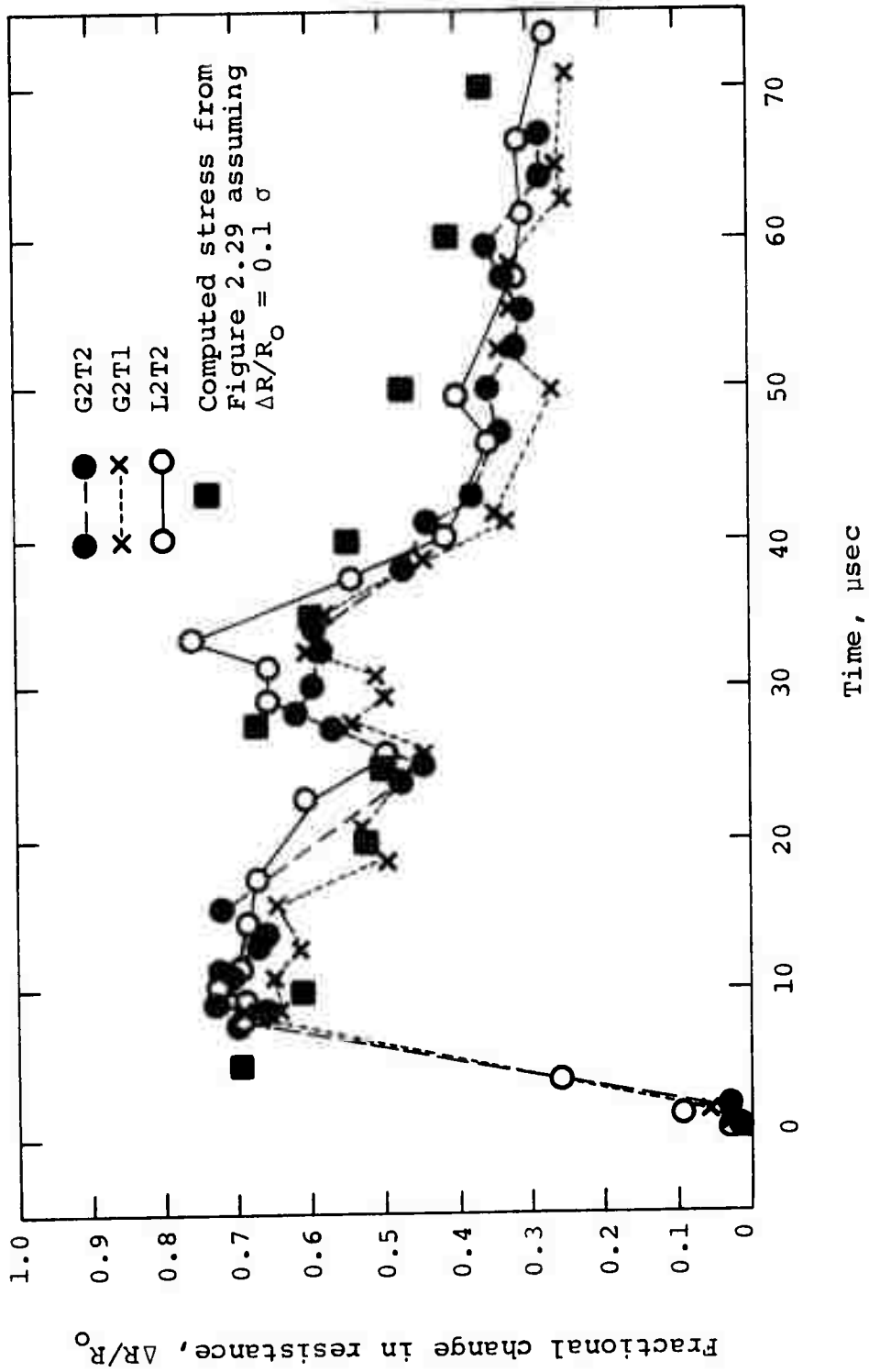


Figure 2.32 Fractional resistance change time histories of three tangential-mode gages.

As the maximum stress far exceeded the von Mises limit of the grout and both the radial and tangential mode gages registered the same peak stresses to within the experimental error, it can be claimed that the tangential mode gage behaved as expected. (Clearly, if the two gage modes had given statistically different peak stresses, then the conclusion would have been that they could not give proper stresses readings in a material that does not behave hydrodynamically at these stress levels.) We have thus successfully completed the first step in the development of a tangential stress gage by showing proper response in a low-impedance, hydrodynamic flow field.

The next step required before fielding the gage system is to obtain the desired gage response in a material which does not behave hydrodynamically and has a high impedance. These requirements may be met in the laboratory by performing the experiment at a lower explosive yield, using a stronger material as the shot medium, or both.

SECTION 3

TECHNICAL REPORT SUMMARY

3.1 TECHNICAL PROBLEMS

The prime directive of this research was to address and solve the theoretical and experimental problems associated with the realization of a gage system to obtain the in-situ constitutive properties for geologic materials. That it is theoretically possible to obtain such information by properly applying the equations of motion to measured histories of ground motion and stress has been long known (Reference 1). However, no investigation into the practical aspects of applying these equations of motion to general field data had been undertaken. The major portion of this work comprises just such an investigation. Results of this investigation then dictated the course of the experimental portion of the contract, which again was cast in the form of solving those problems associated with the realization of a gage system to measure such properties.

3.2 GENERAL METHODOLOGY

The theoretical portion of the work proceeded in three steps. The first step was to generate a data processing code which would solve the equations of motion of continuum mechanics, (Equations 1-1, 1-2, and 1-3) using field data to obtain the constitutive properties of the material from which the data were taken. The second step was to obtain field data on which to

Preceding page blank

operate; these data were generated via computer. In this way the results of our analyses could be calibrated against a precisely known equation of state. Three different sets of data were generated corresponding to three different property models. The first material used was that of a linear elastic solid. The second material was one that had an irreversible compaction, and the third was a model of good-quality structural concrete.

Clearly the data thus generated had to meet the requirements that they closely simulate data that would be obtained in the field from similar materials. This required that the data have no greater than 14 bit accuracy, corresponding to that information obtained from analog-to-digital conversion of field records. Additionally Gaussian white noise could be superimposed on the records when desired.

The third phase was answering several questions that arose naturally during the analyses of these data. The first question posed was that of the practicality of using actual field data to solve the equations of motion. Next, assuming that these equations may yield the constitutive properties of the material, we must know what gages are required for these measurements, the frequency response requirements of the gage elements and of the gage package as a whole, the sensitivity of the analysis technique to recording system noise, and other system requirements such as optimum gage placement and the sensitivity of the system to distortion of the wavefront. As mentioned above, the results of these calculations led, in a natural way, to the definition of the experimental portion of this work. It was found that a very important quantity, the tangential stress, could not, in many cases, be computed from the input data, but had to be a measured quantity itself. Since gages to measure this parameter were not state of the art, the experimental portion of the program was directed to developing and testing a suitable gage.

There are two major physical requirements that such a gage must have. First, it must be small enough that it will not distort the wavefront it is attempting to measure, and second, it must match, as closely as possible, the geologic material in which it is to be placed. This second requirement is to insure that the stress, that is actually reported by the gage is not different from that of the surrounding rock (the parameter we are attempting to measure). The first of these requirements is met by making the dimensions of the gage small. However, if such an instrument is to be used in the field, it must have a relatively high resistance so that it may be impedance matched to the data acquisition system. Such requirements may be met by a gage element that is long and thin and that is placed so that its longest dimension is tangent to the shock front. The material chosen as the active element of the gage is ytterbium as this has a very high piezoresistant coefficient; that is, there is a relatively large change in resistance for a given change in stress. For ease in installation and protection of the gage element against chemical attack, the ytterbium is sandwiched between two backing plates. Again, to satisfy the first criterion, the thickness of these backing plates was approximately 2 mils. The second criterion is met by choosing several different materials as the backing material. We have chosen Lucalox, mica, and glass and have made gages using all three of these backing materials. Tests of the gages were performed using a high explosive LX-04 as the source of the shock wave to be measured by the gages. We used a spherical geometry, as this is the simplest geometry both conceptually and experimentally to give a good test of a tangential stress gage.

3.3 TECHNICAL RESULTS

The first and perhaps the most important conclusion based on our computational investigation was that one should not expect to be able to calculate the tangential stress from measurements of radial stress and radial velocity alone. In most cases, tangential stress must be a measured quantity.

Other results of the calculations are as follows. First, the gage package must include a tangent stress gage, a radial stress gage, and a radial ground motion gage (this may be either a velocity gage or an accelerometer).

In any given experiment there must be a minimum of two such gage packages. In spherical geometry the separation of these gage packages must be about 10 percent of the total distance from the center of the disturbance. The frequency response of the gage package is determined to be the lowest frequency of any of its gage elements. All gages in the same experiment must have the same frequency response. If they do not naturally, then this condition must be imposed artificially by subjecting all of the gage records to the same digital filter during data processing. This insures that all gages have the same risetime and delay.

Actual timing errors of the signals appear in the pressure-volume curve as hysteresis; these may be eliminated by experimenting with the time of arrival of the data itself. Distortion of the wavefront is recognizable by an apparent addition of unrecoverable internal energy. It may be possible to correct for this by two independent and, if desired, simultaneous methods. First the data may be reanalyzed by changing the hypothesis of spherical wave to that of one of either cylindrical or plane. Secondly, if all three principal stresses are measured at each gage station, assuming an isotropic medium, discrepancies in the sphericity of the wavefront may be detected.

The results of the experiments may be summarized as follows: First, the peak stress of the shock wave was well in excess of the von Mises limit of the material in which we shot. This had the effect of making the material behave as if it were hydrodynamic with the subsequent effect that both the radial and tangential stress gages should produce the same stress histories. The experimental data indicated that the peak stresses seen by both types of gages were identical within the experimental error. This indicates that the problems encountered by McKay and Godfrey (Reference 6) were minimized in this work. It must be pointed out that their shot medium was a material (granite) that had a higher impedance than both the grout of this work and the material (epoxy) in which their gage elements were mounted. Further, they quite correctly postulated that a reduction in the thickness of the epoxy layer would tend to mitigate such effects.

The general character of the waveform of Figure 2.24a is that of the tangential gages (Figures 2.25 through 2.27). As is expected, there is a delay in the arrival of the reflection pulse and the risetimes of the two types of gage modes are grossly different. The conclusion is that the tangential mode gage is measuring the equilibrium stress normal to its surface (the tangential stress) to within the limits of its risetime.

Although the evidence is by no means conclusive, it appears the mica-backed gages did not have the time resolution that the other two backing materials afforded, perhaps due to the anisotropy of sheet mica. For that reason it is recommended that mica not be used as the substrate for tangential gages. There was no other obvious effect of the material used as the gage substrate.

The gage failures appeared, in most cases, to be associated with parting the leads and not with destruction of the gage element. With one exception, those gages that yielded more information than the peak stress lasted for greater than 50 μ sec. Certainly, in field applications, where both the flow divergence and shock risetime are expected to be considerably less, loss of gages should be no problem.

3.4 DOD IMPLICATIONS

From a practical standpoint, measured histories of radial stress, tangential stress, and ground motion may be used to obtain the in-situ properties of rock. From an experimental standpoint, the tangential stress gage is required. Although financial and time limitations of the contract precluded many of the experimental investigations needed to insure the viability of such a device, preliminary investigations carried out under this contract indicate that such a gage is practical.

3.5 IMPLICATIONS FOR FURTHER RESEARCH

We have tested a tangential gage design in a low-impedance material that is nearly hydrodynamic at the stress levels attained. It was found that, to within the limits of experimental error, the device performed as desired. The expected field application of such a gage would be in materials having impedances higher than that of the grout used in this work and failure surfaces such that the materials are either elastic or brittle at the stress levels considered here.

We have not demonstrated that all of the difficulties experienced by McKay and Godfrey (Reference 6) have been eliminated. It was postulated that part of their trouble arose

from the fact that the impedance of their shot medium (granite) was greater than that of one of their gage construction components (epoxy). It is thus necessary that the gage concept of this work be tested in a high strength and impedance medium prior to fielding a full gage package for the determination of in-situ properties.

As it is the ultimate goal of this effort to produce a gage system for the determination of in-situ material properties, at least one full-scale field test of a prototype should be performed.

REFERENCES

1. Richard Fowles and Roger F. Williams, "Plane Stress Wave Propagation in Solids," Jour. Appl. Phys. 41, 360 (January 1970).
2. Carl F. Peterson, Stanford Research Institute, private communication.
3. T. F. Stubbs, In-Situ Determination of Constitutive Relations of Geologic Materials, PITR-311, Physics International Company, August 1971.
4. R. P. Swift and I. M. Fyfe, "Elastic/Viscoplastic Theory Examined Using Radial Cylindrical Stress Waves," Trans. ASME, p. 1134, December 1970.
5. "A General Description of PISCESTM 1-DL," Document 1 DL-1, Physics International Company; M. L. Wilkins, Calculation of Elastic-Plastic Flow, UCRL-7322, Revision 1, Lawrence Livermore Laboratory, January 1969.
6. M. W. McKay and C. S. Godfrey, Study of Spherically Diverging Shock Waves in Earth Media, DASA 2223, Physics International Company, March 1969.
7. M. J. Ginsberg, Calibration and Characterization of Ytterbium Stress Transducers, DNA 2742F, Stanford Research Institute, October 1971.
8. D. D. Keough, Development of a High-Sensitivity Piezoresistive Shock Transducer for the Low Kilobar Range, DASA 2508, Stanford Research Institute, March 25, 1970.
9. C. W. Smith, Dynamic Measurements of Stress Pulses in TUFF at Nevada Test Site, DNA 2811F, Stanford Research Institute, August 23, 1971.

Preceding page blank

APPENDIX A
CONSERVATION EQUATIONS FOR SPHERICAL STRESS ANALYSIS

The one-dimensional conservation of mass, momentum, and energy equations in spherical coordinates in a homogeneous, isotropic solid in the absence of body forces, heat conduction, and internal heat sources can be found in any standard text on the subject (Reference A.1). They are:

$$\text{Mass} \quad \frac{1}{\rho} \frac{D\rho}{Dt} + \left(\frac{\partial U}{\partial r} \right)_t + \frac{2}{r} u = 0 \quad (\text{A-1})$$

$$\text{Momentum} \quad \rho \frac{DU}{Dt} = \left(\frac{\partial \sigma_r}{\partial r} \right)_t + \frac{2}{r} (\sigma_r - \sigma_\theta) \quad (\text{A-2})$$

$$\text{Energy} \quad \rho \frac{DE}{Dt} = \sigma_r \left(\frac{\partial U}{\partial r} \right)_t + \frac{2u}{r} \sigma_\theta \quad (\text{A-3})$$

In Eulerian coordinates (r, t) fixed in an inertial frame, the total derivative of a scalar point function $Y(r, t)$ is given by

$$\frac{DY}{Dt} = \left(\frac{\partial Y}{\partial t} \right)_r + u \left(\frac{\partial Y}{\partial r} \right)_t$$

In Lagrangian coordinates (h, t) fixed to mass points of the material in question the total derivative becomes

$$\frac{DY}{Dt} = \left(\frac{\partial Y}{\partial t} \right)_h$$

The two coordinate systems are related by

$$(h, t) = (r(h, 0), t)$$

This gives a particularly clear discussion of the connection between the Eulerian and Lagrangian coordinate frames and equations of motion.

Conservation of mass in Lagrangian coordinates may also be expressed by

$$\rho \cdot J = \rho_0 \quad (\text{A-4})$$

where J is the Jacobian of the transformation from Eulerian to Lagrangian coordinates*

$$J = \frac{\partial V_h}{\partial V_r} = \frac{r^2 dr}{h^2 dh} = \left(\frac{r}{r_0}\right)^2 \left(\frac{\partial r}{\partial h}\right)_t \quad (\text{A-5})$$

Using the general properties of partial derivatives

$$\frac{\partial f}{\partial g}_q = \left(\frac{\partial f}{\partial \lambda}\right)_q \left(\frac{\partial \lambda}{\partial g}\right)_q \quad \text{and} \quad \left(\frac{\partial f}{\partial g}\right)_q = - \left(\frac{\partial f}{\partial q}\right)_g \left(\frac{\partial q}{\partial g}\right)_f \quad (\text{A-6})$$

* W. F. Noh, "CEL: A Time Dependent, Two Space Dimensional, Coupled Eulerian-Lagrange Code," Methods in Computational Physics, Volume 3, Alder, Fernbach, and Rotenberg, eds. (Academic Press, 1964). This gives a particularly clear discussion of the connection between the Eulerian and the Lagrangian coordinate frames and equations of motion.

Equations (A-1), (A-2), and (A-3) become, respectively

$$\frac{1}{\rho} \left(\frac{\partial \rho}{\partial t} \right)_h - \left(\frac{\partial U}{\partial t} \right)_h \left(\frac{\partial t}{\partial h} \right)_u \left(\frac{\partial h}{\partial r} \right)_t + \frac{2}{r} U \quad (\text{A-7})$$

$$\rho \left(\frac{\partial U}{\partial t} \right)_h = - \left(\frac{\partial \sigma_r}{\partial t} \right)_h \left(\frac{\partial t}{\partial h} \right)_{\sigma_r} \left(\frac{\partial h}{\partial r} \right)_t + \frac{2}{r} (\sigma_r - \sigma_o) \quad (\text{A-8})$$

and

$$\rho \left(\frac{\partial E}{\partial t} \right)_h = - \sigma_r \left(\frac{\partial U}{\partial t} \right)_h \left(\frac{\partial t}{\partial h} \right)_u \left(\frac{\partial h}{\partial r} \right)_t + \frac{2}{r} u \sigma_\theta \quad (\text{A-9})$$

Substituting the three definitions

$$Q \equiv \left(\frac{\partial r}{\partial h} \right)_t = \frac{\rho_o}{\rho} \left(\frac{r_o}{r} \right)^2; \quad C_u \equiv \left(\frac{\partial h}{\partial t} \right)_u; \quad \text{and} \quad C_p \equiv \left(\frac{\partial h}{\partial t} \right)_{\sigma_\theta} \quad (\text{A-10})$$

into Equations (A-7), (A-8), and (A-9), the conversion equations at a given gage location (value of h) become:

Conservation of mass

$$dQ = - \frac{du}{C_u} \quad (\text{A-11})$$

Conservation of momentum

$$\frac{1}{QC_p} \frac{\partial \sigma_r}{\partial t} = \frac{r}{2} (\sigma_r - \sigma_\theta) - \frac{1}{V} \frac{du}{dt} \quad (\text{A-12})$$

Conservation of energy

$$dE = - \sigma_r dv - 2V (\sigma_r - \sigma_\theta) \frac{dr}{r} \quad (\text{A-13})$$

REFERENCE

- A.1 Y. C. Fung, Foundations of Solid Mechanics, Chapter 5, Prentice-Hall, Inc., 1965.

APPENDIX B
SUPERIMPOSED GAUSSIAN NOISE

A given data record is prepared for digital processing so that its amplitude entries are equally spaced in time. Let the time ordered sequence (X_i) denote the data record prior to the addition of noise and (Y_i) denote the noisy record. Also denote the maximum entry in (X_i) by X_{\max} . The elements of the clean and noisy sets are related by

$$Y_i = X_i + G_i \cdot \epsilon \cdot X_{\max} \quad (\text{B-1})$$

G_i is a factor chosen randomly for each i so that its distribution is a Gaussian centered at zero with a standard deviation of 1.0. ϵ is an input variable enabling the noise level on the signal to be adjusted. In normal parlance, it is the (noise/peak signal) ratio.

To test the algorithm for generating G_i , 10^4 values were obtained under the conditions of $X_{\max} = 1.0 = \epsilon$ and $X_i = 0$. The resulting histogram plot of Y_i and a true Gaussian curve as given by the Chemical Rubber Handbook is shown in Figure B.1. It is felt that the agreement between the two distributions is sufficient for this purpose.

Signal/noise ratio as commonly used refers to the ratio of the means of the quantities. In this work, the peak value of the signal was chosen as the reference level. Thus a noise/signal ratio of 2 percent, for example, as quoted in this report would be about 4 percent when referred to the means of the signal and noise.

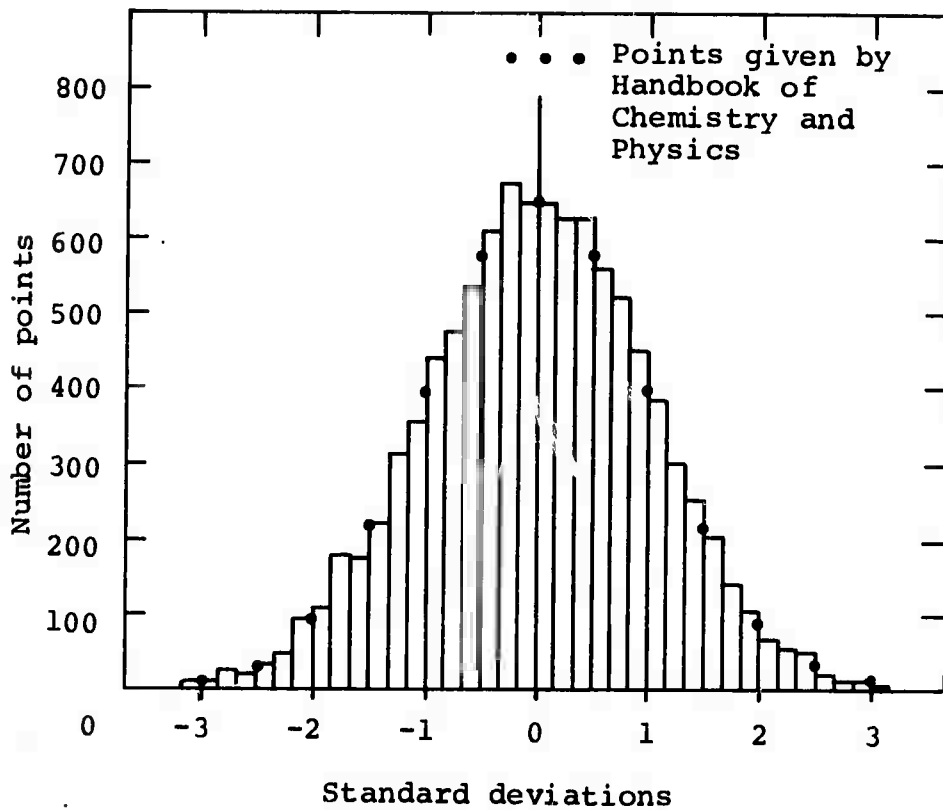


Figure B.1 Test of algorithm for randomly choosing points from a Gaussian distribution.

APPENDIX C
DIGITAL LOW-PASS FILTERING

The analog low-pass filter, upon which the digital filter used in this analysis is based, was taken directly from Reference C.1. It is an all-pole, 12th order Bessel filter modified by a sixth degree numerator polynomial, the zeros of which were determined so that the frequency response near band edge fits a Gaussian curve by the method of least squares. The digital filter was generated from the analog filter by a bilinear-z transform (Reference C.1). This precludes aliasing errors in the filtered data when the digitizing sample rate is of the same order of magnitude as the filter band-edge frequency. Figure C.1 shows the frequency response of the digital filter, with band-edge set at 150 Hz, operating on data digitized at a sample rate of 5000 Hz.

The digital filter consists of a set of coefficients A_{0k} , A_{1k} , B_{1k} and B_{2k} , depending on the zeros and poles of the analog filter and the ratio of the band edge frequency to the sample frequency (digitization rate). Small k takes on the values 1, 2, ---, $K/2$, where K is the number of poles of the analog filter. Let us define (X_n) to be the time-ordered sequence of unfiltered data and (Y_n) the time-ordered sequence of filtered data ($n = 1, 2, \dots, N$). Operation of the filter proceeds in the following manner:

Set

$$P_n = X_n + X_{n-1}$$

and

$$q_{n,k} = P_n - B_{1k} q_{n-1,k} - B_{2k} q_{n-2,k} \quad (C-1)$$

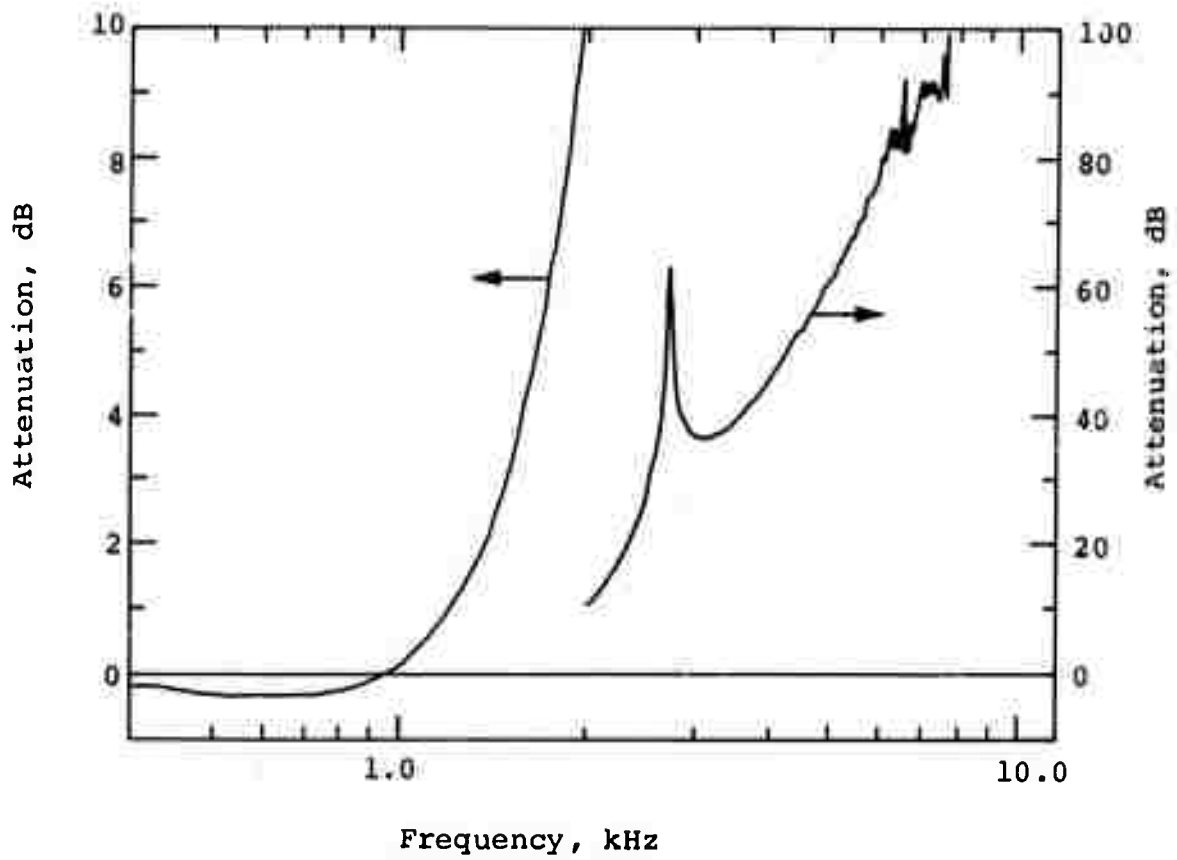


Figure C.1 Frequency response of the low-pass filter.

and

$$r_{n,k} = A_{0k} q_{n,k} + A_{1k} q_{n-1,k}$$

then

$$Y_n = \sum_{k=1}^{K/2} r_{n,k}$$

Assume that the data to be filtered is an impulse, i.e., $(X_n) = (\delta_n^m)$ where δ_n^m is the Dirac function. The filter applied to this through Equation (C-1) yields the "impulse response" (h_n) . Figure C.2 shows the impulse response of the filter with $m = 1$, band edge = 1.50 kHz, and digital sample rate = 50 kHz. This corresponds to an impulse occurring at time zero. Clearly, any arbitrary input sequence of data may be made up of a linear superposition of such impulses:

$$V_n = \sum_{m=1}^N C_m \delta_n^m \quad (C-2)$$

From the linearity shown in Equations (C-1) and (C-2), it is obvious that the elements of the sequence (Y_n) are linear superpositions of the impulse response set.

$$Y_n = \sum_{m=1}^N a_{n,m} h_m \quad (C-3)$$

Figure C.2 shows that the maximum in the impulse response occurs at some time other than the time of the impulse. Assume that this "filter delay" is λ points. That is, the maximal influence

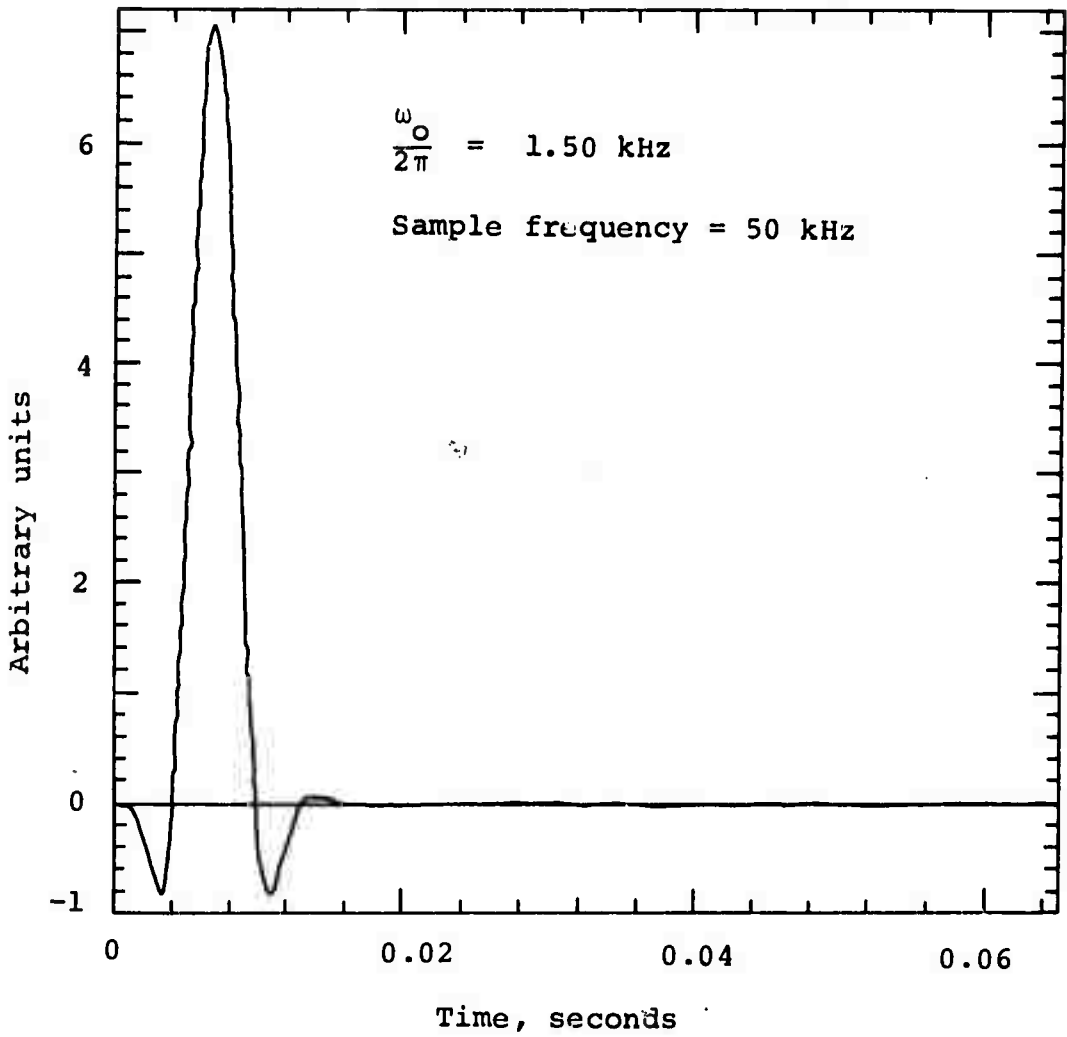


Figure C.2 Impulse response of the low-pass filter.

of the datum X_n manifests itself in the filtered datum element $Y_{n+\lambda}$. In order that (X_k) and (Y_n) have the same time base, the time scale of the filtered data must be shifted by λ points. This is done automatically during data processing.

REFERENCES

- C.1 F. F. Kuo and M. Karnaug, "Approximation of Linear Phase Filters With Gaussian Damped Impulse Response," IEEE Trans. on Arc. Theory, p. 2555, June 1964.
- C.2 Gold and Rader, Digital Processing of Signals, pp. 10-18, (McGraw Hill Book Company: 1969).